Fatigue Life Prediction Based on the Advanced Fatigue Crack Growth Model and the Monte-Carlo Simulation Method

by

Sergey Bogdanov

A thesis
presented to the University of Waterloo
in fulfillment of the
thesis requirement for the degree of
Doctor of Philosophy
in
Mechanical Engineering

Waterloo, Ontario, Canada, 2014

Author's Declaration

I hereby declare that I am the sole author of this thesis. This is a true copy of the thesis, including any required final revisions, as accepted by my examiners.

I understand that my thesis may be made electronically available to the public.

Abstract

It is well-known that loss of the structural stability due to propagation of the dominant crack is one of the main sources of fatigue failures. Therefore, computationally feasible fatigue crack growth model is essential for advanced fatigue life analysis. Appropriate model should be able to calculate the time required for crack to grow: from the initial crack of any size to the final critical length; in any structure; under applied variable loading.

The UniGrow two-parameter total driving force was proposed ten years ago. Since then, the fatigue crack growth model based on it, was enhanced with a set of memory rules and resulted in a sophisticated fatigue crack growth software package which was extensively validated on the basis of available experimental data. Nevertheless, in its previous form the UniGrow model had several serious limitations: it was not able to model the fatigue crack growth under plane-strain conditions; the Neuber rule was the only method used for elastic-plastic stress-strain analysis; the fatigue crack growth prediction was limited to macro-cracks and the variability of the material response to cyclic loading has not been considered. In addition to these shortcomings, there were no preferred method for estimation of the material block size ρ^*, which is one of the main parameters required for the analysis. Therefore, further modeling and validation of the UniGrow concept were required before it could be coupled with the "Monte-Carlo" simulation method.

The main research goal pursued in this work was to improve and remove limitations of the existing fatigue crack growth model and to combine this model with "Monte-Carlo" simulations. Such combination enables the assessment of the reliability of predicted fatigue lives. Thus, the result of this work is an extensive probabilistic fatigue crack growth model which is able to perform the analysis of structures in the plane-strain or plane-stress condition. Comprehensive set of the fatigue crack growth data for aluminum and steel alloys generated under the constant and variable amplitude loading was used for the validation.

Acknowledgements

I would like to thank my supervisor Professor Grzegorz Glinka for his patience, guidance and support. For the past four years of his mentorship I have not only increased my knowledge in the field of fatigue but also learned a lot about how to defend your ideas and how to test new hypotheses.

The Office of Naval Research, USA and Dr. A.K. Vasudevan are gratefully acknowledged for the financial support.

I would like to thank all people who have taken part in the development and validation of the UniGrow model. In particular, I would like to acknowledge Semyon Mikheevskiy, Amir Noroozi for their contributions. Pasi Lindroth and Aditya Chattopadhyay are greatly acknowledged for their gentle criticism and scientific proposals.

Besides my advisor, I would like to thank the rest of my thesis committee: Prof. H. Jakubczak, Prof. M. Pandey, Prof. S. Lambert and Prof. H.J. Kwon.

I am much obliged to people who has shared the pain of learning and doing research in the new environment, people who has been part of the so-called "*russian speaking circle*" - Evdokia Popova, Oxana Skiba, Maria Kapiturova and Yauheni Staraselski. Without them, successful transition to the new country would've been extremely hard.

I want to say special thanks to all my friends who has stayed in Russia but kept in touch over the distance and were always very supportive: Igor Seleznev, Denis Petrov, Andrey Sergeev and Alexander Deryabin.

The last but not the least, I would like to thank my family - Maria Bogdanova, Mikhail Bogdanov, Tatyana Bogdanova, Vasiliy Bogdanov, Denis Bogdanov, Alexandra Bogdanova and Varvara Bogdanova.

Dedication

To my wife Maria and my son Mikhail

Table of Contents

List of Tables

List of Figures

Nomenclature

$[C, \gamma]$ UniGrow fatigue crack growth coefficients

$\Delta\sigma_{th}^{a}$ threshold stress range

ΔK stress intensity factor range

ΔK_{eff} effective stress intensity factor range

ΔK_{th} Threshold stress intensity factor range

$\Delta\kappa$ total driving force

$[C, m]$ fatigue crack growth coefficients

ρ^{*} material block size

σ_{eq} Von-Mises stress

$\sigma_{r}\left(x\right)$ residual stress

σ_{ys} yield stress

$\widetilde{\sigma}_{theor}$ theoretical strength of a material

a crack length

C_p plasticity zone correction factor

CS short crack correction factor

da/dN fatigue crack growth rate

K stress intensity factor

K^* corrected for short crack

K_{IC} fracture toughness

K_r residual stress intensity factor

$m\,(x, a)$ weight function

N number of cycles

R stress ratio

r_p plastic zone size

S_{appl} applied nominal stress

S_{max} maximum applied stress

S_{op} opening stress level

W_p strain energy density

Y geometry factor

Chapter 1

Introduction

The phenomenon of the fatigue failure of engineering structures has been recognized for more than a century. The first designs against fatigue were done on the basis of empirical relationships between the applied nominal stress, S_{appl} and corresponding number of cycles, N the structure can withstand. Nowadays, it is eminent that fatigue failures are due to cracks which initiate and propagate in the structure until the final failure. Therefore a lot of efforts in recent years have been devoted to fatigue crack growth modeling. As a result, a variety of fatigue crack growth models and software packages are available nowadays to engineers.

The finite element analysis method is a widely used tool for the structural analysis, and at first it seems also to be a promising technique for modeling of the fatigue crack growth. By using the finite element method, the stress analysis of complex bodies can be carried out with a high degree of precision but this advantage comes at a cost of enormous computational time in the case of cyclic loading histories. Also, since the crack propagates through the analyzed medium, continuous "*remeshing*" of the 3D model is

required and this is not a trivial feature to implement. A typical fatigue crack growth model in turn employs available stress intensity factor solutions for stress analysis of the cracked bodies and therefore provides satisfactory accuracy in exchange for reasonable amount computational costs.

The UniGrow two-parameter total driving force concept [1] was derived more than ten years ago. Since then, the UniGrow fatigue crack growth model has been enhanced with set of memory rules to account for load-interaction effects, which has resulted in an extensive fatigue crack growth software package. A comprehensive set of available fatigue crack growth data [2, 3, 4, 5, 6] obtained under constant and variable loading conditions was used for the validation of the model. The materials tested include different aluminum and steel alloys (such as Al 7075-T6 and Al 2024-T3, St 4130 and A36).

Despite the fact that the UniGrow model is capable of predicting numerous fatigue crack growth scenarios, its performance was unstatisfactory in several instances and thus further development and expansion of the model was required. First, the UniGrow model in its current form can be applied only to structures under the plane-stress condition. Second, the UniGrow model uses Neuber rule for the elastic-plastic stress-strain analysis of a cracked body. The ESED method is an alternative for the Neuber rule and it is based on the equivalence of the strain-energy density. Therefore, implementation of the ESED method for the elastic-plastic stress analysis and comparison of obtained results using both methods was required. Third, short cracks pose a well-known problem which wasn't previously accounted for in the UniGrow fatigue crack growth model. Finally, numerous different methods were proposed to estimate the microstructural material parameter, ρ^*. It was found that the effect of the ρ^* value on the fatigue crack growth analysis needed additional studies as well.

Another shortcoming of deterministic fatigue crack growth models is that they do not

account for the varying material fatigue crack growth resistance inherent to the real-world structures. To counter that, the "Monte-Carlo" method had to be combined with the improved UniGrow fatigue crack growth model. One of two alternative approaches can be used to account for the material properties variability and the scatter of the initial flaw size. They are so-called random variables and random process methods. The first method asserts that every produced part is made of a material with a deterministic resistance to the cyclic load but that resistance is changing from part to part. The second focuses on the erratic fatigue crack growth behavior and respectively advocates the use of Markov Chains for the analysis [7]. Following the analysis of both methods, the choice of the random variables approach has been justified and combination of the deterministic fatigue crack growth UniGrow model with the "Monte-Carlo" simulation method has been undertaken.

The goal of this research is to analyze common engineering problems with the fatigue crack growth modeling, improve the deterministic UniGrow fatigue crack growth model, and propose the method to account for the scatter of the material resistance and of the initial flaw size. In more details, the objectives of this research are as follows:

- To assess limitations of the UniGrow fatigue crack growth model proposed and developed by Noroozi [1] and Mikheevskiy [8].
- To modify the UniGrow fatigue crack growth model, such that it can be applied to structures in plane-strain condition
- To extend it to be capable of analyzing fatigue growth of short cracks.
- To implement the capability of the elastic-plastic stress-strain analysis based on the ESED rule.

- To review methods for evaluation of the ρ^* parameter, develop a unified approach for its estimation, and study its impact on the fatigue crack growth analysis.
- To analyze random variables and random process approaches for probabilistic fatigue crack growth modeling, to study the UniGrow model bias and combine the UniGrow model with the "Monte-Carlo" simulation method.
- To validate proposed modifications to the UniGrow model, and apply the probabilistic analysis to fatigue life evaluation.

Tasks carried out to accomplish the objectives listed above: Alternative methods to perform stress-strain analysis ahead of a crack tip under plane-strain conditions in a combination with the ESED and Neuber rule were proposed and incorporated into the extended and improved UniGrow model. The short-crack correction factor for Creager-Paris solution was introduced and validated. A special algorithm to search for the ρ^* parameter has been established and the sensitivity of the UniGrow model to the variability of this parameter was studied. In order to account for the material variability in the fatigue crack growth, random process and random variables approaches were studied. Ability to input the initial crack length which follows the prescribed probability distribution was incorporated. Potential applications of the developed model were presented.

The structure of this dissertation is as follows. Available fatigue crack growth models are presented and analyzed in the literature review, then the UniGrow model in its current form is thoroughly reviewed, and finally available methods to account for the inherent randomness of the fatigue crack growth are described. Modifications and adjustments of the UniGrow model are presented in chapter 3. Analysis and new method for evaluation of the material parameter, ρ^* are described in the Chapter 4. The probabilistic analysis based on the combination of the improved UniGrow model with the "Monte-Carlo" method

is reviewed in the Chapter 5. Afterward, several potential applications of the developed model are presented. The thesis is concluded with a brief summary, conclusions and recommendations for future research.

Chapter 2

Literature Review

Paul Paris, in 1963, performed critical analysis of available crack propagating laws [9] and his conclusion was that the fatigue crack growth rate, da/dN can be described as a function of the stress intensity factor range, ΔK :

$$\frac{da}{dN} = C\left(\Delta K\right)^m \tag{2.1}$$

It is widely accepted since then that fatigue crack propagation rate is related to the range of the applied stress intensity factor, given that the plastic zone in the vicinity of the crack tip is small in comparison with the crack length and cross-section dimensions.

2.1 The stress intensity factor

The stress intensity factor, K is a scalar value which was derived by Irwin [10] during studies on stress and displacement fields in a cracked linear elastic body. Irwin has pre-

sented the stress distribution ahead of an infinitely sharp crack (see Figure 2.1a) subjected to an arbitrary external load in a form:

$$\begin{aligned}
\sigma_x &= \frac{K}{\sqrt{2\pi r}} \cos\frac{\phi}{2}\left[1 - \sin\frac{\phi}{2}\sin\frac{3\phi}{2}\right] + \dots \\
\sigma_y &= \frac{K}{\sqrt{2\pi r}} \cos\frac{\phi}{2}\left[1 + \sin\frac{\phi}{2}\sin\frac{3\phi}{2}\right] + \dots \\
\tau_{xy} &= \frac{K}{\sqrt{2\pi r}} \cos\frac{\phi}{2}\sin\frac{\phi}{2}\cos\frac{3\phi}{2} + \dots
\end{aligned} \tag{2.2}$$

where (r, ϕ) are polar coordinates with r=0 at the crack tip.

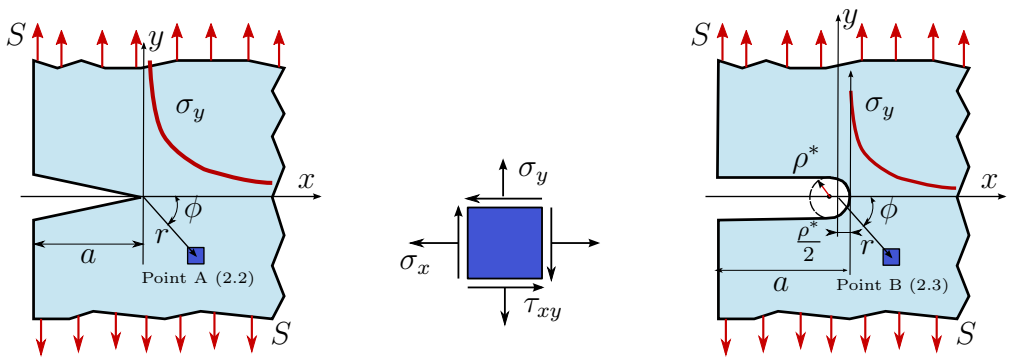

(a) Sharp crack (b) Stress cube (c) Blunt crack

Figure 2.1: Ideally sharp and blunt cracks in a linear elastic domain.

The solution of equation (2.2) returns infinite stress at the crack tip, that is physically impossible. Therefore, it seems reasonable to model the crack tip as a notch with a small but finite radius ρ^* , as shown in Figure 2.1c. For this case, the stress distribution in a similar to (2.2) form was obtained by Creager and Paris [11]:

$$\begin{aligned}
\sigma_x &= -\frac{K}{\sqrt{2\pi r}}\frac{\rho^*}{2r}\cos\frac{3\phi}{2} + \frac{K}{\sqrt{2\pi r}}\cos\frac{\phi}{2}\left[1 - \sin\frac{\phi}{2}\sin\frac{3\phi}{2}\right] + \dots \\
\sigma_y &= \frac{K}{\sqrt{2\pi r}}\frac{\rho^*}{2r}\cos\frac{3\phi}{2} + \frac{K}{\sqrt{2\pi r}}\cos\frac{\phi}{2}\left[1 + \sin\frac{\phi}{2}\sin\frac{3\phi}{2}\right] + \dots \\
\tau_{xy} &= -\frac{K}{\sqrt{2\pi r}}\frac{\rho^*}{2r}\sin\frac{3\phi}{2} + \frac{K}{\sqrt{2\pi r}}\sin\frac{\phi}{2}\cos\frac{3\phi}{2}\cos\frac{\phi}{2} + \dots
\end{aligned} \tag{2.3}$$

One can notice that the stress at the blunt crack tip (see Figure 2.1c,$r = \rho^*/2$) is finite

2.1.1 Ready-made solutions

Since the stress intensity factor is a key parameter to estimate stress and displacement fields ahead of a crack tip, there has to be a robust way to calculate it for any given "*geometry-load*" combination. The stress intensity factor as commonly defined by equation (2.4), contains the geometry correction factor Y.

$$K = S\sqrt{\pi a}\cdot Y \tag{2.4}$$

It is possible to estimate the Y factor through extensive stress analysis using finite element methods or by the application of available ready-made solutions. The most comprehensive collection of ready-made Y factor solutions is contained in the handbooks compiled by Murakami [12], Tada [13] and Sih [14]. Unfortunately, solutions presented in those handbooks are limited to specific loading conditions and have limited geometrical range of applicability. The most well-known and used Y factor solutions for compact tension (CT, Figure 2.2a) and middle-tension (MT, Figure 2.2b) specimens under tension loading are

presented in equations (2.5) and (2.6) accordingly.

$$Y = 16.7\left(\frac{a}{W}\right)^{0.5} - 104.7\left(\frac{a}{W}\right)^{1.5} + 369.9\left(\frac{a}{W}\right)^{2.5} - 573.8\left(\frac{a}{W}\right)^{3.5} + 360.5\left(\frac{a}{W}\right)^{4.5} \quad (2.5)$$

$$Y = \frac{1}{\sqrt{1.0 - \left(\frac{a}{W}\right)}}\left[1.0 - 0.5\left(\frac{a}{W}\right) + 0.37\left(\frac{a}{W}\right)^{2} - 0.044\left(\frac{a}{W}\right)^{3}\right] \quad (2.6)$$

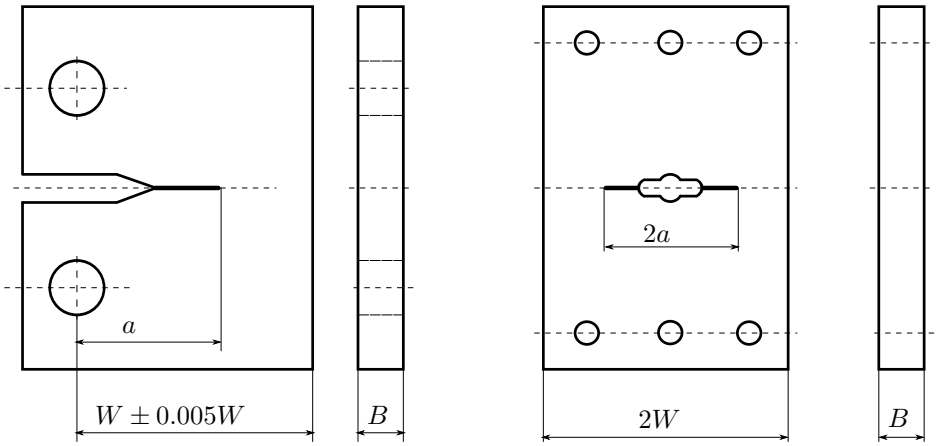

Figure 2.2: (a) Compact-tension and (b) middle-tension specimens [15]

2.1.2 The weight function method

In order to overcome limitations of the ready-made stress intensity factor solutions approach, Moftakhar and Glinka [16] have developed a methodology for efficient calculation of stress intensity factors for cracks in complex stress fields by using the weight function method. Originally proposed by Bueckner [17] and Rice [18], the weight function method is based on the principle of superposition. The stress intensity factor for a crack body

subjected to external loading, S, (Figure 2.3a) can be obtained by determining the stress intensity factor in a geometrically identical body with the local stress field $\sigma(x)$ applied to the crack faces (Figure 2.3c). The local stress field $\sigma(x)$ induced by the external load S in the prospective crack plane should be determined by neglecting the presence of the crack (Figure 2.3b).

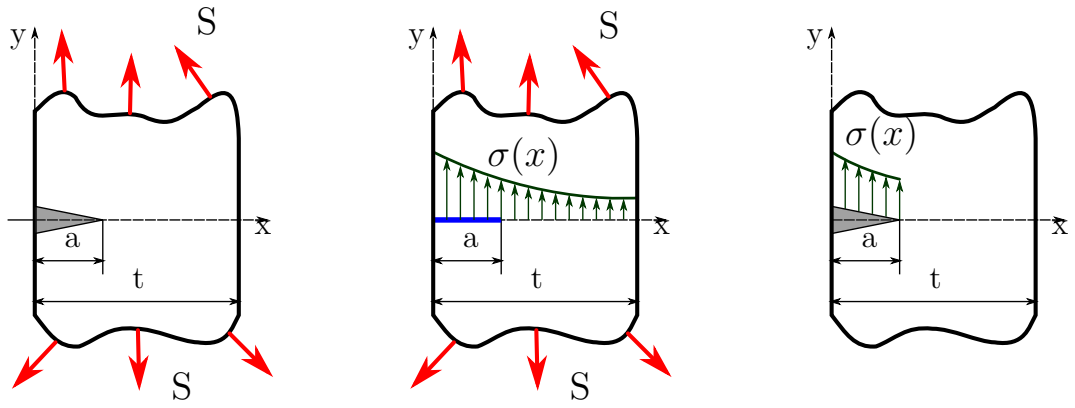

(a) Cracked body with externally applied stress

(b) Geometrically identical body without crack

(c) Geometrically identical body with local stress applied to the crack faces

Figure 2.3: Weight function method

Therefore, the stress intensity factor takes a form of the following definite integral (2.7):

$$K = \int_0^a \sigma(x)\, m(x,a)\, dx \tag{2.7}$$

where $m(x,a)$ is the weight function and $\sigma(x)$ is the stress distribution, induced by the loads in the uncracked body

The most significant advantage of the weight function method is its universality. It is sufficient to derive the weight function for a given cracked body and it can later be used to estimate the stress intensity factor induced by any externally applied load. A variety of cracked bodies were studied in recent years by Glinka et. al [19]. Weight functions obtained from theses studies can be used to estimate the stress intensity factors for cracks in plates, disks or cylinders [20, 21]. In addition to the available collection of weight functions, an efficient integration procedure was implemented in the UniGrow software package. Therefore, an immense number of fatigue crack growth cases can be studied with the deterministic UniGrow fatigue crack growth model.

2.2 Correlation between fatigue crack growth rate and the stress intensity factor

Every available fatigue crack growth model requires a significant amount of basic experimental material data. Raw fatigue crack growth data sets come in the form of the "*a versus N*" relationship (see Figure 2.4a). The CT or MT specimens tested under constant amplitude loading are the most often used configurations to map the relationship between the crack length and the number of loading cycles. In order to use such data for future fatigue life esimations, the set of $[N_i, a_i]$ points from the fatigue crack growth experiment has to be transformed into the set of $[\Delta K_i, (da/dN)_i]$ pairs. Examples of the original and transformed fatigue crack growth data sets are presented in Figures 2.4a and 2.4b. It is obvious that the conversion technique plays an important role for further fatigue crack growth analysis, and therefore it had to be standardized.

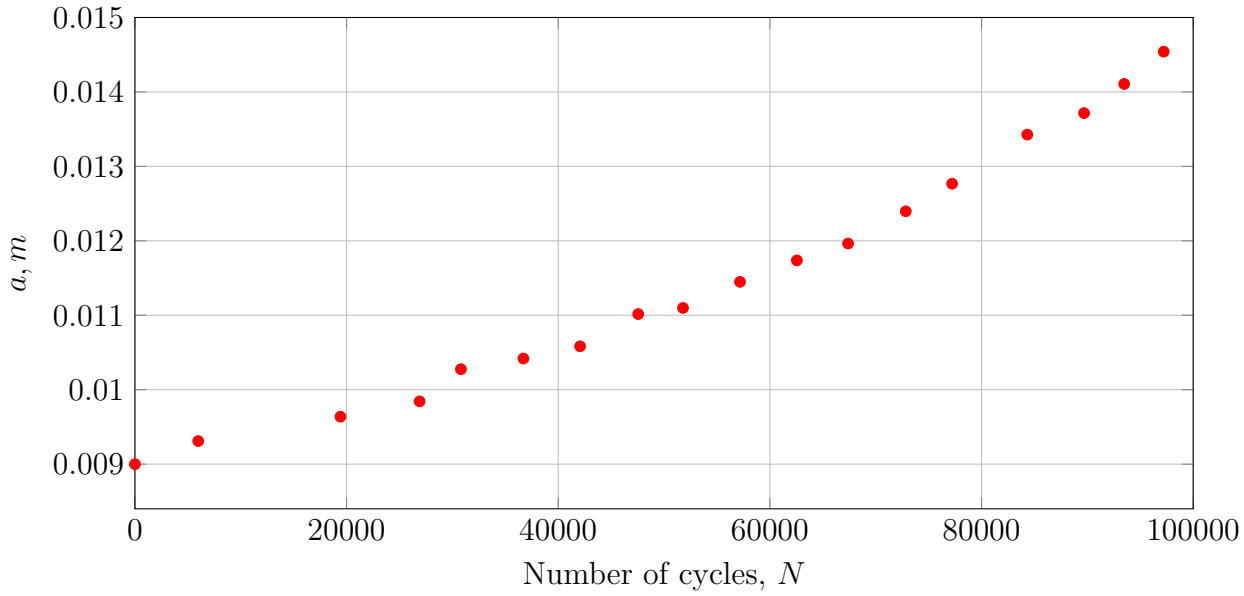

(a)

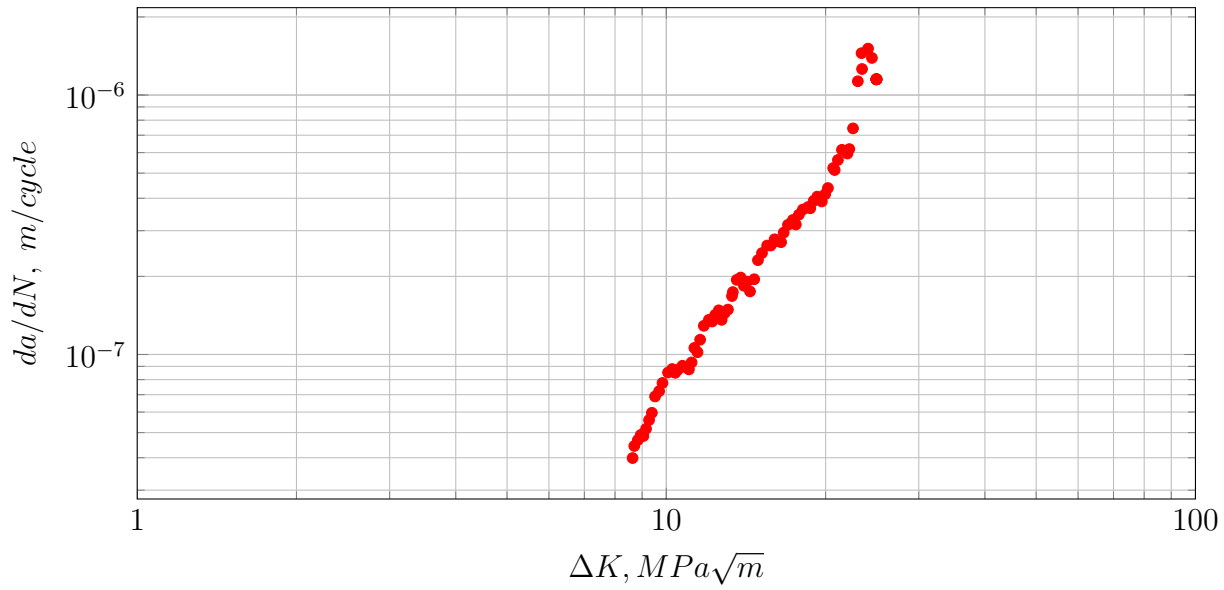

(b)

Figure 2.4: Typical experimental fatigue crack growth data in (a) $avs.N$ and (b) da/dN $vs.$ Δ K [3]

The ASTM E647 [15] is the standard which currently governs the fatigue crack growth test procedure and transformation methods. The development of the current standard has been preceded by two comprehensive inter-laboratory round-robin studies [2, 5]. The first round-robin program was organized by a special task group E24.04.01 of the ASTM around forty five years ago. Fifteen laboratories from the United States and United Kingdom performed fatigue crack growth experiments on specimens made of the 10Ni-8Co-1Mo high strength steel and 2219-T851 aluminum alloys. The objectives of this study were: to measure variability in the fatigue crack growth experiments within each and between all participating laboratories; to study the specimen geometry effect on the fatigue crack growth rate, and to test which of the selected five data processing techniques used would provide the best outcome. As a result, two out of five data processing techniques (incremental polynomial and secant) were recommended for the use. Test specimen bias was concluded not to pose any practical problem for fatigue crack growth rate testing. Typical variability factor within a single laboratory was about 2 to 1 and the scatter of fatigue crack growth data between laboratories was about 3 to 1 for da/dN given the ΔK level.

The second round-robin program started in early 2000's and was focused on the improvement of the existing standard. New techniques to measure the crack length, different materials and geometries as well as a variety of loading R ratio were tested in eighteen laboratories across the world. Needless to say that the new crack measurement techniques developed in recent years provided more reliable data in comparison with the first round-robin program. But the important result was that the fatigue crack growth rate of specimens made of steel (St 4140 in particular) exhibited significantly less variability than similar specimens made of aluminum alloys (Al 7075-T6 and Al 2024-T3). The general conclusion from both round-robin programs was that it is possible to obtain reproducible data from fatigue crack growth experiments.

2.2.1 Material models and the stress ratio, R effect

Once the computational procedure to estimate the stress intensity factor for a given "*geometry-load*" configuration is in place, it is important to decide which material fatigue crack growth model to use for the fatigue crack growth analysis. The "*Paris Law*" is the simplest fatigue crack growth material model but it has several limitations. First, equation (2.1) fails to imitate sigmoidal shape of a typical experimental fatigue crack growth data set (as seen in Figure 2.5a) unless a set of $[C_i, m_i]$ parameters is used. Second, the "*Paris Law*" fails to predict the spread of $(\Delta K, da/dN)$ curves obtained at different R ratios (see Figure 2.5b).

A variety of fatigue crack growth laws have been proposed in recent years and interested readers can be referred to the review made by Miller [22]. Two material models proposed at the end of 60's - the Forman [23] and the Walker law [24] are worth mentioning due to their wide acceptance. Interestingly, most of the later descriptions of fatigue crack growth models are formally similar or they are derivatives of those two models.

The empirical fatigue crack growth relationship proposed by Forman in 1967 correlates (2.8) the fatigue crack growth rate to the combination of the stress intensity factor range ΔK, the fracture toughness K_{IC} and the load ratio, R :

$$\frac{da}{dN} = \frac{C\left(\Delta K_{appl}\right)^m}{\left(1-R\right)K_c - \Delta K_{appl}} \tag{2.8}$$

Forman's law describes a wide range of da/dN data given by correctly chosen $[C, m]$ values and also is able to account for the R ratio effect.

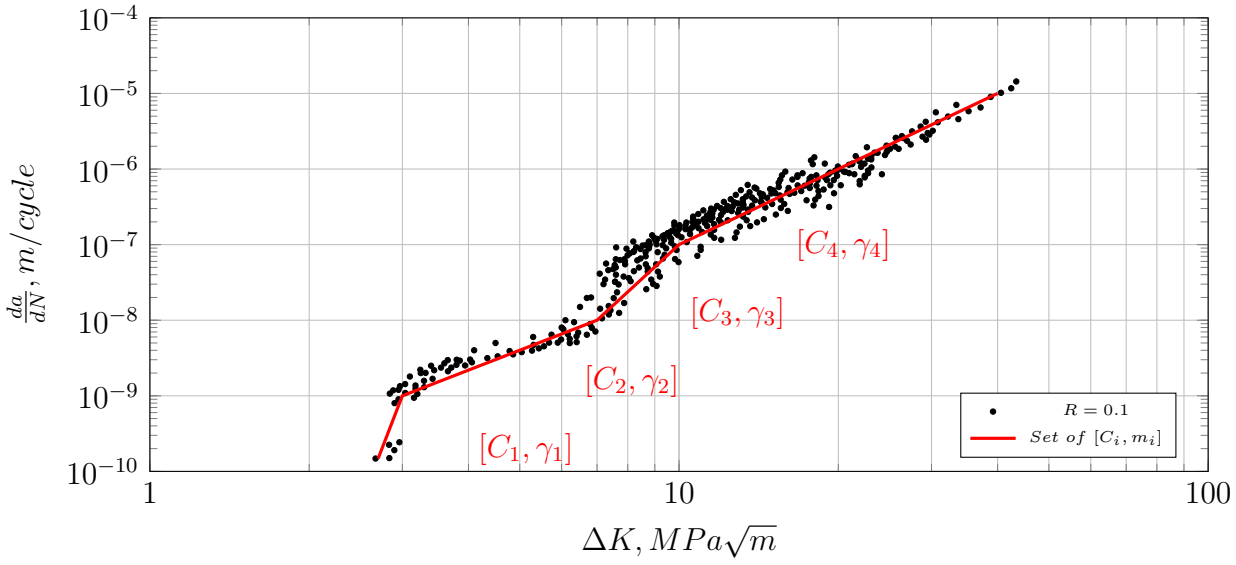

(a)

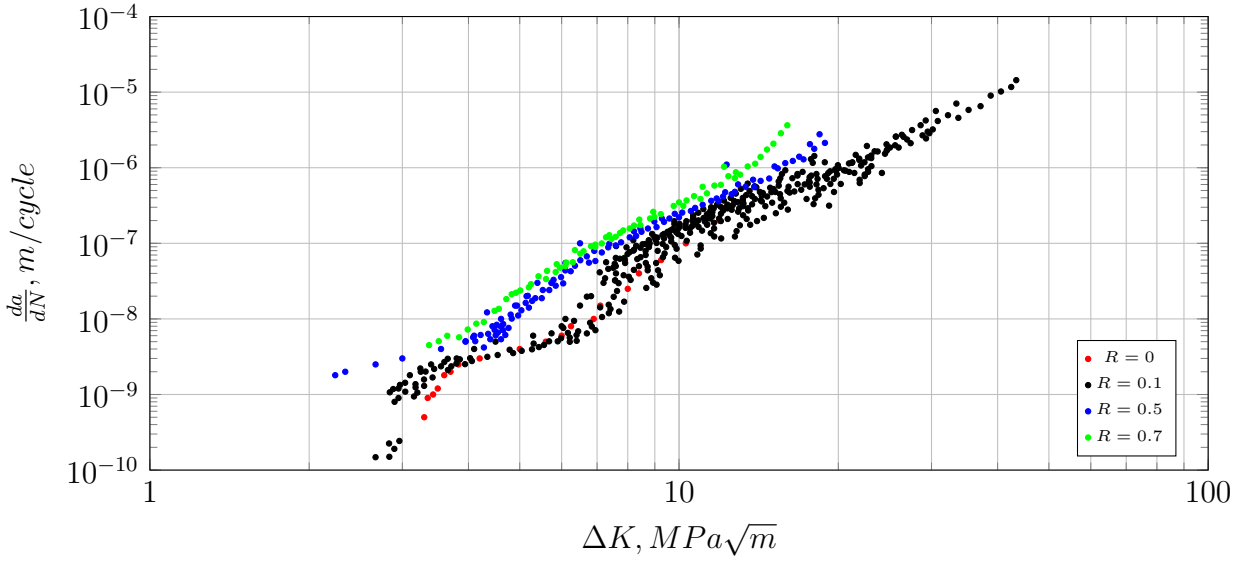

(b)

Figure 2.5: Fatigue crack growth data for Al 2024-T3 aluminum alloy obtained at (a) $R = 0.1$ and (b) various R ratios [25]

The Walker model [24] constitutes that the R ratio effect has to be accounted for via the effective stress $\bar{\sigma} = \sigma_{max}^{(1-n)} \Delta\sigma^n$ parameter. One can derive from this assumption the effective stress intensity factor, $\bar{K} = K_{max}^{(1-n)} \Delta K^n$ and relate it to the fatigue crack growth rate da/dN:

$$\frac{da}{dN} = C \left(\bar{K}\right)^m \tag{2.9}$$

Similar to the "*Paris law*", the Walker model fails to account for the sigmoidal shape of the experimental fatigue crack growth data. Thus, a set of $[C_i, m_i]$ constants has to be used for the description of the complete fatigue crack growth curve.

Application of the Paris (2.1), Forman (2.8) or Walker (2.9) material model for fatigue life analysis under constant amplitude loading is straightforward. After the initial crack size, a_0, is set, the cycle-by-cycle crack growth analysis can be initiated and carried out till the crack reaches its final size a_N. Diagram 2.6 shows the series of steps required to estimate the current crack growth increment Δa_i induced by a given loading cycle. The first step (#1 from Figure 2.6) requires estimation of the stress intensity factor range using the ready-made solution approach (2.4) or the weight-function method (2.7) for the current crack length a_i and the applied loading cycle. In the second step (#2 from Figure 2.6) selected material fatigue crack growth model combined with appropriate $[C_i, m_i]$ parameters is used to estimate the crack growth increment Δa_i. Finally, in the last step (#3 from Figure 2.6) of the fatigue crack growth analysis, the new crack length $a_i = a_i + \Delta a_i$ is checked against the final crack length a_f and corresponding cycle count is updated $N = N + 1$.

The described above cycle-by-cycle algorithm relies on the experimental fatigue crack growth data. Such data in turn can obtained at different stress ratios, R. The "*Paris law*" doesn't have means to account for the spread of fatigue crack growth data. Therefore, in

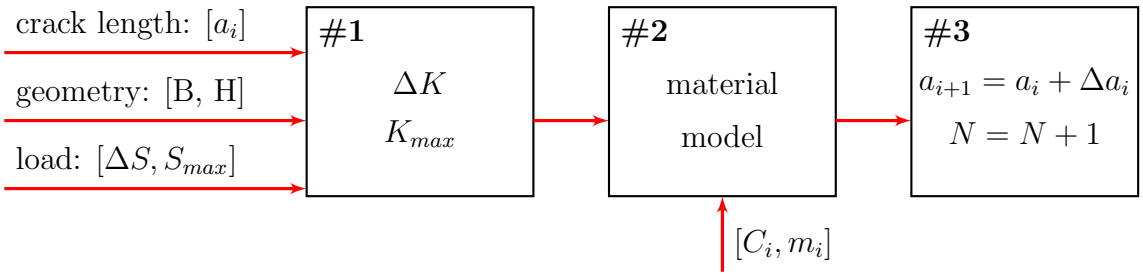

Figure 2.6: Cycle-by-cycle analysis of the fatigue crack growth

order to predict the fatigue life of component subjected to the cyclic constant amplitude load of stress ratio, $R = 0.2$, the experimental fatigue crack growth data obtained at the same R is required. The Forman and Walker laws, in turn are only partially able to collapse fatigue crack growth data obtained at different R ratios and the quality of the "*collapse*" changes with the da/dN level. Therefore, another approach for explanation of the R ratio effect was needed.

It is widely accepted at present that the plastically deformed material left in the wake of a propagating crack distorts the fatigue crack growth rate but Elber was the first to point it out. In the paper on "*The Significance of Fatigue Crack Closure*" [26] Elber has presented the measurements of the strain displacements in the wake of a crack tip in the compact tension specimen under cyclic loading (see Figure 2.7a) and argued that the non-linearity of the stress-displacement path from points **B** to **C** (see Figure 2.7b) "*can be explained by crack closure only*". Assuming that the crack tip partially remains closed even under the fully tensile applied loading cycle, Elber proposed to use the effective stress intensity factor range, ΔK_{eff}, based on the range between maximum applied, S_{max} and opening stress , S_{op} (2.10).

$$\Delta K_{eff} = (S_{max} - S_o)\sqrt{\pi a}F \tag{2.10}$$

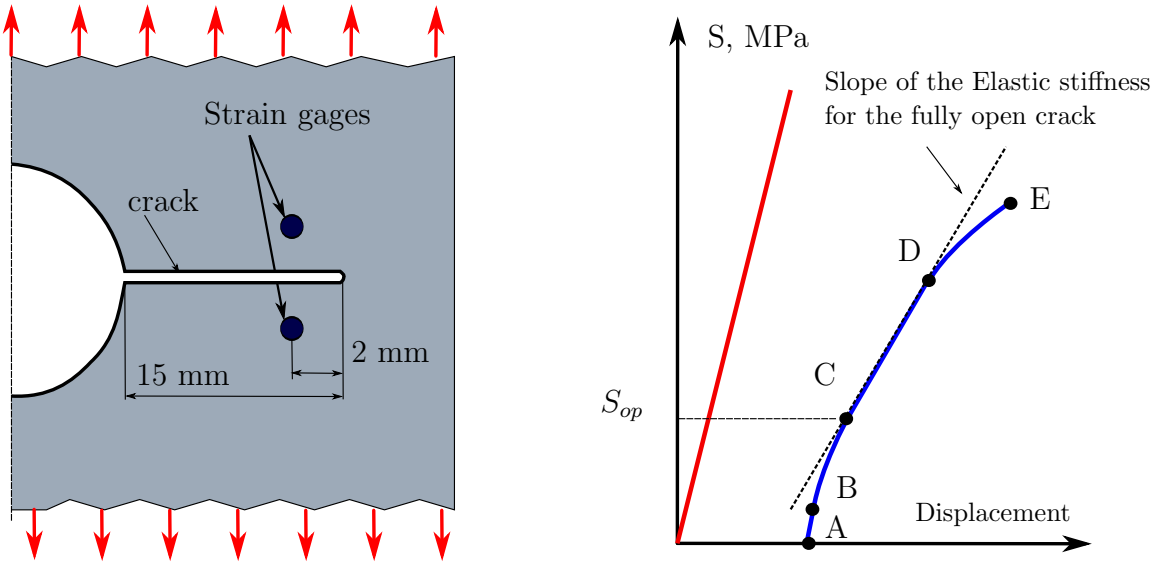

(a) Strain displacement measurement

(b) Stress vs. displacement

Figure 2.7: The crack tip closure concept according to Elber [26].

Therefore, the fatigue crack growth law, proposed by Elber has the form:

$$\frac{da}{dN} = C\left(\Delta K_{eff}\right)^m \tag{2.11}$$

Unfortunately it is impossible to estimate the opening stress, S_{op}, for the large variety of loading and geometry configurations encountered in practice. That is why, Elber has proposed [26] an empirical relationship for determining the effective stress intensity factor range, ΔK_{eff} :

$$\Delta K_{eff} = U \cdot \Delta K \tag{2.12}$$

For the Al 2024-T3 aluminum alloy, the crack tip closure parameter U was empirically correlated to the stress ratio R as:

$$\Delta K_{eff} = (0.5 + 0.4R) \cdot \Delta K \tag{2.13}$$

It was argued later that the crack closure has three distinct regions in the da/dN range [27]. This led to the conclusion that equation (2.13) was inadequate and parameter U could not be formulated in terms of only the R ratio parameter. For this reason Newman have proposed [28] to modify the Forman law (2.8) by taking into account the effective stress in a different way:

$$\frac{da}{dN} = C_1 \left(\Delta K_{eff}\right)^{C_2} \left[\frac{1 - \left(\frac{\Delta K_o}{\Delta K_{eff}}\right)^2}{1 - \left(\frac{K_{max}}{C_5}\right)^2}\right] \tag{2.14}$$

where

$$\Delta K_o = C_2 \left(1 + C_4 \frac{S_o}{S_{max}}\right) \tag{2.15}$$

Equation (2.15) has gone in time through a series of modification and now it is referred to as NASGRO equation [29] given in the form of:

$$\frac{da}{dN} = C \left(\frac{1 - S_o/S_{max}}{1 - R} \Delta K\right)^n \frac{\left(1 - \frac{\Delta K_{th}}{\Delta K}\right)^p}{\left(1 - \frac{K_{max}}{K_c}\right)^q} \tag{2.16}$$

While Newman has used the Forman law (2.8) as a basis for further modifications and fatigue crack growth analysis, many other researchers decided to use the original Walker approach [24]. Donald and Paris [30] were the first to combine the two-parameter fatigue crack growth material model obtained by Walker with the crack closure concept. The out-

come of their proposal was the normalized stress intensity factor (2.17) which theoretically was also supposed to account for the R ratio effect (2.18).

$$\Delta K_{norm} = \Delta K_{eff}^{(1-n)} K_{max}^{n} \tag{2.17}$$

$$\frac{da}{dN} = C\left(\Delta K_{norm}\right)^{m} \tag{2.18}$$

Another modification to the Walker law was suggested by Kujawski [31]. Instead of using the crack closure concept, Kujawski has proposed to use the total driving force in a form of the geometric mean of the positive stress intensity factor range and the maximum stress intensity factor $\left(\Delta K^{+} K_{max}\right)^{0.5}$. This model was later generalized to the form (2.19):

$$K^{*} = K_{max}^{\alpha}\left(\Delta K^{+}\right)^{1-\alpha} \tag{2.19}$$

By using only the positive part of the stress intensity factor range ΔK^{+} Kujawski managed to show a reasonable correlation of the load ratio effect on fatigue crack growth in a variety of aluminum alloys [32]

The UniGrow total driving force

The two parameter total driving force, $\Delta\kappa$, used in the UniGrow model is also similar to Walker's parameter. Glinka and Noroozi have argued [1] that since the strain-life method and fatigue crack growth analysis describe the same phenomenon, then it should be possible to derive the fatigue crack growth law based on the strain-life relationship (2.20) proposed by Manson and Coffin [33]. Glinka and Noroozi have postulated that the crack tip geometry can be approximated by the finite radius ρ^{*} and that the material surrounding it can be modeled as a set of material blocks of the same size (see Figure 2.8).

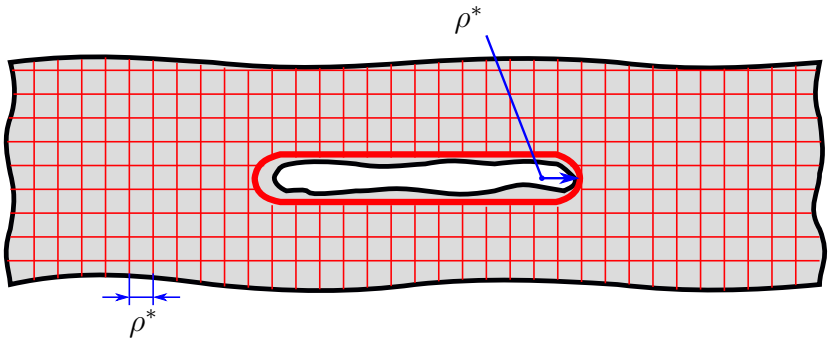

Figure 2.8: The crack model according to the UniGrow model

Fatigue crack growth rate da/dN was first related to the average number of cycles required to "*destroy*" such a block, ρ^*/N. Then, using the Smith-Watson-Topper damage parameter [34], the fatigue crack growth relationship in the form (2.21) was obtained:

$$\frac{\Delta\varepsilon}{2} = \frac{\sigma_f^{'}}{E}\left(2N\right)^b + \varepsilon_f^{'}\left(2N\right)^c \tag{2.20}$$

$$\frac{da}{dN} = \frac{\rho^*}{N} = C\left(\Delta\kappa\right)^\gamma \tag{2.21}$$

Where $\Delta\kappa$ is the total driving force (2.22) and $[C, \gamma]$ are fatigue crack growth coefficients which should be obtained from available fatigue crack growth data.

$$\Delta\kappa = \left(\Delta K + K_r\right)^{1-p}\left(K_{max} + K_r\right)^p \tag{2.22}$$

The K_r from equation (2.22) is the residual stress intensity factor. This parameter enables to account for the generated plastic deformation in the vicinity of the crack tip. The K_r can be evaluated by using the weight function method:

$$K_r = \int_0^a \sigma_r\left(x\right) m\left(x, a\right) dx \tag{2.23}$$

Where $\sigma_r(x)$ is the residual stress distribution. The exponent p in relationship (2.22) is related to the cyclic strain hardening exponent n':

$$p = \frac{n'}{n' + 1} \tag{2.24}$$

In summary, the fatigue crack growth material model chosen for the analysis will have a profound effect on the prediction of the number of cycles required for the crack to grow from the initial size a_0 to the specified final crack length a_f. The most advanced material models available today are the NASGRO (2.16), the Donald law (2.18), the relationship proposed by Kujawski (2.19) and the UniGrow total driving force $\Delta\kappa$ (2.21). What all these model have in common is that they impose some sort of plasticity corrections to the combination of the applied K_{max} and ΔK. Adjusted cycle-by-cycle fatigue crack growth analysis procedure is presented in Figure 2.9. Two differences between diagrams 2.6 and 2.9 should be noted. The first distinction is the presence of plasticity corrections. Second distinction is that the notation of the fatigue crack growth constants was changed from $[C, m]$ to $[C, \gamma]$, since the experimental fatigue crack growth data required for the analysis has to be adjusted accordingly.

2.3 State-of-the-art fatigue crack growth modeling

Application of the fatigue crack growth material model for constant amplitude loading scenarios is pretty straight-forward. Unfortunately, real stress histories often deviate from the constant amplitude loading and fatigue lives are known to be dependent on the applied loading history. The very first fatigue crack growth studies of the effect of the variable amplitude loading on the fatigue life took place in early 50's of the last century [35] and

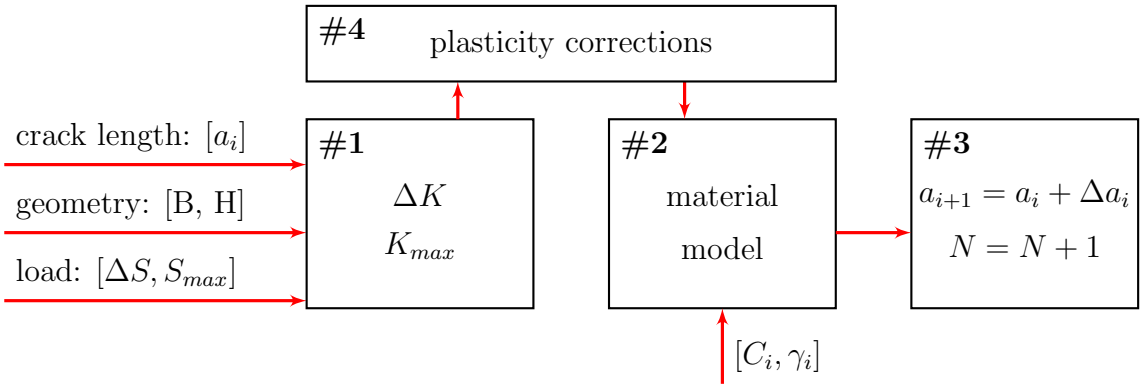

Figure 2.9: Adjusted cycle-by-cycle analysis of the fatigue crack growth

lots of experimental fatigue crack growth data has been accumulated since then. The very first tests were done to study the effect of a single overload (2.10a), underload (2.10b) or their combination (2.10c) under predominantly constant amplitude loading history.

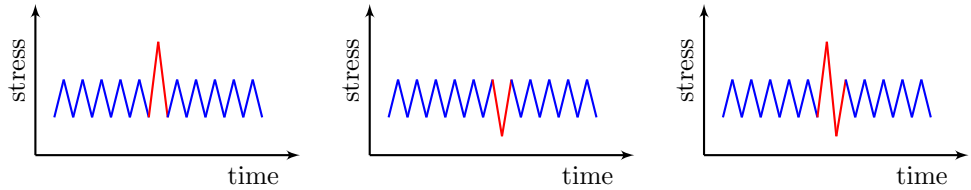

Figure 2.10: (a) Single overload, (b) single underload and (c) their combination.

The following trends were observed while studying the effects of single overloads and underloads on a predominantly constant loading history:

- Application of a single or repeated positive overloads led to increase in fatigue life when compared to the life of only constant amplitude loading. [35].
- Single or repeated underloads applied to the predominantly constant amplitude loading history had no significant effect on the final fatigue life of a structure [3]

- Underload applied immediately after the overload diminishes the beneficial effect of a single overload [36]

Expected loading histories in real machines are supposedly random and thus has to be approximated in advance. For aerospace applications a variety of flight-simulation spectra are known (such as FALSTAFF, TWIST, TURBISTAN, P3, etc. [37]). In case of ground vehicles, expected terrain profiles are usually transformed into loading sequences. As an example, part of aircraft flight spectrum loading is shown in Figure 2.11.

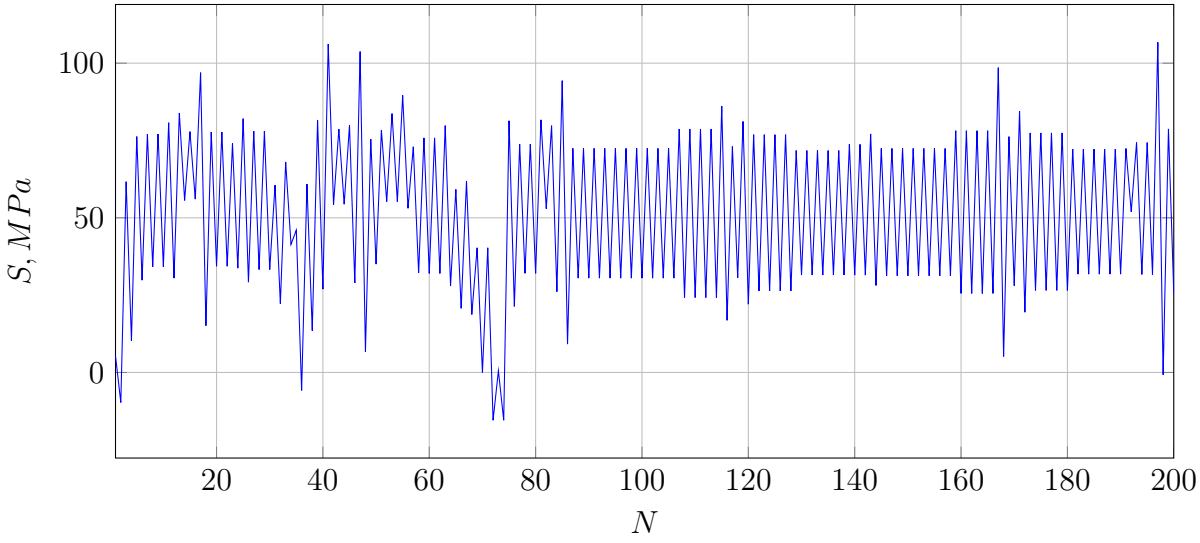

Figure 2.11: Excerpt from the P3 loading spectra.

No matter how complicated the loading sequence is, the fatigue life can be approximately predicted by a computational model capable of accounting for the effect of single overloads and underloads. To verify that hypothesis, a variety of loading sequences have been tested in previous years and experimental data obtained by McMillan and Pelloux for Al 2024-T3 [38] might be of particular interest.

2.3.1 The Willenborg and Wheeler model

The main concepts used to explain the retardation and acceleration effects imposed by loading spectra on the fatigue crack growth are: the crack tip plasticity, the plasticity induced crack closure and residual stresses. Crack tip plasticity models were introduced at the beginning of the 1970s by Wheeler [39] and Willenborg [40] and they are still used today in software packages like AFGROW [41]. The explanation of the retardation effect according to those models is as follows. A single overload in a predominantly constant amplitude loading sequence produces larger plasticity zone ahead of the crack tip, than basic constant amplitude fluctuations. This phenomenon causes the growth rate of the crack to decrease (see Figure 2.12) after application of the overload.

In order to account for the temporary increase of the plastic zone ahead of a crack tip, Wheeler has proposed to use the C_p correction factor (2.25) in the cycle-by-cycle analysis (2.26) of the crack growth.

$$C_p = \left(\frac{R_y}{a_p - a} \right)^m \tag{2.25}$$

$$a_r = a_0 + \sum_{i=1}^{r} C_{pi} f\left(\Delta K_i\right) \tag{2.26}$$

Parameter m in equation (2.25) is the shaping exponent which has to be found from the experimental constant amplitude loading fatigue crack growth data with single overloads. This poses an obvious challenge: the amount of required experimental data necessary for further fatigue crack growth analysis becomes very extensive, i.e. impractical in reality to obtain.

Willenborg argued [40] that the effective stress range influencing fatigue crack growth is reduced due to a larger plasticity zone generated by the overload. Therefore, it can be used to model the retardation phenomenon. The retardation factor, analogous to C_p, is determined from the difference between the position of the plastic zone boundary coming from the currently generated overload and the previous cycle. After the calculated effective stress is found, it can be used in conjunction with the Forman law (2.8) or other material fatigue crack growth model. The main disadvantage of all models based on the crack tip plasticity effect is that they are not capable of explaining the underload effect, thus they have a very limited application range and might give non-conservative predictions for loading histories with multiple underloads.

2.3.2 The crack tip closure based fatigue crack growth model

Even though the crack closure concept was questioned by many researchers [42, 43], it is still being widely used to explain variable amplitude loading effects. The most advanced model based on the crack closure considerations is FASTRAN [44] and it has been developed by Newman while working at NASA/Langley research center [45]. The FASTRAN model is schematically illustrated in Figure 2.13. Three zones can be distinguished in the crack tip neighborhood:

- The wake of the crack without stresses (Zone 1)
- The plastically yielded region of the crack tip of size ρ (Zone 2)
- The elastic continuum with a present crack of size $a + \rho$ (Zone 3)

The first and second zones consists of perfectly rigid plastic bar elements and the third zone is regarded as linear elastic region. It is important to note that under any applied stress, the bar elements can be in one of the two states: broken or intact.

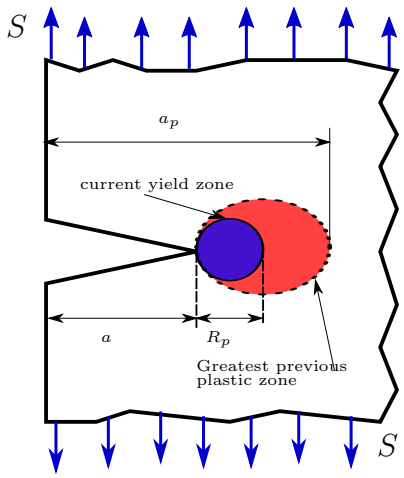

Figure 2.12: Crack tip yield zones due to overload.

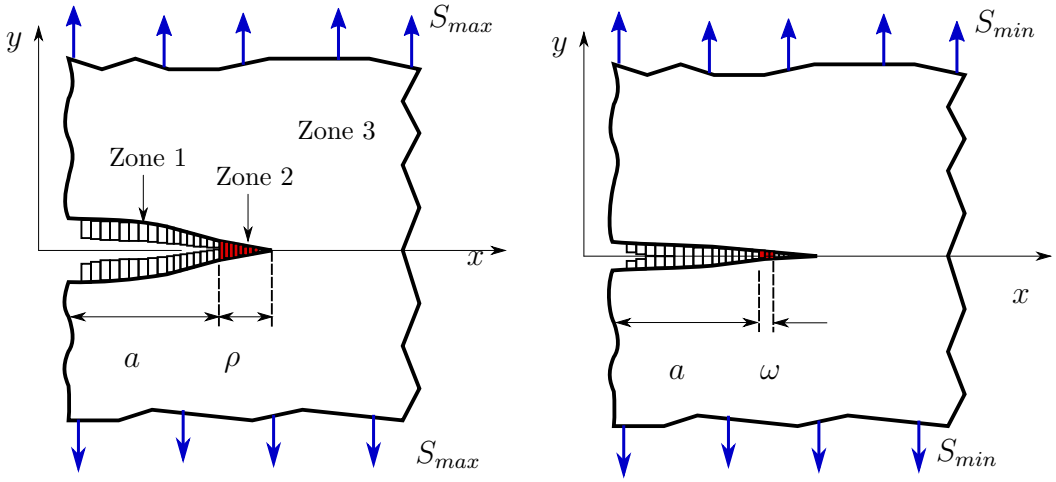

(a) Maximum stress

(b) Minimum stress

Figure 2.13: The Newman crack tip closure module based on a Dugdale yield-strip concept [28].

The main goal of the crack closure model is to determine the opening stresses level resulting from the applied load. The estimation of the opening stress level is based on the modified Dugdale strip-yield model [46]. The essence of the adjustment proposed by Newman [28] is as follows: the plastically deformed material is left in the wake of the propagating crack, which leads to impediment of the growth of the crack. The set of equations required to calculate the opening stress level, S_{op}, for the positive (2.27) and negative (2.28) R ratios are presented in (2.27) and (2.28).

For $R \geq 0$

$$\frac{S_o}{S_{max}} = A_0 + A_1 R + A_2 R^2 + A_3 R^3 \tag{2.27}$$

For $-1 \leq R < 0$

$$\frac{S_o}{S_{max}} = A_0 + A_1 R \tag{2.28}$$

where the coefficients are:

$$\begin{aligned} A_0 &= \left(0.825 - 0.34\alpha 0.05 + \alpha^2\right) \left[\cos \frac{\pi S_{max}}{2\sigma_o}\right]^{1/\alpha} \\ A_1 &= \left(0.415 - 0.071\alpha\right) S_{max}/\sigma_o \\ A_2 &= 1 - A_0 - A_1 - A_3 \\ A_3 &= 2A_0 + A_1 - 1 \end{aligned} \tag{2.29}$$

The solution of equations (2.27) and (2.28) requires introduction of the accommodating "*constraint parameter,* α". This parameter [28] is supposed to simulate plane-stress or plane-strain conditions and it ranges from 1 to 3. It is also worth mentioning that expression (2.27) is empirical and it applies mostly to aluminum alloys.

When the procedure to estimate the opening stress level is established, it is important to setup the cycle-by-cycle analysis procedure. The FASTRAN model approximates the

extension of the crack by an incremental value calculated at the highest applied stress level from a block of 300 cycles, which is an empirically chosen number. The crack increment is then arbitrarily set to be equal to:

$$\Delta a^* = 0.05\rho^{max} \tag{2.30}$$

where the ρ^{max} is the plastic zone size caused by the maximum applied stress. The estimated opening stress level is held constant while the crack is growing under the cyclic loading over the length Δa^*. The number of cycles to generate the crack increment Δa is calculated then with the NASGRO equation (2.16). When the sum of those crack growth increments reaches Δa^*, the analytical crack closure model is executed. If the increment of the number of loading cycles reaches $\Delta N = 300$, the crack closure model is invoked regardless whether or not the total crack increment Δa^* was reached. Main steps of this analysis can be summarized as follows:

1. Apply the minimum and maximum stress, (S_{min} and S_{max}) at crack length of "a"
2. Extend the crack length by the increment, Δa^* (2.30) and calculate the corresponding number of cycles ΔN (2.16)
3. Apply the current minimum stress S_{min} at $a + \Delta a^*$ and calculate the opening stress level, S_o
4. Re-calculate the crack growth increment Δa^*
5. Repeat steps 1-5 while the crack size is less than $a + \Delta a^*$ or the number of cycles of applied load ΔN is less than 300 cycles

These steps are repeated till the crack reaches the prescribed final crack length. The drawback of the FASTRAN model is that obtained results will depend on the arbitrary assumed 300 cycles interval.

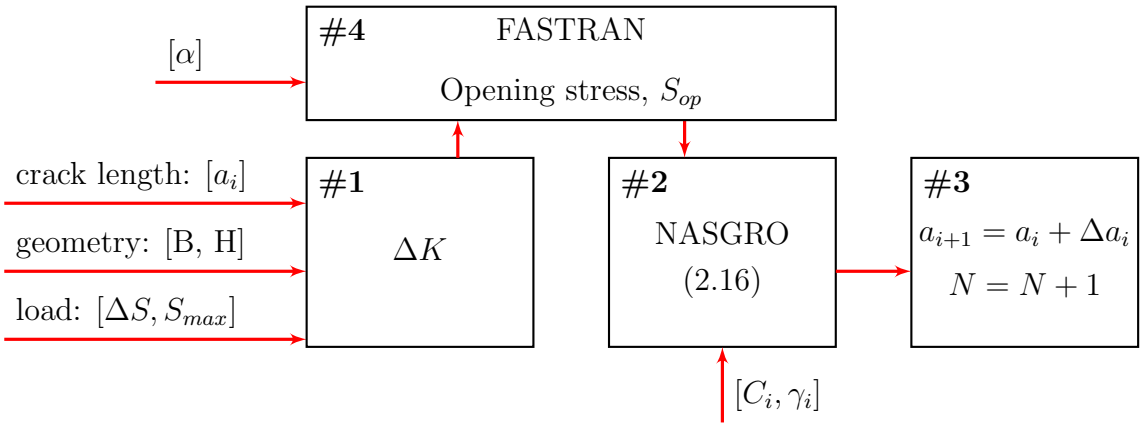

Figure 2.14: Advanced crack tip closure-based cycle-by-cycle analysis of fatigue crack growth.

In addition to the above mentioned AFGROW and FASTRAN software packages, the NASGRO software package [29] is also currently available as a standalone program for fatigue crack growth analyses. While there are minor technical differences in implementation, conceptually none of those software packages are significantly different. The most advanced closure based setup for the cycle-by-cycle fatigue crack growth analysis is presented in Figure 2.14. This diagram features the FASTRAN [44] model for plasticity corrections and NASGRO (2.16) material model.

2.3.3 The UniGrow fatigue crack growth model

The UniGrow fatigue crack growth model developed partially earlier is an advanced software package which uses the total driving force $\Delta\kappa$ and a set of memory rules accounting

for the loading sequence effects. A schematic illustration of how the crack growth increment Δa_i is being calculated by the UniGrow model is shown in the Figure 2.15.

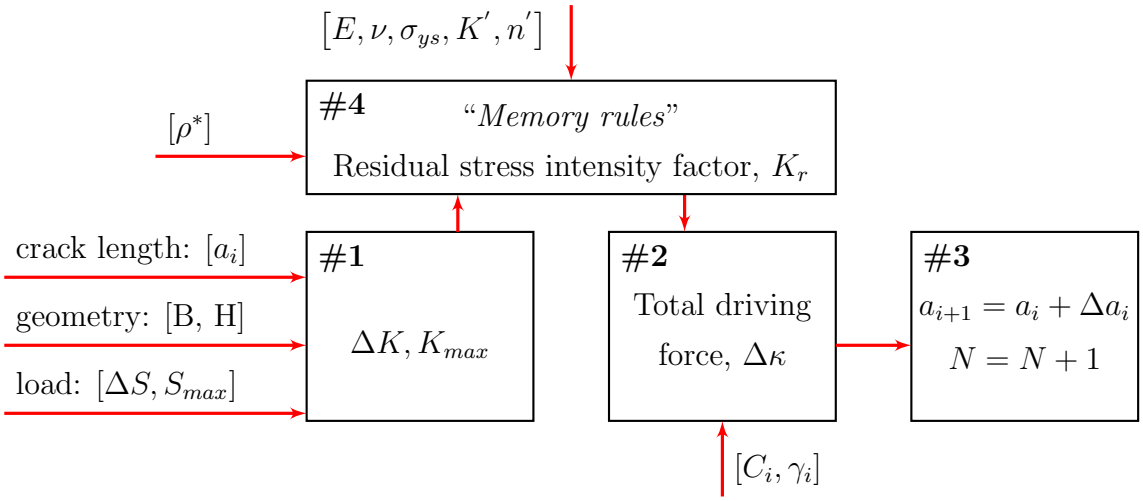

Figure 2.15: Cycle-by-cycle analysis of fatigue crack growth based on the UniGrow model.

Contrary to the crack tip closure-based fatigue crack growth models, the UniGrow model uses the residual stress distribution created around the crack tip (**#4** from 2.15). The plastically deformed region left in the crack tip zone according to the UniGrow model needs to be transformed into the residual stress intensity factor K_r. This parameter is then used to calculate the total driving force, $\Delta\kappa$ (2.22) which subsequently is related to the fatigue crack growth rate da/dN as per (2.21).

The detailed description of memory rules was given by Mikheevskiy in reference [47]. Therefore, only a short descriptive example is presented here. Let's consider a model of a "*virgin*" crack in a complex body (see Figure 2.16a) subjected to a variable amplitude loading (as shown in Figure 2.16b). Suppose that the applied loading sequence is given in the form of the stress intensity factor, K_i, so the step #1 from diagram 2.15 can be omitted. Let's put an axis defined as $\mathbf{x}$ with a starting point at the origin of the crack

(if the crack is symmetrical it is then at the center). Changes in the stress profile in the vicinity of the crack tip invoked by the cyclic loading are of special interest and the stress distribution along the **x** axis in particular.

The very first step is to increase the applied load from 0 to K_2 (see Figure 2.17b). This applied tensile load reversal produces the crack increment Δa_0 and generates the stress distribution shown in Figure 2.17a. Since it was assumed that the crack was "*virgin*", residual stresses ahead of the crack tip are absent, thus $K_r = 0$ during the load reversal from 0 to K_2. The applied stress intensity factor range is evaluated as $\Delta K = K_2 - 0 = K_2$ and maximum applied stress intensity factor, K_{max} is obviously equal to K_2. Therefore, the crack growth increment can be estimated as $\Delta a_0 = C\left[(K_2)^p (K_2)^{1-p}\right]^\gamma$ where C and γ are fatigue crack growth material parameters.

The UniGrow model assumes that crack propagates during the increasing load reversal and creates a residual stress zone after unloading. Therefore, once the crack has propagated from a_0 to $a_1 = a_0 + \Delta a_0$, the drop in the applied load from K_2 to K_1 (see 2.18b) results in the residual stress profile, as presented in Figure 2.18a.

The first memory rule states that integration region for calculation of the residual stress intensity factor K_r is bounded by the distance X_f. The X_f was defined by Mikheevskiy [47] as an interval from the crack tip to the point where the residual stress σ_r from given cycle becomes equal to 0. Respectively, the residual stress profile (see Figure 2.18a) has to be remembered until the crack reaches the length $a = a_0 + \Delta a_0 + X_{f,1}$ and coordinates of point **A** are to be stored in the memory.

The next step is the application of the second loading cycle ($K_1 - K_3 - K_1$ as depicted in Figure 2.19b). The ascending reversal of the loading cycle (K_1 to K_3) leads to increase of the crack length by the increment Δa_1. Since the residual stress distribution in the vicinity

of the crack tip (i.e. from 0 to a_1 is still absent, the residual stress intensity factor K_r is equal to zero and $\Delta a_1 = C\left[(K_3 - K_1)^p (K_3)^{1-p}\right]^\gamma$.

The unloading portion of the cycle (from K_3 to K_1) produces the residual stress distribution presented in Figure 2.19a. The second memory rule states that if the next loading cycle produces residual stress distribution partially or completely outside of the previous one, then the residual stress distributions should be combined. Therefore, coordinates of the intersection point **B** and coordinates of point **C**, where the maximum residual stress occurs (Figure 2.19a) should be stored in the memory for further analysis.

The third applied cycle ($K_1 \rightarrow K_2 \rightarrow K_1$, Figure 2.20b) is the last one to be considered in this example. At first, the fatigue crack growth increment Δa_2 generated by current reversal needs to be estimated. This time, in order to calculate the current crack growth increment, the residual stress distribution left in the wake of the crack tip has to be translated into the residual stress intensity factor, K_r (2.23). The residual stress profile from 0 to a_2 can be represented by two parts. The first part, where the residual stress $\sigma_r = 0$ goes from 0 to A^* (Figure 2.20a). The second part is where the residual stress σ_r follows the path $A - B$. The total area for integration is shown as filled in Figure 2.20a for clarity. The integration procedure [16] is used to estimate the residual stress intensity factor $K_{r,A-B}$. As a result, $\Delta a_2 = C\left[(K_2 - K_1 + K_{r,A-B})^p (K_3 + K_{r,A-B})^{1-p}\right]^\gamma$.

The residual stress profile estimated for the unloading portion of the third cycle happens to be fully inside of previous residual stress profiles which leads to the use of the third memory rule which states that such distributions are supposed to be forgotten. Therefore, only coordinates of point **D** (Figure 2.20a) should be stored in the memory. This concludes a brief summary of how the memory rules proposed by Mikheevskiy [47] are used to impose plasticity corrections on fatigue crack growth in the UniGrow model.

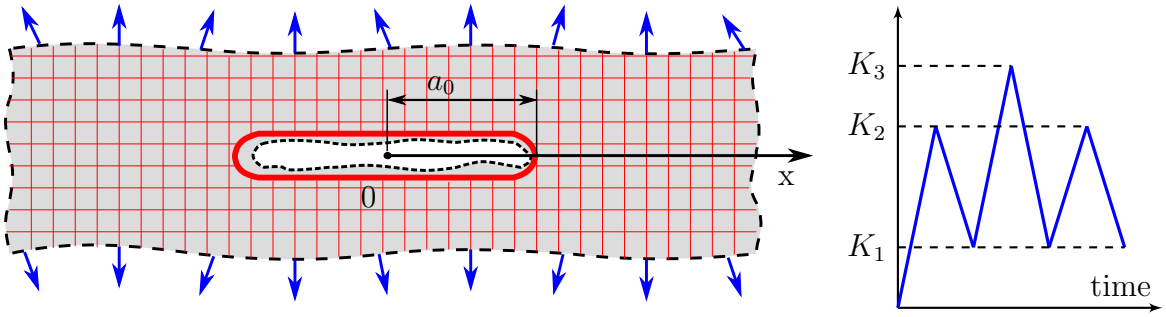

(a) Cracked body (b) Loading history

Figure 2.16: Model of the "*virgin*" crack in a complex body.

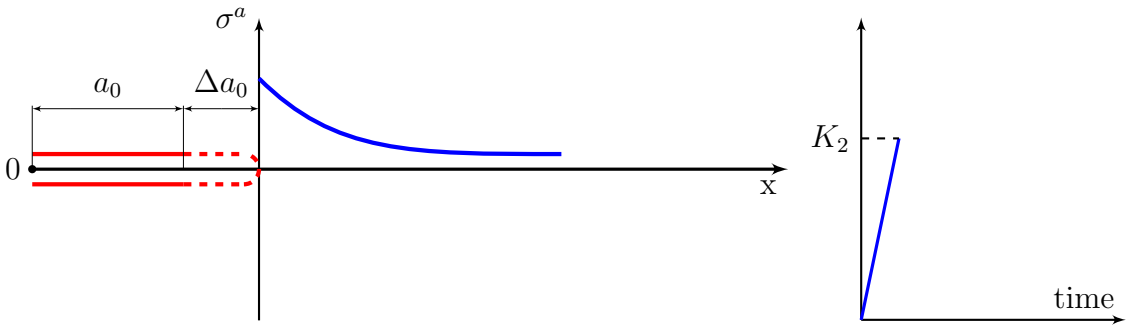

(a) (b)

Figure 2.17: Crack progression according to the UniGrow model: the first step.

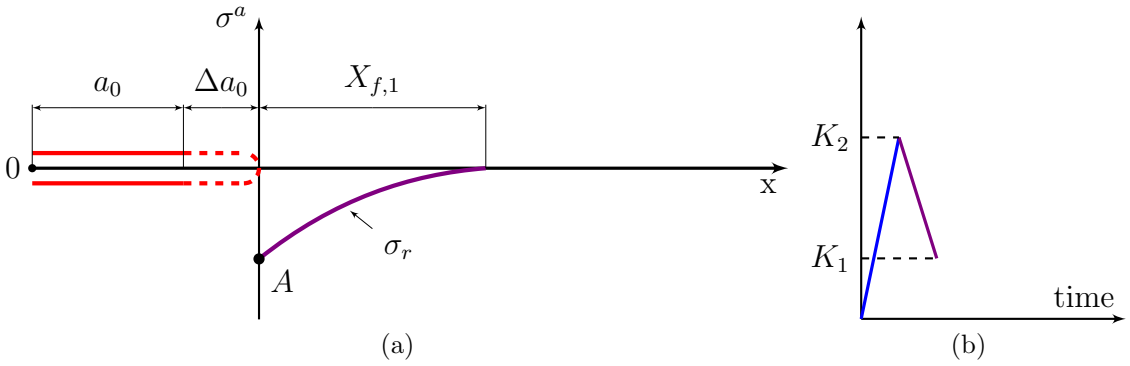

(a) (b)

Figure 2.18: Crack progression according to the UniGrow model: the second step.

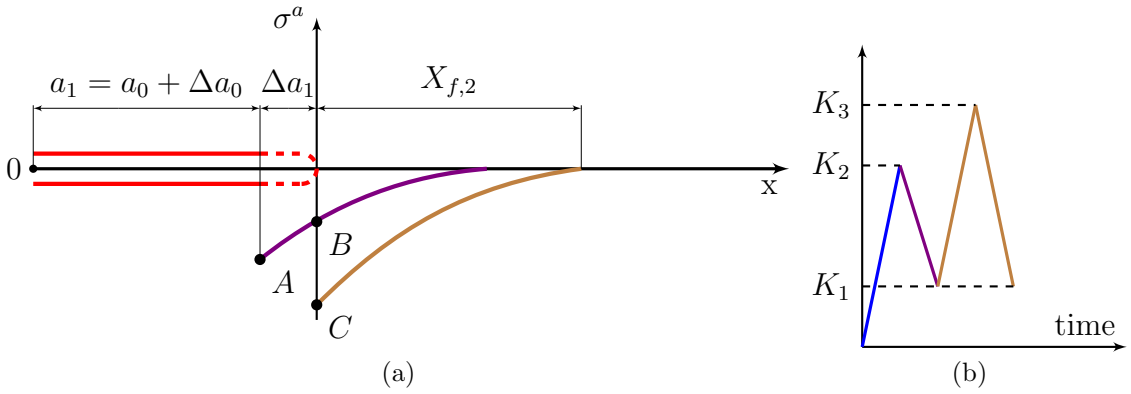

Figure 2.19: Crack progression according to the UniGrow model: the third step.

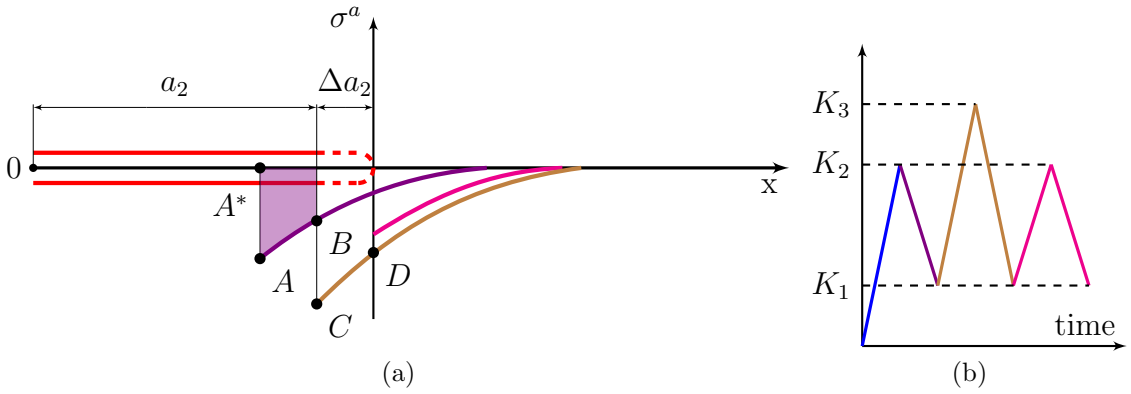

Figure 2.20: Crack progression according to the UniGrow model: the fourth step.

It should be noted that such implementation of the model is impossible without sufficiently accurate estimation of residual stresses. The solution to this problem can be split into two steps. In the first step, the distribution of the elastic stress components ahead of the crack tip $\sigma_x^{el}(x)$, $\sigma_y^{el}(x)$ and $\tau_{xy}^{el}(x)$ need to be obtained from the Creager-Paris solution [11] for given stress intensity factor and the crack tip radius, ρ^*. The second step is the estimation of actual elastic-plastic strains and stresses $\sigma_x^a(x)$, $\sigma_y^a(x)$ and $\tau_{xy}^a(x)$. Mikheevskiy has stated [47] that this can be done by using the multiaxial Neuber [48] or ESED [49] method assuming a plane-stress or plane-strain state around the crack tip.

Accordingly, four methods to obtain the actual stress distribution ahead of a crack tip are possible, but only the Neuber rule for cracked bodies under plane-stress has been used so far. Therefore, a more generalized solution involving the four methods and their effect on the predicted fatigue crack growth is of great interest.

Finally, it has to be remembered that a set of fatigue crack growth parameters $[C_i, \gamma_i]$ for the UniGrow model reflects the correlation between the fatigue crack growth rate, da/dN and the total driving force, $\Delta\kappa$, rather than the stress intensity factor range,ΔK. Therefore, before any fatigue crack growth analysis based on the UniGrow model can be undertaken, a set of standard experimental fatigue crack growth data, $[\Delta K_i, (da/dN)_i]$ has to be transformed into the $[\Delta\kappa_i, (da/dN)_i]$ format. The purpose of the transformation is the derivation of the master $da/dN - \Delta\kappa$ material curve valid for all possible stress ratios R. Examples of such transformation for Al 2024-T3 aluminum alloy is presented in Figure 2.21. More details on how to perform the transformation will be discussed in following chapters.

2.4 Random nature of the fatigue crack growth

The scatter of the material fatigue resistance to cyclically applied loads is often the reason for differences between deterministically predicted fatigue lives and those observed in service [50]. Those differences can be sometimes very large regardless of the fatigue life prediction method and are often attributed without justification to imperfections of fatigue crack growth models. While none of the models described above are able to account for the discrepancies caused by the random nature of fatigue crack growth, several approaches aimed at the quantification of this phenomenon exist [51].

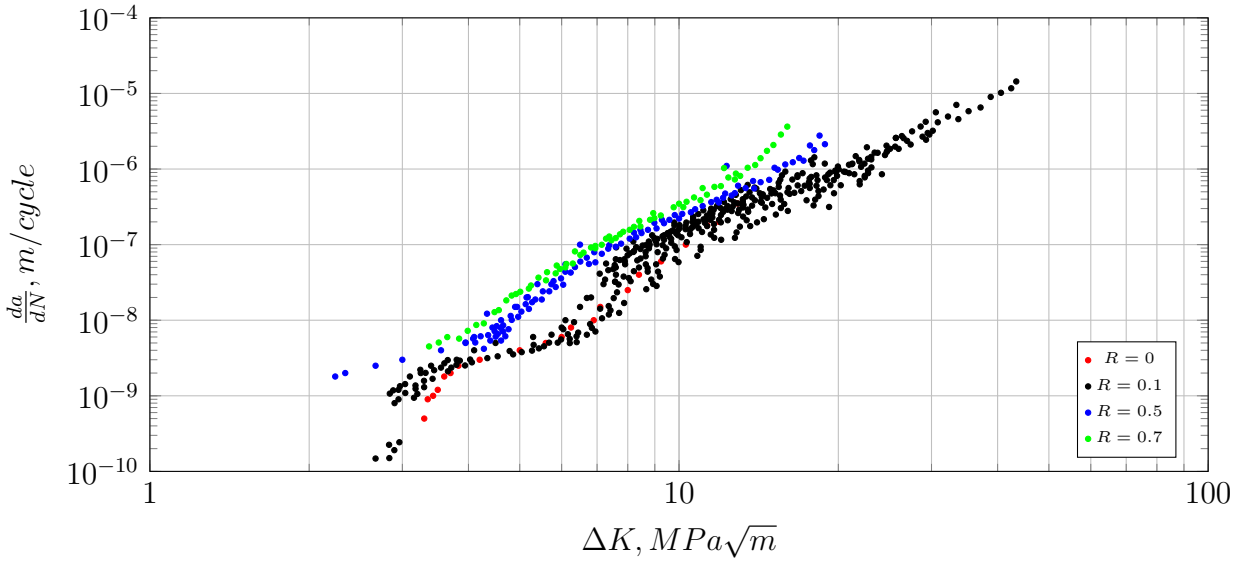

(a)

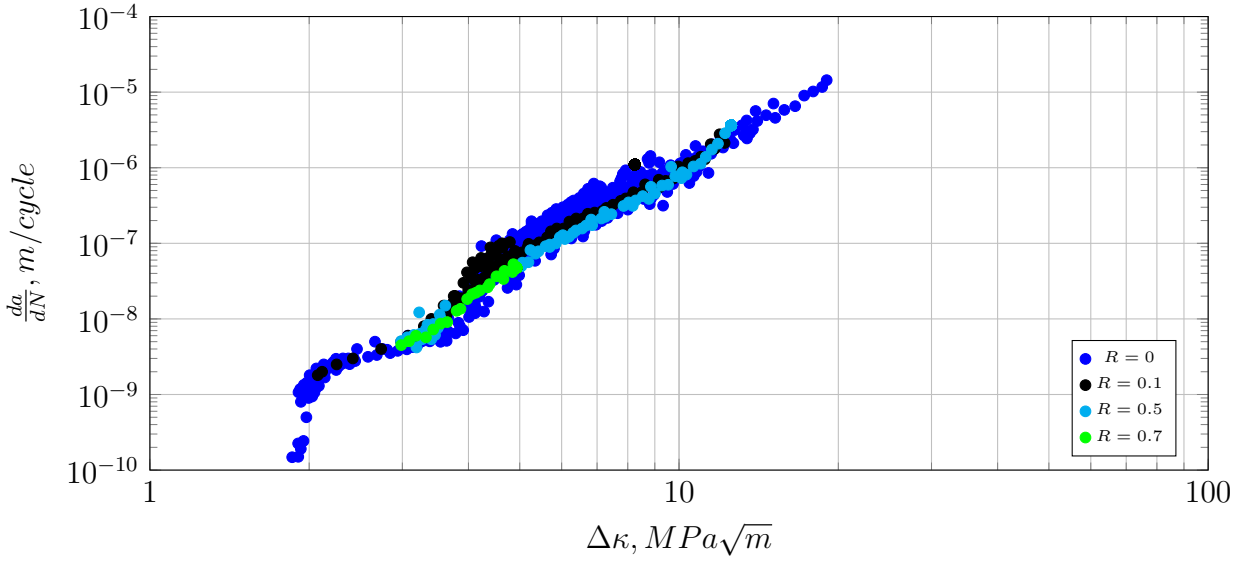

(b)

Figure 2.21: Example of fatigue crack growth data transformed from $[\Delta K, da/dN]$ to $[\Delta\kappa, da/dN]$ form for the Al 2024-T3 aluminum alloy [25].

2.4.1 Uncertainty of material properties

Randomness inherent to the fatigue crack growth process can be classified into the scatter "*within the specimen*" and the "*specimen to specimen*" scatter. For brevity they will be referred to as *intraspecimen* and *interspecimen* variability. The former comes from non-homogeneity of the material within a single machine component or specimen and can be quantified as the measure of the spread around the smooth, i.e. "*ideal*", (N_i, a_i) curve. Intraspecimen variability is a measure of randomness of a single fatigue crack growth experiment.

Interspecimen variability on the other hand is the reason why two identical fatigue crack growth experiments performed on specimens made of the same material might result in significantly different fatigue lives. This scatter comes from the inherent variability of the manufacturing process. In order to quantify this scatter, significant amount of fatigue crack growth experiments in the controlled environment were needed. Virkler [4] in 1978 took 68 identical specimen made of Al 2024-T3 aluminum alloy and carried out a series of fatigue crack growth experiments. While on average it took 270×10^3 cycles to propagate the crack from 9 to 49.8 mm in the middle-tension specimen (Figure 2.22a), the experimental span of obtained fatigue lives was $224 \times 10^3 \div 323 \times 10^3$ cycles (Figure 2.22b) obtained under the same cyclic loading history.

Let's denote a number of cycles required to propagate a crack from the initial a_0 to the final a_f crack size as N_f. It is of interest to construct all the N_f values from statistical experiment, into the corresponding probability distribution. It is also of interest to test whether distribution type of the number of cycles N_i is going to change depending on the corresponding crack size, a_i. It was hypothesized and confirmed by Virkler [4] and others [6] that the collection of N_f associated with given crack size a_i is best described

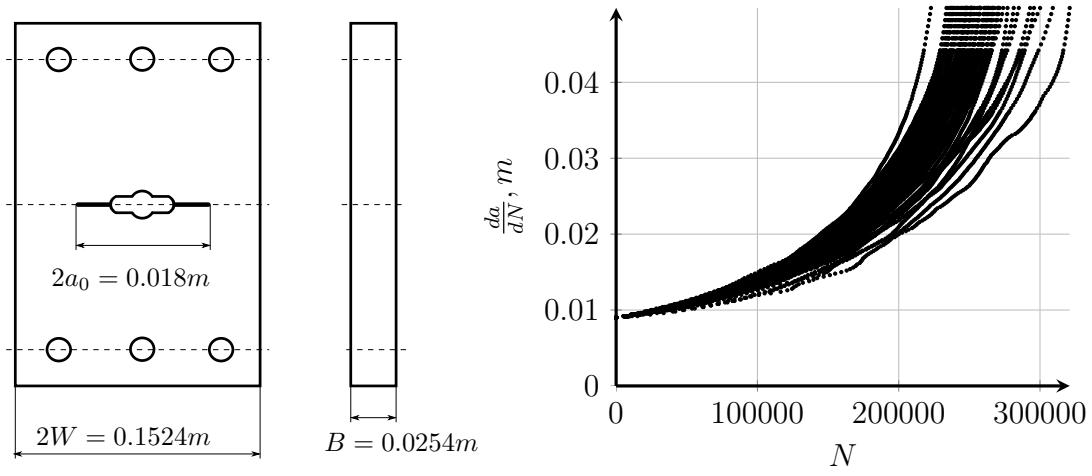

(a) (b)

Figure 2.22: (a) Geometry and (b) result of the fatigue crack growth experiments performed by Virkler [4]

by the log-normal distribution. Thus, the histogram of $ln\,(N_f)$ is supposed to follow a bell-shaped curve. In order to demonstrate it, experimental fatigue crack growth results of form (N_i, a_i) from the Virkler experiment [4] were "*cut*" as shown in the Figure 2.23 at $a_f = 0.0498m$. Resultant histogram obtained from this "*cut*" together with fitted lognormal probability density function ($\lambda = 12.45$, $\zeta = 0.066$) are shown in Figure 2.24.

2.4.2 The stochastic modeling of fatigue crack growth

Any field of science relies on the reproducibility of results. When statistically significant results can't be obtained from laboratory tests, then solely a probabilistic model might be an option. This is not the case for fatigue crack growth analysis, since intra-laboratory studies performed by ASTM committees have shown that fatigue crack growth data can be successfully reproduced by variety of laboratories.

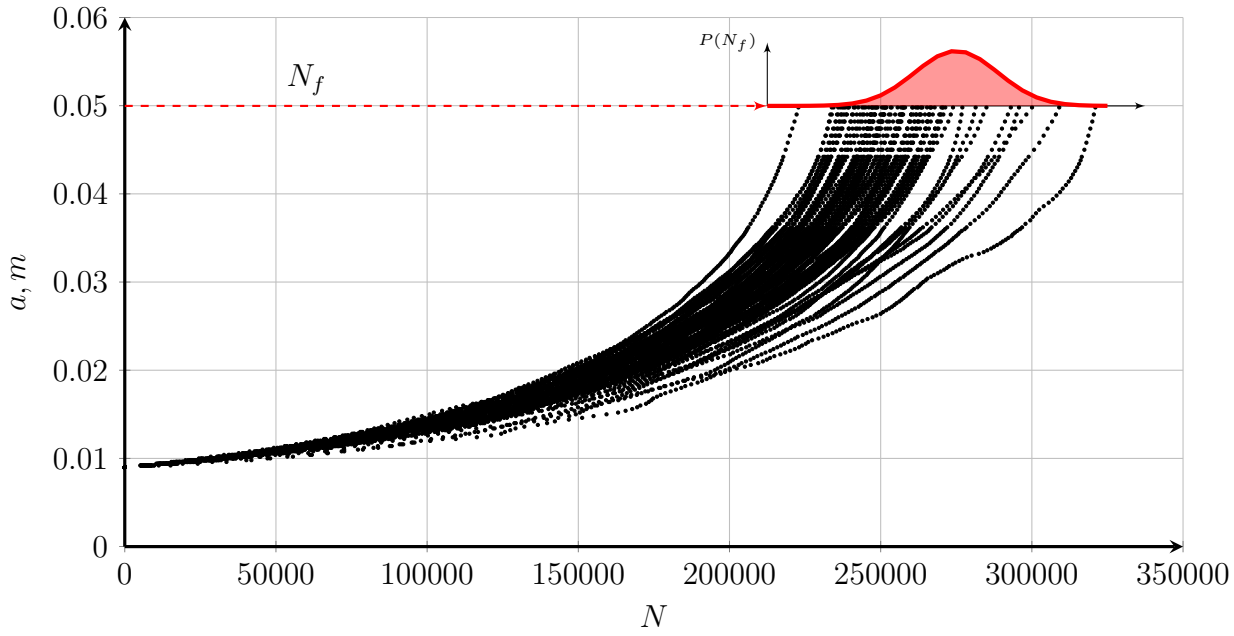

Figure 2.23: Evaluation of the Virkler experimental data [4]

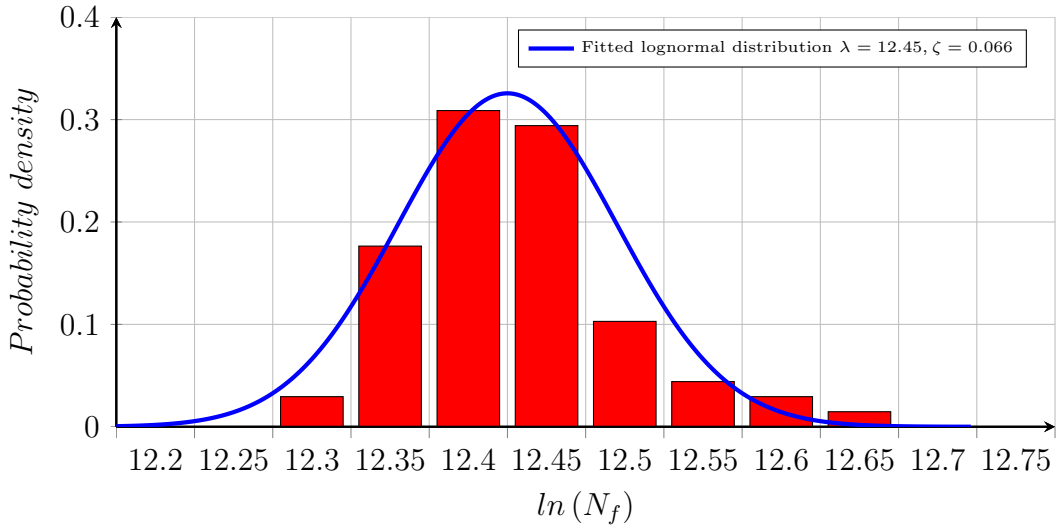

Figure 2.24: Probability density histograms obtained from the Virkler data [4].

In order to get reliability estimations, one can run a significant number of laboratory fatigue tests but such an approach is costly and time consuming. Therefore, it is common to perform a vast number of numerical fatigue crack growth experiments via computer modeling by using the "Monte-Carlo" method. Two philosophically different approaches exist. The first approach is focused on modeling the intraspecimen variability. For this purpose, propagation of the crack is treated as a single realization of a stochastic process. The second approach assumes that intraspecimen variability is negligible but every specimen has its own mean fatigue crack growth resistance. The former is labeled as a random process approach, while latter is characterized as random variable modeling.

A general random process based model, uses a deterministic fatigue crack growth rate multiplied by a chosen stochastic process and indexed by the number of loading cycles. The resulting equation in this case can be written as:

$$\frac{da}{dN} = X(N) \times f(\Delta K) \tag{2.31}$$

where $X(N)$ represents the stochastic process indexed by the number of cycles and $f(\Delta K)$ is the material model as outlined in previous section (see #2 from 2.9). Equation (2.31) is a differential one and its solution can be found from the integration of the stochastic process over the desired time interval. For that purpose, the distribution of the integral of the appropriate stochastic process has to be known or determined. Only a few closed form expressions, describing distributions of stochastic integrals exist. The Gaussian random process is one of the exceptions and that is why it is used in the model proposed by Yang [52]. Other models worth mentioning were proposed by Bogdanoff and Kozin [7], Ortiz [53] and Ghonem [6]. Unfortunately, the random process modeling approach is not always feasible due to complications with calculations of the crack size and distribution of

the number of cycles. Also, inference of the parameters from an existing limited statistical fatigue crack growth data is very complicated.

Random variable modeling is based on the introduction of uncertainty into the deterministic fatigue crack growth model by imposing the probability distribution to one or more of its dependent parameters. Those distributions have to be obtained in advance, while propagation of the crack in the medium is then considered deterministic. If intraspecimen fatigue crack growth variability can be treated as negligible, then this approach is of great value even though it may fail to capture irregularity of a single realization of the fatigue crack growth experiment. One of the advantages of the random variables approach is that it is able to account simultaneously for variability in many parameters, such as: material properties, the initial flaw size, etc. Once the probability distribution of essential input parameters are known, they have to be combined with the "Monte-Carlo" simulation method.

Chapter 3

Improvement of the UniGrow fatigue crack growth model

The state-of-the-art fatigue crack growth model is essential for reliability fatigue life analysis. While there are several models (UniGrow, FASTRAN, AFGROW, NASGRO) available to carry out the fatigue crack growth analysis, the UniGrow model is the only model which doesn't depend on a vaguely defined opening stress level. The UniGrow model has been also extensively validated on the basis of available experimental fatigue crack growth data. Therefore, it was chosen as a basis for further analysis and necessary improvements.

The UniGrow model carries cycle-by-cycle fatigue crack growth analysis as it was described in the literature review. First, the applied stress intensity factor range, ΔK has to be calculated. Since the stress intensity factor for cracks of small size can be largely underestimated, it was concluded that the UniGrow model was not able to predict behavior of short cracks. This was considered as the first item for possible improvements. The stress intensity factor range, ΔK in combination with the material block size ρ^* and the material cyclic stress-strain curve are used in the next step to calculate the actual stress distribution ahead of the crack tip and to subsequently calculate the residual stress intensity factor,

K_r. Solution to this problem can be carried out with either the Neuber or ESED method imposing the plane-strain or plane-stress condition at the crack tip. Since only the Neuber rule in combination with the plane-stress assumption has been implemented earlier, it was of great importance to derive a general solution, i.e. implement and study the effect of all possible approaches concerning the elastic-plastic stress-strain analysis near the crack tip. Successful implementation of these tasks was a prerequisite for further probabilistic fatigue crack growth analysis.

3.1 The short crack correction factor

The prediction of fatigue lives based on the fatigue crack growth analysis starts from the assumption of an initial crack-like defect. Two things should be considered here. First, initial defects which lead to the final failure are in the scale of micrometers [54]. Second, final fatigue life is highly dependent on the value of approximated initial crack size [55]. Therefore, it is of importance to define what can be considered as the smallest crack in a material. Bao-Tong for example has stated [56] that "*cracks are considered to be cracks only if they are deeper than 3μm*" but in the guidelines of the United States Air Forces, the initial crack size is assumed to be equal to 0.25 mm [57]. While there is no standardized definition of what is meant by a crack, the categorization by length proposed by Miller [58] seems to be the most appropriate one:

- microstructurally short crack, $a \approx$ grain size
- physically short cracks, $a \in 50 - 500,\ \mu m$
- long cracks, $a \geq 0.5\ mm$

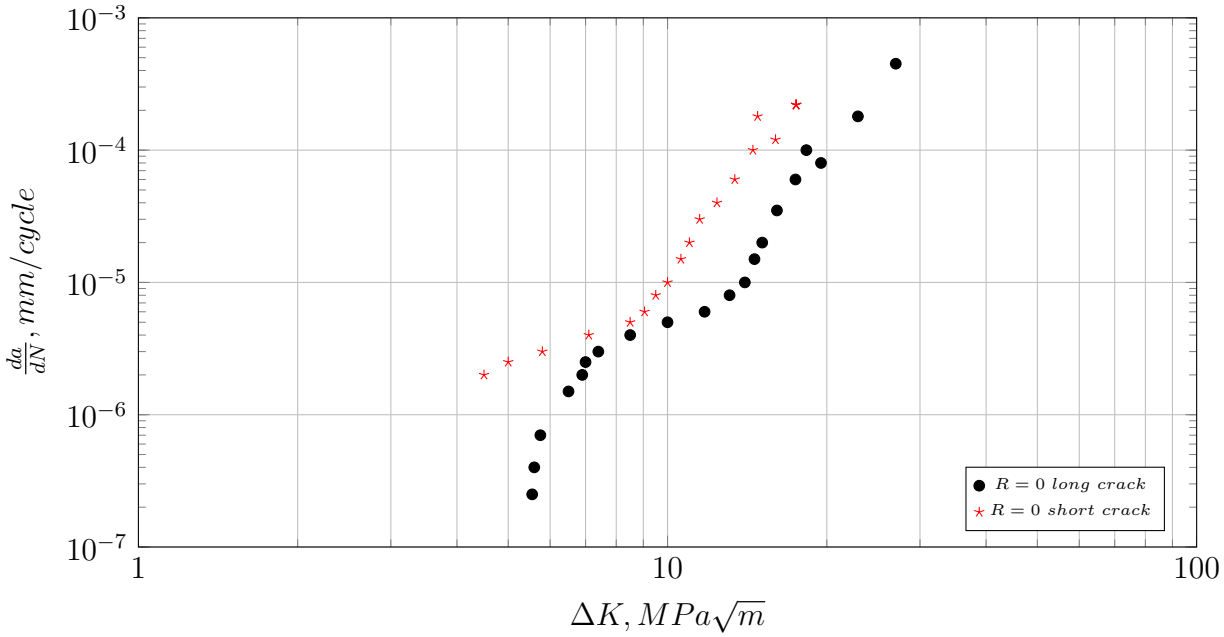

Figure 3.1: The fatigue crack growth data of short and long cracks (Al 2024-T3 aluminum alloy) [25]

The UniGrow fatigue crack growth model is theoretically limited to the crack size greater than the ρ^* parameter. However, it couldn't predict well the fatigue crack growth of cracks comparable in size with the ρ^* parameter, called as *short cracks*. This was due to fact that fatigue crack growth rates of small cracks are higher than those of a long crack (see Figure 3.1) even when subjected to the same applied stress intensity factor range, ΔK.

The short crack problem can be further broken down into two issues. First, the linear elastic fracture mechanics isn't able to quantify the behavior of small cracks. Second, small cracks are of a three dimensional nature, thus considerations concerning the stress state are very important.

In order to predict the fatigue crack growth of short cracks, models based on the crack closure concept use the data obtained from testing the fatigue crack growth of short cracks [59]. In this case, during the fatigue crack growth analysis, when a crack reaches sufficiently large size, the program used for calculations has to switch to the fatigue crack growth data obtained for long cracks data. This way, for example, the short crack phenomenon is tackled in the FASTRAN [44] software. Such an approach is complicated since it requires significant amount of extra experimental data and it depends on the accepted definition of the short crack.

The essential property of the stress intensity factor, is that it accounts simultaneously for the load and geometry effects. Thus, small cracks in combination with a high load theoretically should result in the same stress intensity factor value as long cracks with a respectively low load. Unfortunately, the stress intensity factor for cracks of a smaller size is being underestimated. That is why, applicability of the linear elastic fracture mechanics to short cracks was questioned by several researchers [25, 60]. In order to overcome this limitation, it is possible to use the different approach such as elastic-plastic fracture mechanics or to appropriately correct the stress intensity factor obtained from the linear elastic fracture mechanics solution.

It is also known, that stresses at the crack tip obtained from the Creager-Paris (2.3) solution are underestimated for small cracks and in reality stresses at the crack tip of a short crack are higher (see Figure 3.2) than in the case of long crack even if the same stress intensity factor range, ΔK is applied in both cases. This is one of several potential explanations why the crack propagation rates of short cracks are higher than those of long cracks.

In order to determine appropriate crack tip stresses, it was proposed to adjust the classical stress intensity factor for the length of the crack a relative to the crack tip radius

ρ^*. The maximum stress ahead of the crack tip (equation (2.3) for $\phi = 0, r = \rho^*/2$) can be determined from the Creager-Paris solution [11] as:

$$\sigma_{CG} = \frac{2K}{\sqrt{\pi\rho^*}} = \frac{2S\sqrt{\pi a}}{\sqrt{\pi\rho^*}} \tag{3.1}$$

The actual stress obtained by solving the classical linear elastic boundary problem of an elliptical notch ($\phi = 0, r = \rho^*/2$) is presented by equation (3.2).

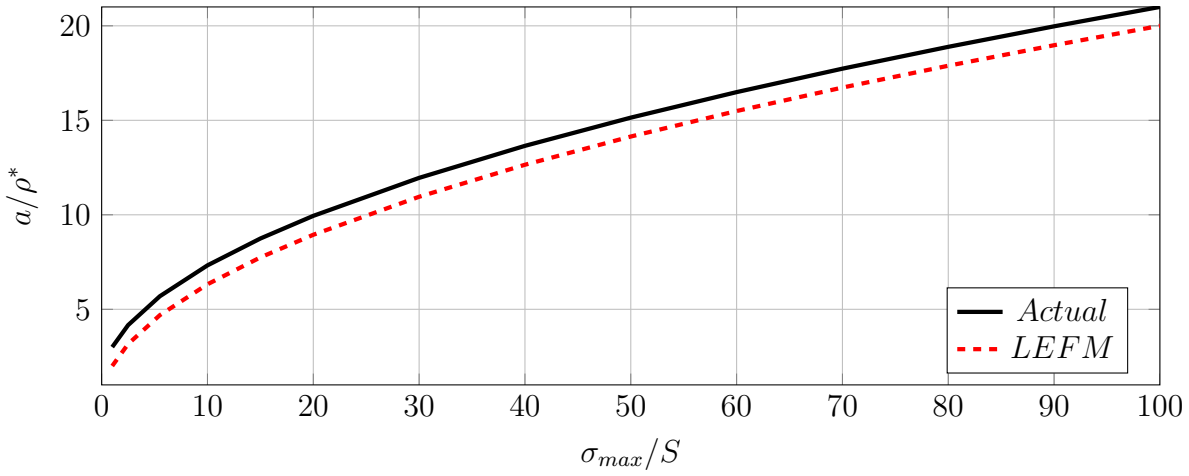

Figure 3.2: The LEFM and the actual crack tip stress

$$\sigma_{actual} = S\left(1 + 2\sqrt{\frac{a}{\rho^*}}\right) \tag{3.2}$$

Thus, the ratio of the maximum stresses obtained from the fracture mechanics and Creager-Paris solution [11] and the classical elliptical notch solution is:

$$\frac{\sigma_{actual}}{\sigma_{CG}} = \frac{S\left(1 + 2\sqrt{\frac{a}{\rho^*}}\right)}{\frac{2S\sqrt{\pi a}}{\sqrt{\pi\rho^*}}} = 1 + \frac{1}{2}\sqrt{\frac{\rho^*}{a}} \tag{3.3}$$

Therefore, the classical fracture mechanics solution (and the stress intensity factor, K) needs to be corrected in order to obtain the correct stress level at the crack tip.

$$\sigma_{actual} = \sigma_{CG}\left(1+\frac{1}{2}\sqrt{\frac{\rho^*}{a}}\right) = \frac{2K}{\sqrt{\pi\rho^*}}\left(1+\frac{1}{2}\sqrt{\frac{\rho^*}{a}}\right) = \frac{2K^*}{\sqrt{\pi\rho^*}} \tag{3.4}$$

The corrected stress intensity factor, K^* , can be subsequently used to predict the behavior of short cracks:

$$K^* = K\left(1+\frac{1}{2}\sqrt{\frac{\rho^*}{a}}\right) = K\cdot CS \tag{3.5}$$

where $CS = \left(1+\frac{1}{2}\sqrt{\frac{\rho^*}{a}}\right)$ is the short crack correction factor. The correction factor CS is presented in Figure 3.3 as a function of the a/ρ^* parameter

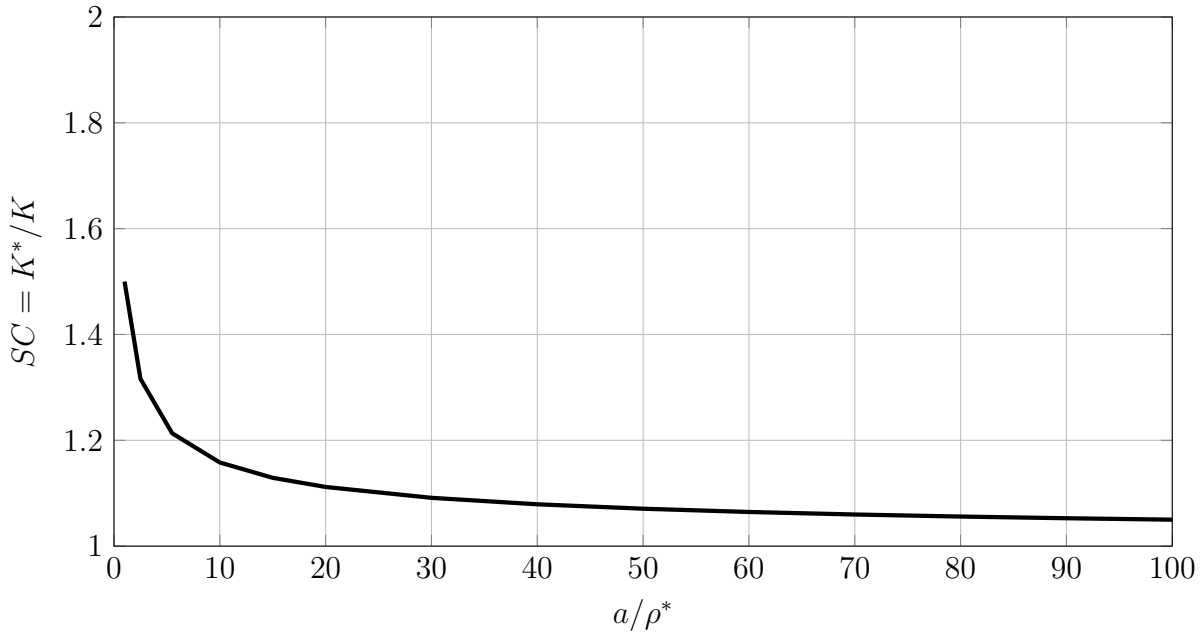

Figure 3.3: The short crack correction factor

3.2 The stress analysis of a cracked body

The knowledge of the actual stress field in a cracked body is required for the estimation of the effect of the plastically deformed material in the vicinity of the crack tip. This effect is quantified in the UniGrow fatigue crack growth model with the help of the residual stress intensity factor, K_r, resulting from the residual stress created around the crack tip (2.23).

The stress data necessary for fatigue crack growth analysis can be obtained for either the plane-stress or plane-strain state condition, by using the Neuber [48] or the ESED [49] rule. The importance of the implementation of the stress analysis under the plane-strain conditions comes from following observation: if the UniGrow model is to be used to predict the fatigue crack growth in a machine or structural components having different thicknesses then it is going to yield the same results, regardless of the thickness and contrary to the experimental observations [61].

The need to implement the ESED rule comes from the following observation. It is known that when the Neuber rule is used actual stresses are being overestimated and when the ESED rule is used actual stresses are underestimated [62]. While overestimation of the actual stresses leads to conservative design when static theories of failure are involved (such as Tresca or Von-Mises [55]) it is opposite for the fatigue crack growth analysis based on the UniGrow model. The logic is as follows. Use of the ESED rule leads to underestimated actual stresses in the vicinity of the crack tip. Since the actual stresses estimated using the ESED rule are lower then the ones estimated with the Neuber rule, than the residual stress intensity factor, K_r is consequently lower. While the applied stress intensity factor range ΔK and the applied maximum stress intensity factor K_{max} are going to be the same using either of methods (Neuber or ESED), the lower K_r value as per (2.22) will result in a higher total driving force $\Delta\kappa$. Accordingly, the fatigue crack growth rate da/dN is going

to be higher when the ESED rule is used. Finally, the total number of cycles to failure will be less when ESED rule will be employed. This will result in the conservative and safe design.

3.2.1 Elastic crack tip stresses and the plastic zone correction factor, C_p

The solution to the elastic-plastic crack problem starts first from the well-known [11] linear elastic stress problem. Let's assume an arbitrary cracked body loaded with known stress intensity factor, K as shown in Figure 3.4a. If the crack is approximated by an elliptical notch, then the elastic stress distribution can be written down as a function of coordinates (r, ϕ) with the origin at the focal point. It is obvious that the highest stress occurs at $\phi = 0$ and $r = \rho^*/2$. Thus in the Cartesian system of coordinates the equation set (2.3) transforms into (3.6). An example of the distribution of the stress component σ^e_{22} along the **x** axis is schematically shown in Figure 3.4b.

$$\begin{aligned}
\sigma^e_{33} &= -\frac{K}{\sqrt{2\pi r}}\frac{\rho^*}{2r}\cos\frac{3\phi}{2} + \frac{K}{\sqrt{2\pi r}}\cos\frac{\phi}{2}\left[1 - \sin\frac{\phi}{2}\sin\frac{3\phi}{2}\right] + \dots \\
\sigma_{22} &= \frac{K}{\sqrt{2\pi r}}\frac{\rho^*}{2r}\cos\frac{3\phi}{2} + \frac{K}{\sqrt{2\pi r}}\cos\frac{\phi}{2}\left[1 + \sin\frac{\phi}{2}\sin\frac{3\phi}{2}\right] + \dots
\end{aligned} \tag{3.6}$$

Elastic stresses at the crack (3.6) are finite but they significantly exceed the material yield limit, σ_{ys} . Therefore, the material will deform plastically in the crack tip neighborhood. The region in which the plastic deformation take place will be referred to as the crack tip plastic zone. For the linear elastic fracture mechanics to be applicable this region have to be small in comparison with other dimensions of the cracked body. Several methods were proposed to account for the effect of the plastic zone. Two most known methods

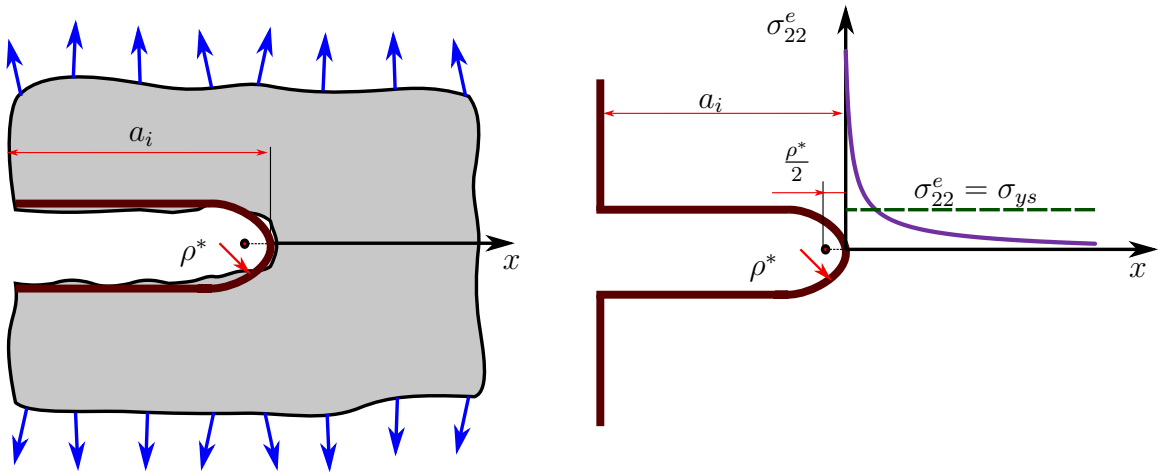

(a) Arbitrary cracked body

(b) Elastic stress distribution

Figure 3.4: Elastic stress distribution in a cracked body.

used for the crack analysis were obtained by Irwin [10] and Dugdale-Barenblatt [46]. Main steps in those models are - first estimate the size of plastic zone based on the linear elastic stress field and the yield limit σ_{ys} and then find how much more the zone will extend due to the redistribution of the linear elastic stress field (see Figure 3.5).

The plasticity zone correction factor C_p for a notched body was proposed by Glinka [63] and used later by Noroozi for derivation of the total driving force, $\Delta\kappa$ [64].

$$C_p = \frac{\sigma_{corrected}}{\sigma_{elastic}} \tag{3.7}$$

Where $\sigma_{corrected}$ is an elastic stress increased due to the presence of the plastic zone.

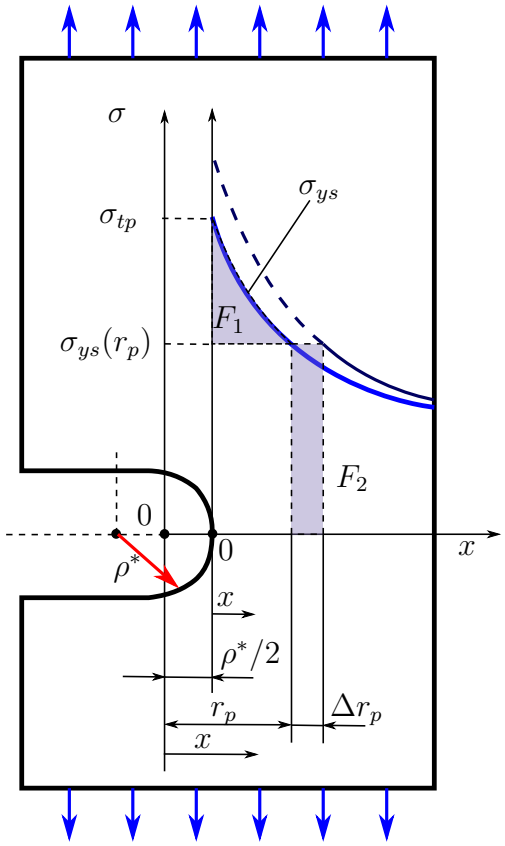

Figure 3.5: Plastic yielding and the elastic stress redistribution ahead of a crack tip [63]

$$C_p = \sqrt{1 + \frac{\Delta r_p}{r_p}} \times \sqrt{\frac{1 + \frac{3}{4}\left[\frac{\rho^*}{x+\frac{\rho^*}{2}} \times \left(1 + \frac{\Delta r_p}{r_p}\right)\right]^2}{1 + \frac{3}{4} \times \left[\frac{\rho^*}{x+\frac{\rho^*}{2}}\right]^2}} \tag{3.8}$$

where r_p is the initial plastic zone size which shall be found from the linear-elastic stress field and Von-Mises criterion, σ_{eq} :

$$\sigma_{ys}\left(r_p\right) = \sigma_{eq} \tag{3.9}$$

By substituting the Creager-Paris solution (3.6) into of the left side of equality (3.9), the following general cubic equation can be obtained:

$$\left(\frac{1}{r_p}\right)^3 + A \times \left(\frac{1}{r_p}\right) + B = 0 \tag{3.10}$$

Coefficients A and B of equation (3.10) depend on whether the plane-stress (3.11) or the plane-strain (3.12) condition is used in the analysis.

$$plane-stress: \begin{cases} A & = \frac{4}{3} \times \left(\frac{1}{\rho^*}\right)^2 \\ B & = -\frac{4}{3} \times \left(\frac{1}{\rho^*}\right)^2 \times \left(\frac{\sigma_{ys}\sqrt{2\pi}}{K_I}\right)^2 \end{cases} \tag{3.11}$$

$$plane-strain: \begin{cases} A & = \frac{4}{3} \times \left(\frac{1}{\rho^*}\right)^2 \times \left[4\nu^2 - 4\nu + 1\right] \\ B & = -\frac{4}{3} \times \left(\frac{1}{\rho^*}\right)^2 \times \left(\frac{\sigma_{ys}\sqrt{2\pi}}{K_I}\right)^2 \end{cases} \tag{3.12}$$

Finally, the extension of the plastic zone size Δr_p can be found from equation (3.13)

$$\Delta r_p = 2r_p \frac{\left(1 - \frac{\rho^*}{2r_p}\right)}{\left(1 + \frac{\rho^*}{2r_p}\right)} - \rho^* \left(\frac{r_p}{\rho^*} - \frac{1}{2}\right) \tag{3.13}$$

The plastic zone correction factor C_p (3.8) has to be determined before the ESED or Neuber method can be applied for determination of the elastic-plastic stress field.

3.2.2 Estimation of actual stresses ahead of the crack tip

Two methods are known to provide a reasonable transformation from the linear elastic stress state σ_{ij}^{e} to the actual elastic-plastic stress state σ_{ij}^{a} at the crack tip providing that the material stress-strain relationship $\varepsilon_{eq}^{pa} = f\left(\sigma_{eq}^{a}\right)$ is known. These methods are the Neuber rule [48] and the ESED approach [49]. Since the crack tip in the UniGrow fatigue crack growth model is defined by the finite radius ρ^{*}, the modified multiaxial notch stress-strain analysis [65] has to be applied.

The stress state around the crack tip

Let's consider the stress-state near the crack tip under both plane-stress and plane-strain conditions. These stress-states can be described by tensors (3.14) and (3.15) respectively.

$$plane-stress: \sigma_{i,j} = \begin{bmatrix} 0 & 0 & 0 \\ 0 & \sigma_{22}^{a} & \sigma_{23}^{a} \\ 0 & \sigma_{32}^{a} & \sigma_{33}^{a} \end{bmatrix} \varepsilon_{i,j} = \begin{bmatrix} \varepsilon_{11}^{a} & 0 & 0 \\ 0 & \varepsilon_{22}^{a} & \varepsilon_{23}^{a} \\ 0 & \varepsilon_{32}^{a} & \varepsilon_{33}^{a} \end{bmatrix} \tag{3.14}$$

$$plane-strain: \sigma_{i,j} = \begin{bmatrix} \sigma_{11}^{a} & 0 & 0 \\ 0 & \sigma_{22}^{a} & \sigma_{23}^{a} \\ 0 & \sigma_{32}^{a} & \sigma_{33}^{a} \end{bmatrix} \varepsilon_{i,j} = \begin{bmatrix} 0 & 0 & 0 \\ 0 & \varepsilon_{22}^{a} & \varepsilon_{23}^{a} \\ 0 & \varepsilon_{32}^{a} & \varepsilon_{33}^{a} \end{bmatrix} \tag{3.15}$$

Due to the equilibrium condition, the shear stress components are $\sigma_{23}^{a} = \sigma_{32}^{a}$ and $\varepsilon_{23}^{a} = \varepsilon_{32}^{a}$. Also the shear stress $\sigma_{23}^{el} = 0$ at $\phi = 0$ according to the equation (2.3). Thus, only five unknowns have to be determined for the plane-strain $[\sigma_{11}^{a}, \sigma_{22}^{a}, \sigma_{33}^{a}, \varepsilon_{22}^{a}, \varepsilon_{33}^{a}]$ and the plane-stress cases $[\sigma_{22}^{a}, \sigma_{33}^{a}, \varepsilon_{11}^{a}, \varepsilon_{22}^{a}, \varepsilon_{33}^{a}]$. Three out of five required independent equations can be derived from the constitutive material model. Additional equations come from the

generalized Neuber or the ESED rule.

Hencky's total deformation equations of plasticity (3.16) in combination with Prandtl-Reuss flow rule constitute the material model.

$$\varepsilon_{ij}^{a} = \frac{1+\nu}{E}\sigma_{ij}^{a} - \frac{\nu}{E}\sigma_{kk}^{a}\delta_{ij} + \frac{3}{2}\frac{\varepsilon_{eq}^{pa}}{\sigma_{eq}^{a}}S_{ij}^{a} \tag{3.16}$$

where S_{ij}^{a} is a deviatoric stress component and δ_{ij} is a Kronecker delta.

$$S_{ij}^{a} = \sigma_{ij}^{a} - \frac{1}{3}\sigma_{kk}^{a}\delta_{ij} \tag{3.17}$$

and σ_{eq}^{a} is an equivalent or Von-Mises stress

$$\sigma_{eq}^{a} = \sqrt{\frac{3}{2}\sigma_{ij}^{a}\sigma_{ij}^{a} - \frac{1}{2}\left(\sigma_{kk}^{a}\right)^{2}} \tag{3.18}$$

The plastic term of the stress-strain curve $\varepsilon_{eq}^{pa} = f\left(\sigma_{eq}^{a}\right)$ and the multiaxial stress-strain relationships are to be obtained from the uniaxial material stress-strain experimental curve

$$\varepsilon_{eq}^{pa} = \frac{df\left(\sigma_{eq}^{a}\right)}{d\sigma_{eq}^{a}}\sigma_{eq}^{a} \tag{3.19}$$

Due to the fact that $\sigma_{23}^{el} = 0$ at $\phi = 0$ (see equation (2.3)) the number of unknowns and the number of equations can be decreased by one. Final equations obtained from the material constitutive model for the plane-stress state:

$$\begin{aligned}
\varepsilon_{11}^{a} &= \frac{1}{E}\left[-\nu\left(\sigma_{22}^{a}+\sigma_{33}^{a}\right)\right]+\frac{1}{E_p}\left[-\frac{1}{2}\left(\sigma_{22}^{a}+\sigma_{33}^{a}\right)\right] \\
\varepsilon_{22}^{a} &= \frac{1}{E}\left[\sigma_{22}^{a}-\nu\left(+\sigma_{33}^{a}\right)\right]+\frac{1}{E_p}\left[\sigma_{22}^{a}-\frac{1}{2}\left(+\sigma_{33}^{a}\right)\right] \\
\varepsilon_{33}^{a} &= \frac{1}{E}\left[\sigma_{33}^{a}-\nu\left(\sigma_{22}^{a}\right)\right]+\frac{1}{E_p}\left[\sigma_{33}^{a}-\frac{1}{2}\left(\sigma_{22}^{a}\right)\right]
\end{aligned} \tag{3.20}$$

Final equations obtained from the material constitutive model for the plane-strain state:

$$\begin{aligned}
\varepsilon_{11}^{a} &= \frac{1}{E}\left[\sigma_{11}^{a}-\nu\left(\sigma_{22}^{a}+\sigma_{33}^{a}\right)\right]+\frac{1}{E_p}\left[\sigma_{1}-\frac{1}{2}\left(\sigma_{22}^{a}+\sigma_{33}^{a}\right)\right] \\
\varepsilon_{22}^{a} &= \frac{1}{E}\left[\sigma_{2}-\nu\left(\sigma_{11}^{a}+\sigma_{33}^{a}\right)\right]+\frac{1}{E_p}\left[\sigma_{22}^{a}-\frac{1}{2}\left(\sigma_{11}^{a}+\sigma_{33}^{a}\right)\right] \\
0 &= \frac{1}{E}\left[\sigma_{33}^{a}-\nu\left(\sigma_{22}^{a}+\sigma_{11}^{a}\right)\right]+\frac{1}{E_p}\left[\sigma_{33}^{a}-\frac{1}{2}\left(\sigma_{22}^{a}+\sigma_{11}^{a}\right)\right]
\end{aligned} \tag{3.21}$$

The Neuber rule and the ESED method

Graphical representation of the Neuber rule and the ESED method are schematically shown in Figure 3.6. Those rules are used to estimate the actual stress-strain state ahead of the crack tip based on their relationship with the fictitious linear elastic stresses induced by the applied stress intensity factor.

The general form of the Neuber and the ESED rule for a multiaxial stress state is given in the form of equation (3.22).

$$\sigma_{ij}^{e}\varepsilon_{ij}^{e}=\left[\frac{2\left(1+\nu\right)}{3E}+\frac{1-2\nu}{3E}\left(\frac{\sigma_{kk}^{a}}{\sigma_{eq}^{a}}\right)^{2}\right]\cdot\left(\sigma_{eq}^{a}\right)^{2}+W_{p} \tag{3.22}$$

where W_p is the strain energy density contribution, which depends on whether the Neuber (3.23) or the ESED (3.24) rule is to be used.

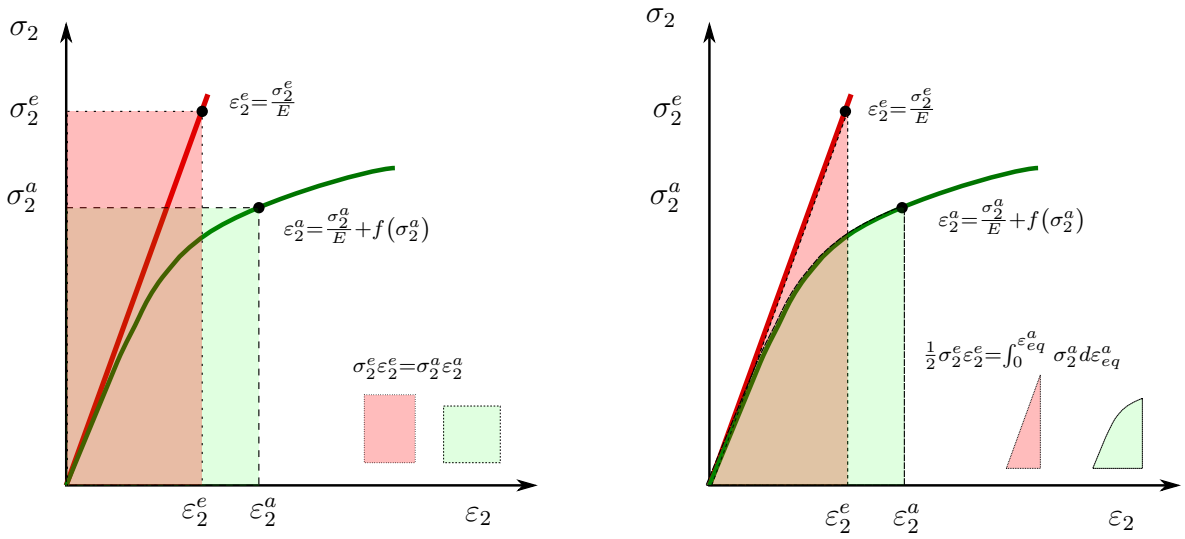

(a) Neuber

(b) ESED

Figure 3.6: Graphical representation of the Neuber (a) and the ESED rule (b).

$$The\ Neuber\ rule:\ W_p = \sigma_{eq}^a \varepsilon_{eq}^{pa} \tag{3.23}$$

$$The\ ESED\ rule:\ W_p = 2\int_0^{\varepsilon_{eq}^{pa}} \sigma_{eq}^a d\varepsilon_{eq}^{pa} \tag{3.24}$$

The equivalent plastic strain ε_{eq}^{pa} as it was stated earlier is obtained from the uniaxial material stress-strain curve, described by the Ramberg-Osgood stress-strain relationship (3.25). It should be noted that due to the Bauschinger effect the uniaxial stress-strain relationship follows so-called "*doubled*" $\varepsilon - \sigma$ curve when the second and further loading reversals are applied.

$$ascending\ first\ reversal:\ \varepsilon_2^a = \frac{\sigma_2^a}{E} + \left(\frac{\sigma_2^a}{K'}\right)^{\frac{1}{n'}} \tag{3.25}$$

$$descending\ reversal:\ \frac{\Delta\varepsilon_2^a}{2} = \frac{\Delta\sigma_2^a}{2E} + \left(\frac{\Delta\sigma_2^a}{2K'}\right)^{\frac{1}{n'}} \tag{3.26}$$

When the stress-strain relationship is approximated by the Ramberg-Osgood equation, the plastic energy density in the case of the Neuber rule takes the form of the expression (3.27).

$$W_p = \left(\frac{1}{K'}\right)^{\frac{1}{n'}} \left(\sigma_{eq}^a\right)^{\frac{n'}{n'+1}} \tag{3.27}$$

Equation (3.28) represents the strain energy density, W_p derived for the ESED rule.

$$W_p = \frac{2}{n'+1}\left(\frac{1}{K'}\right)^{\frac{1}{n'}} \left(\sigma_{eq}^a\right)^{\frac{n'}{n'+1}} \tag{3.28}$$

For the descending reversal (doubled stress-strain curve), the strain energy density W_p under the plane-strain and plane-stress condition takes the form of expression (3.29).

$$W_{p,double} = \left(\frac{1}{2}\right)^{1/n'-1} \cdot W_p \tag{3.29}$$

As a result, the fourth equation for calculating the actual strains and stresses generated by the ascending load reversal takes the form of equation presented below:

• The Neuber rule and the plane-stress state:

$$\sigma_{22}^{e}\varepsilon_{22}^{e}+\sigma_{33}^{e}\varepsilon_{33}^{e}=\left[\frac{2\left(1+\nu\right)}{3E}+\frac{1-2\nu}{3E}\left(\frac{\sigma_{22}^{a}+\sigma_{33}^{a}}{\sigma_{eq}^{a}}\right)^{2}\right]\cdot\left(\sigma_{eq}^{a}\right)^{2}+ \\ +\left(\frac{1}{K'}\right)^{\frac{1}{n'}}\left(\sigma_{eq}^{a}\right)^{\frac{n'}{n'+1}} \tag{3.30}$$

• The Neuber rule and the plane-strain state:

$$\sigma_{22}^{e}\varepsilon_{22}^{e}+\sigma_{33}^{e}\varepsilon_{33}^{e}=\left[\frac{2\left(1+\nu\right)}{3E}+\frac{1-2\nu}{3E}\left(\frac{\sigma_{11}^{a}+\sigma_{22}^{a}+\sigma_{33}^{a}}{\sigma_{eq}^{a}}\right)^{2}\right]\cdot\left(\sigma_{eq}^{a}\right)^{2}+ \\ +\left(\frac{1}{K'}\right)^{\frac{1}{n'}}\left(\sigma_{eq}^{a}\right)^{\frac{n'}{n'+1}} \tag{3.31}$$

• The ESED rule and the plane-stress state:

$$\sigma_{22}^{e}\varepsilon_{22}^{e}+\sigma_{33}^{e}\varepsilon_{33}^{e}=\left[\frac{2\left(1+\nu\right)}{3E}+\frac{1-2\nu}{3E}\left(\frac{\sigma_{22}^{a}+\sigma_{33}^{a}}{\sigma_{eq}^{a}}\right)^{2}\right]\cdot\left(\sigma_{eq}^{a}\right)^{2}+ \\ +\frac{2}{n'+1}\left(\frac{1}{K'}\right)^{\frac{1}{n'}}\left(\sigma_{eq}^{a}\right)^{\frac{n'}{n'+1}} \tag{3.32}$$

• The ESED rule and the plane-strain state:

$$\sigma_{22}^{e}\varepsilon_{22}^{e}+\sigma_{33}^{e}\varepsilon_{33}^{e}=\left[\frac{2\left(1+\nu\right)}{3E}+\frac{1-2\nu}{3E}\left(\frac{\sigma_{11}^{a}+\sigma_{22}^{a}+\sigma_{33}^{a}}{\sigma_{eq}^{a}}\right)^{2}\right]\cdot\left(\sigma_{eq}^{a}\right)^{2}+ \\ +\frac{2}{n'+1}\left(\frac{1}{K'}\right)^{\frac{1}{n'}}\left(\sigma_{eq}^{a}\right)^{\frac{n'}{n'+1}} \tag{3.33}$$

The fourth equation for calculation of actual stresses during the descending loading takes the following forms:

• The Neuber rule and the plane-stress state:

$$\sigma_{22}^{e}\varepsilon_{22}^{e}+\sigma_{33}^{e}\varepsilon_{33}^{e}=\left[\frac{2\left(1+\nu\right)}{3E}+\frac{1-2\nu}{3E}\left(\frac{\sigma_{22}^{a}+\sigma_{33}^{a}}{\sigma_{eq}^{a}}\right)^{2}\right]\cdot\left(\sigma_{eq}^{a}\right)^{2}+ \\ +\left(\frac{1}{2}\right)^{1/n^{'}-1}\cdot\left(\frac{1}{K^{'}}\right)^{\frac{1}{n^{'}}}\left(\sigma_{eq}^{a}\right)^{\frac{n^{'}}{n^{'}+1}} \tag{3.34}$$

• The Neuber rule and the plane-strain state:

$$\sigma_{22}^{e}\varepsilon_{22}^{e}+\sigma_{33}^{e}\varepsilon_{33}^{e}=\left[\frac{2\left(1+\nu\right)}{3E}+\frac{1-2\nu}{3E}\left(\frac{\sigma_{11}^{a}+\sigma_{22}^{a}+\sigma_{33}^{a}}{\sigma_{eq}^{a}}\right)^{2}\right]\cdot\left(\sigma_{eq}^{a}\right)^{2}+ \\ +\left(\frac{1}{2}\right)^{1/n^{'}-1}\cdot\left(\frac{1}{K^{'}}\right)^{\frac{1}{n^{'}}}\left(\sigma_{eq}^{a}\right)^{\frac{n^{'}}{n^{'}+1}} \tag{3.35}$$

• The ESED rule and the plane-stress state:

$$\sigma_{22}^{e}\varepsilon_{22}^{e}+\sigma_{33}^{e}\varepsilon_{33}^{e}=\left[\frac{2\left(1+\nu\right)}{3E}+\frac{1-2\nu}{3E}\left(\frac{\sigma_{22}^{a}+\sigma_{33}^{a}}{\sigma_{eq}^{a}}\right)^{2}\right]\cdot\left(\sigma_{eq}^{a}\right)^{2}+ \\ +\left(\frac{1}{2}\right)^{1/n^{'}-1}\cdot\frac{2}{n^{'}+1}\left(\frac{1}{K^{'}}\right)^{\frac{1}{n^{'}}}\left(\sigma_{eq}^{a}\right)^{\frac{n^{'}}{n^{'}+1}} \tag{3.36}$$

• The ESED rule and the plane-strain state:

$$\sigma_{22}^{e}\varepsilon_{22}^{e}+\sigma_{33}^{e}\varepsilon_{33}^{e}=\left[\frac{2\left(1+\nu\right)}{3E}+\frac{1-2\nu}{3E}\left(\frac{\sigma_{11}^{a}+\sigma_{22}^{a}+\sigma_{33}^{a}}{\sigma_{eq}^{a}}\right)^{2}\right]\cdot\left(\sigma_{eq}^{a}\right)^{2}+ \\ +\left(\frac{1}{2}\right)^{1/n^{'}-1}\cdot\frac{2}{n^{'}+1}\left(\frac{1}{K^{'}}\right)^{\frac{1}{n^{'}}}\left(\sigma_{eq}^{a}\right)^{\frac{n^{'}}{n^{'}+1}} \tag{3.37}$$

The final equation required for the complete formulation of the crack tip problem comes from the proportionality assumption:

$$\frac{\sigma_{ii}^{a}}{\sigma_{eq}^{a}} = \frac{\sigma_{kk}^{e}}{\sigma_{eq}^{e}} \tag{3.38}$$

Unfortunately, the resulting system of five independent equations with five unknowns, corresponding to the desired combination: plane-stress - plane-strain; Neuber - ESED during the ascending or descending load reversals does not have a closed form analytical solution and therefore it has to be solved numerically. As an example, total set of 5 equations for the ESED rule and the plane-strain state is presented in equation (3.39). It should be also noted that this is set for the ascending reversal.

$$\begin{cases} \textbf{1}. \quad \varepsilon_{11}^{a} = \dfrac{1}{E}\left[\sigma_{11}^{a} - \nu\left(\sigma_{22}^{a} + \sigma_{33}^{a}\right)\right] + \dfrac{1}{E_p}\left[\sigma_1 - \dfrac{1}{2}\left(\sigma_{22}^{a} + \sigma_{33}^{a}\right)\right] \\ \textbf{2}. \quad \varepsilon_{22}^{a} = \dfrac{1}{E}\left[\sigma_2 - \nu\left(\sigma_{11}^{a} + \sigma_{33}^{a}\right)\right] + \dfrac{1}{E_p}\left[\sigma_{22}^{a} - \dfrac{1}{2}\left(\sigma_{11}^{a} + \sigma_{33}^{a}\right)\right] \\ \textbf{3}. \quad 0 = \dfrac{1}{E}\left[\sigma_{33}^{a} - \nu\left(\sigma_{22}^{a} + \sigma_{11}^{a}\right)\right] + \dfrac{1}{E_p}\left[\sigma_{33}^{a} - \dfrac{1}{2}\left(\sigma_{22}^{a} + \sigma_{11}^{a}\right)\right] \\ \textbf{4}. \quad \sigma_{22}^{e}\varepsilon_{22}^{e} + \sigma_{33}^{e}\varepsilon_{33}^{e} = \left[\dfrac{2\left(1+\nu\right)}{3E} + \dfrac{1-2\nu}{3E}\left(\dfrac{\sigma_{11}^{a} + \sigma_{22}^{a} + \sigma_{33}^{a}}{\sigma_{eq}^{a}}\right)^2\right] \cdot \left(\sigma_{eq}^{a}\right)^2 + \\ \qquad + \dfrac{2}{n^{'}+1}\left(\dfrac{1}{K^{'}}\right)^{\frac{1}{n^{'}}} \left(\sigma_{eq}^{a}\right)^{\frac{n^{'}}{n^{'}+1}} \\ \textbf{5}. \quad \dfrac{\sigma_{ii}^{a}}{\sigma_{eq}^{a}} = \dfrac{\sigma_{kk}^{e}}{\sigma_{eq}^{e}} \end{cases} \tag{3.39}$$

3.2.3 Analysis of the residual stress distribution profiles obtained from various formulations of the elastic-plastic stress-strain crack tip problem

Before implementation of the stress calculation procedure into the fatigue crack growth analysis, the special computer program was developed with the purpose to study residual stress profiles induced by the cyclic loading (see Figure 3.7). This program takes as an input all required material properties (cyclic stress-strain curve and the ρ^* parameter) and based on the applied loading cycle defined by the stress intensity factor range ΔK and the maximum stress intensity factor K_{max} (see Figure 3.8a) calculates the residual stress distribution (as shown in Figure 3.8b). Results of the residual stress analysis obtained for aluminum and steel alloys (Al 2024-T3 and A36) are presented below. Material properties for both materials used in the program are summarized in Table 3.1.

Table 3.1: Material properties used for the elastic-plastic stress strain analysis

	$\rho^*,\ m$	E, MPa	ν	$\sigma_{ys},\ MPa$	$K^{'},\ MPa$	$n^{'}$
Al 2024-T3	$1.36E-05$	73100	0.33	428	662	0.07
A36	$4E-05$	190786	0.3	324	991	0.18

Since the length of the crack is already accounted for through the applied stress intensity factor, the origin of the **x** axis for the program has been set at the crack tip. Numerical solution of the total set of equation similar to the one presented in equation (3.39) coded into the program can be carried for any combination of the ESED - Neuber and Plane-Strain - Plane-Stress options.

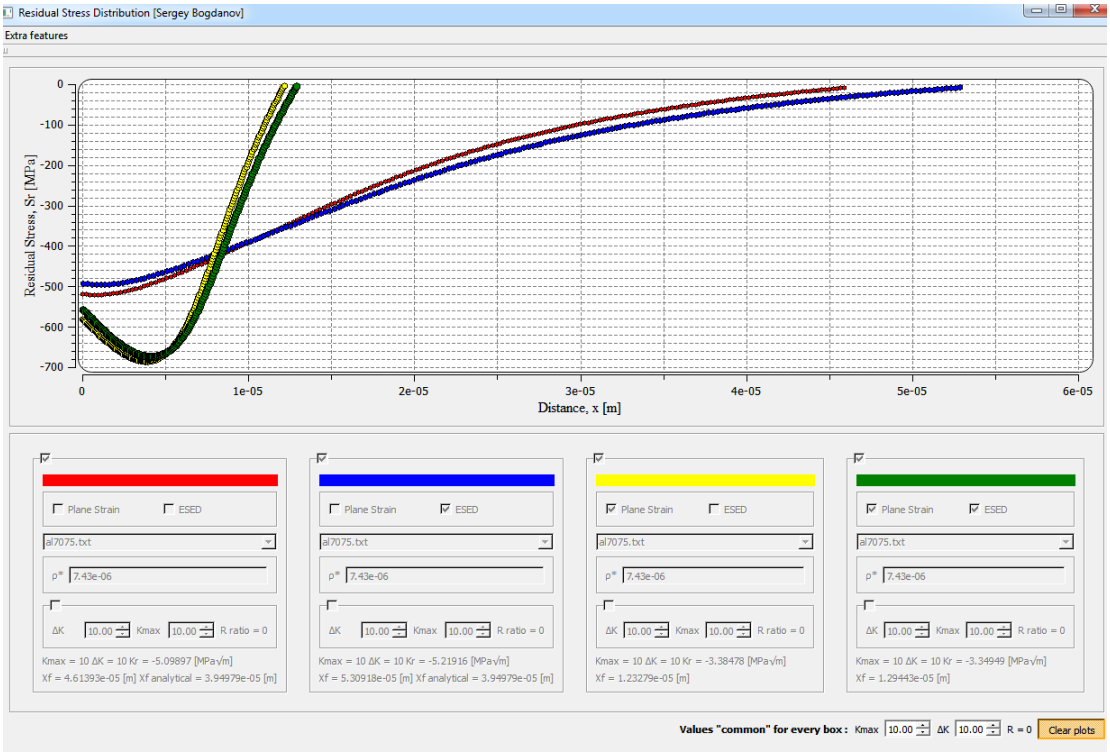

Figure 3.7: The Graphic User Interface of the residual stress distribution $\sigma_r(x)$ computer program

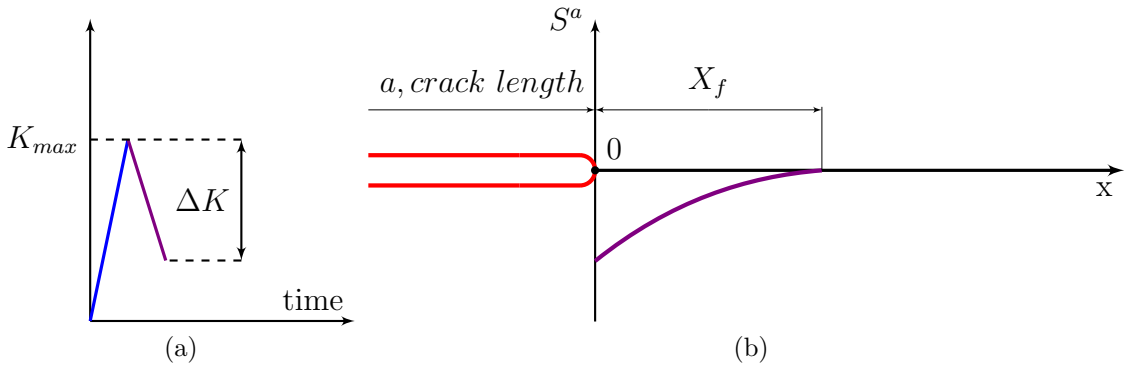

Figure 3.8: Residual stress distribution based on the applied loading cycle

The goal of the first step in the entire project was to study the effect of the applied stress ratio R on the residual stress profile resulting from the application of the plane-stress/plane-strain - ESED method and the plane-stress/plane-strain - Neuber rule. The maximum stress intensity factor, K_{max} was set to $15, MPa\sqrt{m}$ and the applied stress intensity factor range, ΔK was varied from $15, MPa\sqrt{m}$ to $3, MPa\sqrt{m}$. Aluminum alloys appeared to have a non-zero (visible) residual stress profiles even at relatively high R ratios, such as $R = 0.8$. In the case of the A36 steel alloy, residual stress distribution disappeared at the stress ratio $R \geq 0.5$. This correlates well with experimental observations of available fatigue crack growth data for steel and aluminum alloys. Loading conditions for which, the residual stress profiles were calculated and plotted for the aluminum Al 2024-T3 and A36 steel alloys are summarized in Table 3.2.

Table 3.2: Loading conditions used for the elastic-plastic stress strain analysis

Al 2024-T3	**A36**
$\Delta K = 15, K_{max} = 15, MPa\sqrt{m}$ (R=0)	$\Delta K = 15, K_{max} = 15, MPa\sqrt{m}$ (R=0)
$\Delta K = 7.5, K_{max} = 15, MPa\sqrt{m}$ (R=0.5)	$\Delta K = 12, K_{max} = 15, MPa\sqrt{m}$ (R=0.2)
$\Delta K = 3, K_{max} = 15, MPa\sqrt{m}$ (R=0.8)	$\Delta K = 9, K_{max} = 15, MPa\sqrt{m}$ (R=0.4)

The residual stress profiles of cracked bodies under the plane-strain or plane-stress conditions vary significantly. On contrary, similar profiles obtained using the ESED method and the Neuber rule are fairly close to each other. As it appeared from the studies, the residual stress profile obtained from the ESED method resulted in a larger X_f zone but the lowest point of the distribution was always higher than the one obtained from the

Neuber rule. For demonstration purposes, residual stress profiles which are supposed to appear in the vicinity of the crack tip after application of the stress intensity factor range $\Delta K = 15, MPa\sqrt{m}$ and maximum stress intensity factor, $K_{max} = 15, MPa\sqrt{m}$ to the cracked body made of Al 2024-T3 calculated using the Neuber and ESED methods are presented in Figures 3.17 and 3.18. Nevertheless, analysis of the residual stress intensity factor, K_r obtained from the studies of these residual stress distributions has revealed the following. In general, values of K_r corresponding to the ESED method are slightly lower than K_r values obtained under the same conditions but using the Neuber rule. It means that total driving force, $\Delta\kappa$ values obtained from equation (2.22) will be in general larger for the ESED method. This leads to the higher crack growth rates Δa_i and consequently to lower number of cycles to failure, N_f. Therefore, the ESED method can be regarded as conservative in comparison with the Neuber rule.

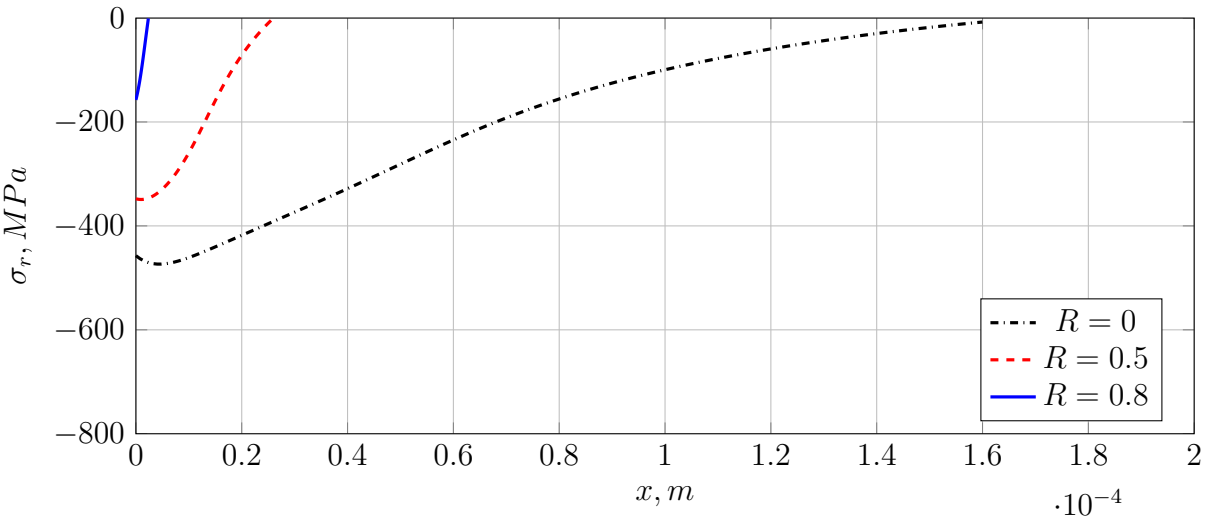

Figure 3.9: Residual crack tip stress distributions induced by the cycle loading of $K_{max} = 15\ MPa\sqrt{m}$ and various stress ratios R. Aluminum alloy Al 2024-T3. The Neuber rule and the plane-stress state.

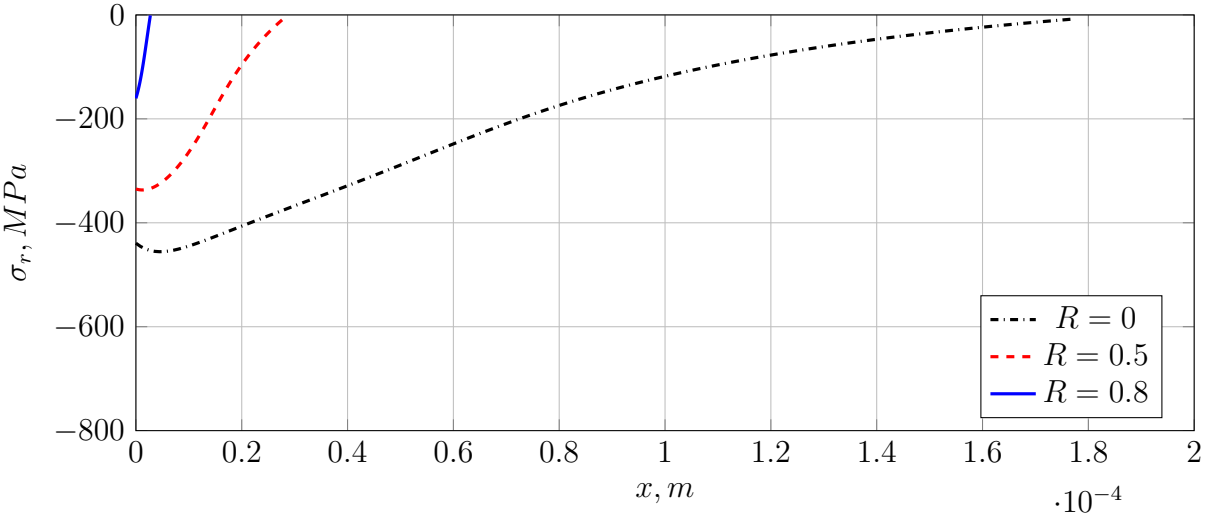

Figure 3.10: Residual crack tip stress distributions induced by the cycle loading of $K_{max} = 15\ MPa\sqrt{m}$ and various stress ratios R. Aluminum alloy Al 2024-T3. The ESED rule and the plane-stress state.

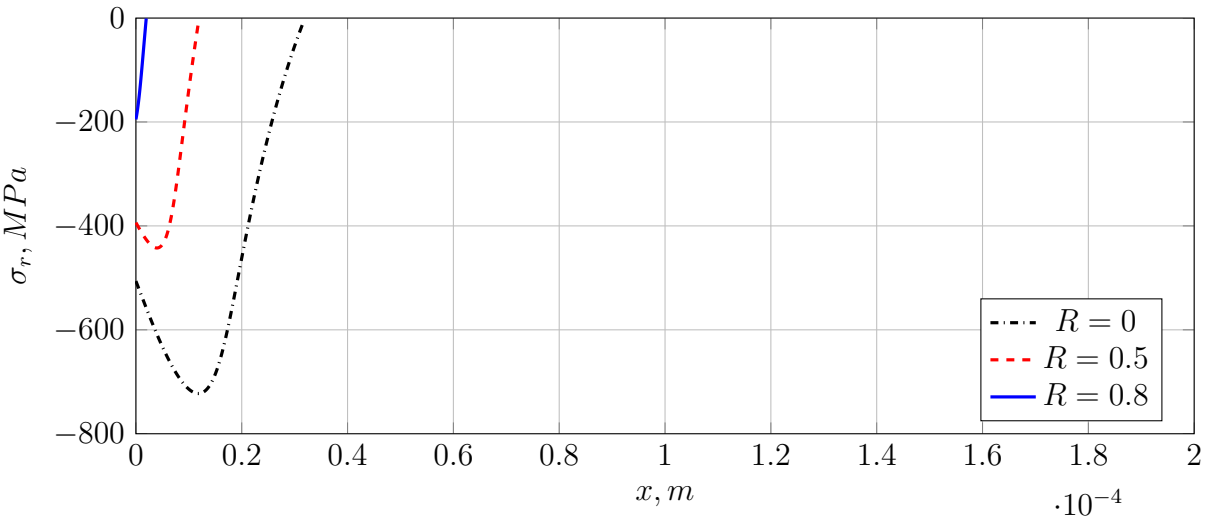

Figure 3.11: Residual crack tip stress distributions induced by the cycle loading of $K_{max} = 15\ MPa\sqrt{m}$ and various stress ratios R. Aluminum alloy Al 2024-T3. The Neuber rule and the plane-strain state.

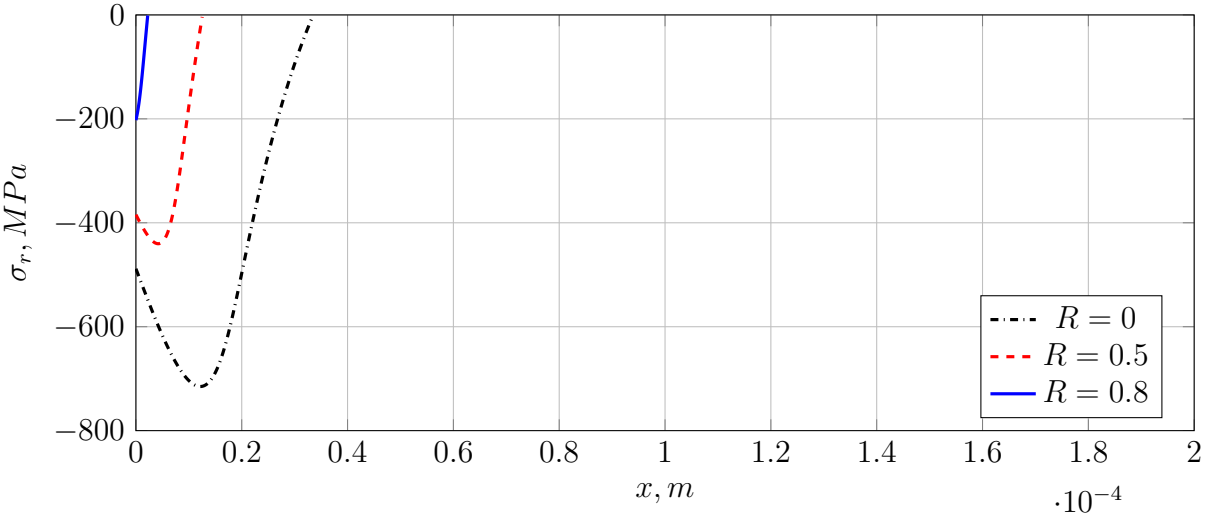

Figure 3.12: Residual crack tip stress distributions induced by the cycle loading of $K_{max} = 15\ MPa\sqrt{m}$ and various stress ratios R. Aluminum alloy Al 2024-T3. The ESED rule and the plane-strain state.

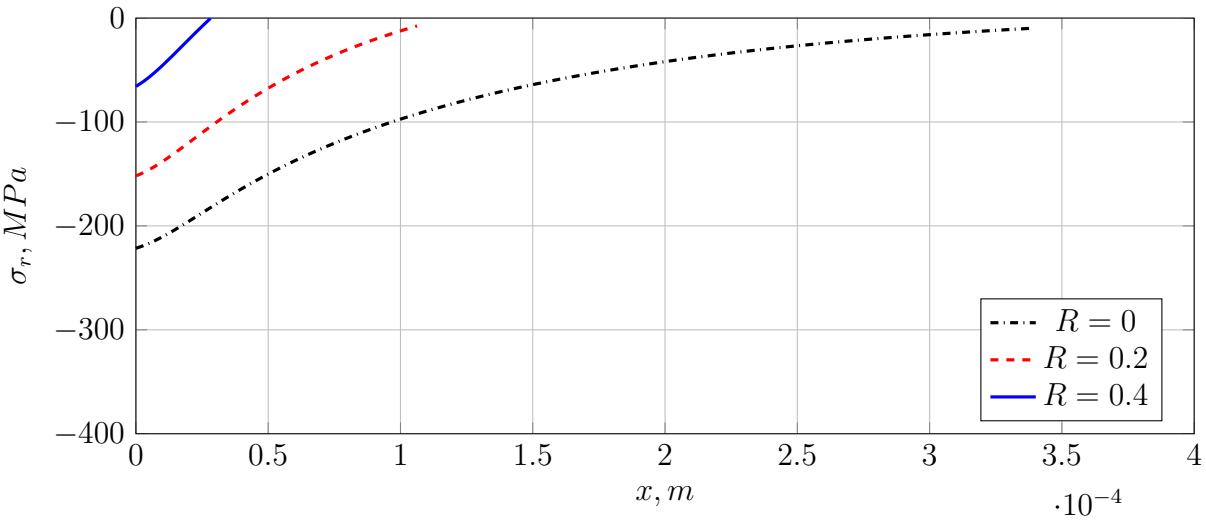

Figure 3.13: Residual crack tip stress distributions induced by the cycle loading of K_{max} $MPa\sqrt{m}$ and various stress ratios R. Steel alloy A36. The Neuber rule and the plane-stress state.

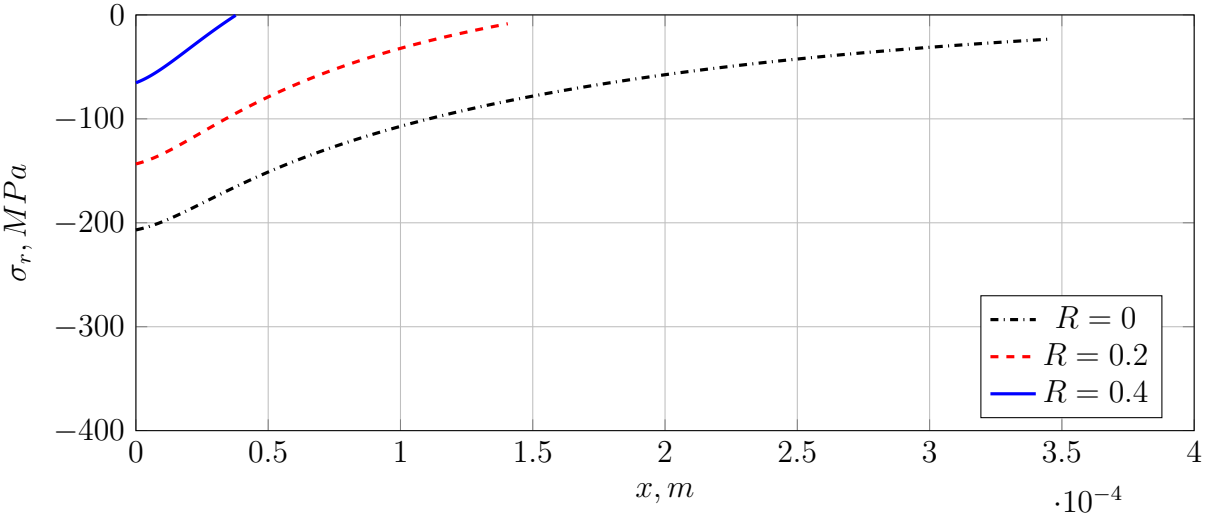

Figure 3.14: Residual crack tip stress distributions induced by the cycle loading of $K_{max} = 15$ $MPa\sqrt{m}$ and various stress ratios R. Steel alloy A36. The ESED rule and the plane-stress state.

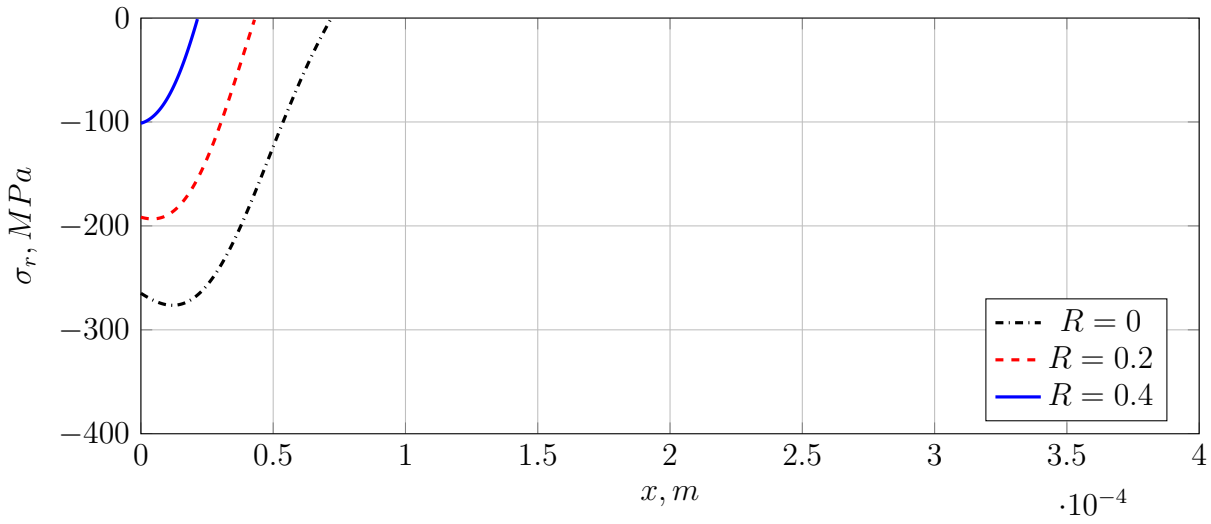

Figure 3.15: Residual crack tip stress distributions induced by the cycle loading of $K_{max} = 15\ MPa\sqrt{m}$ and various stress ratios R. Steel alloy A36. The Neuber rule and the plane-strain state.

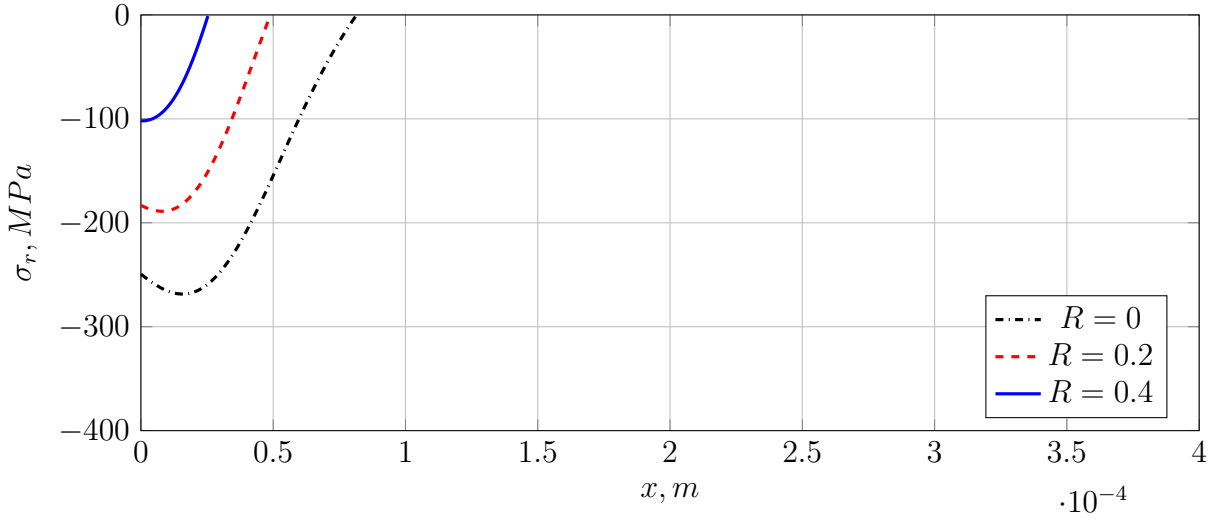

Figure 3.16: Residual crack tip stress distributions induced by the cycle loading of $K_{max} = 15\ MPa\sqrt{m}$ and various stress ratios R. Steel alloy A36. The ESED rule and the plane-strain state.

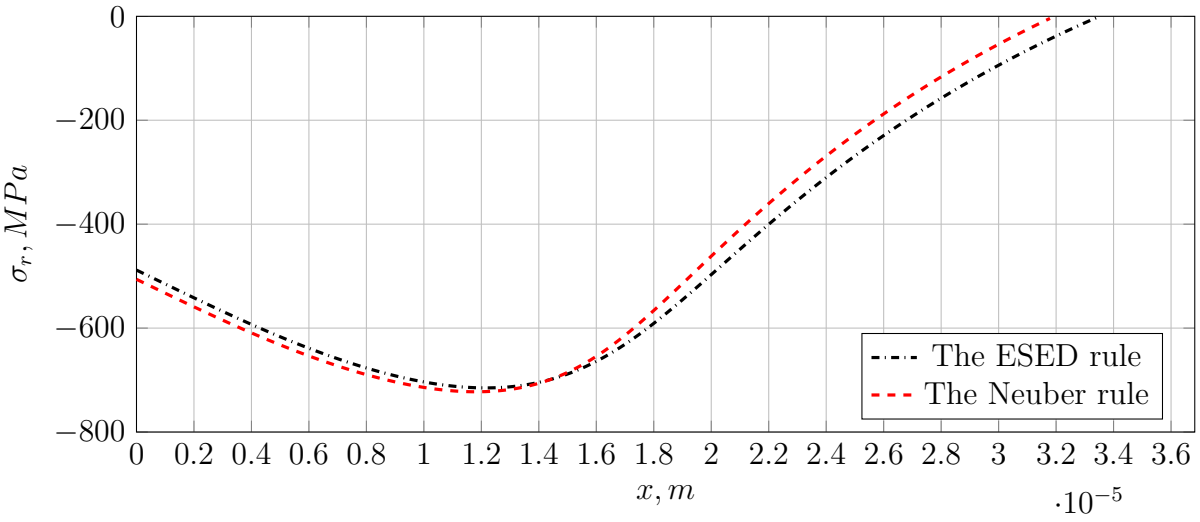

Figure 3.17: Comparison of residual stress profiles calculated using the Neuber rule and the ESED method in plane-strain condition (Al 2024-T3 aluminum alloy, $\Delta K = 15\ MPa\sqrt{m}$, $K_{max} = 15\ MPa\sqrt{m}$).

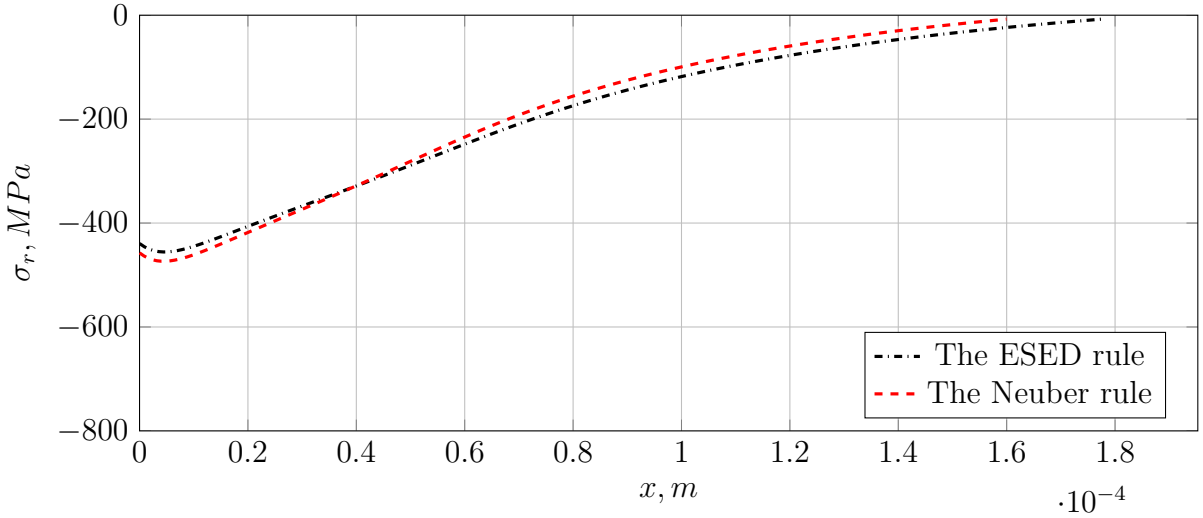

Figure 3.18: Comparison of residual stress profiles calculated using the Neuber rule and the ESED method in plane-stress condition (Al 2024-T3 aluminum alloy, $\Delta K = 15\ MPa\sqrt{m}$, $K_{max} = 15\ MPa\sqrt{m}$).

Chapter 4

Analysis and estimation of the ρ^* parameter

The very important and initially unknown parameter ρ^* of the UniGrow fatigue crack growth model was originally viewed as an effective crack tip radius and as an "*average dimension of inhomogeneous material blocks*" [1]. These definitions constitute the dual nature of the ρ^* parameter and for evaluation purposes should be regarded as equally important. The value of the ρ^* parameter is directly used in the UniGrow computational algorithm since it approximates the effective crack tip radius and consequently enables the estimation of stresses and strains at the crack tip. From the other side, assumption of the ρ^* parameter as a material block size sets some constraints on evaluation of the ρ^* parameter. For example, the magnitude of the ρ^* parameter has to be greater than an average grain size of the material used in the analysis. This is due to the fact that bulk material properties such as Young's modulus, E, Poisson's ratio, ν and etc. were used in derivation of the total driving force, $\Delta\kappa$ in its current form (2.22). Therefore, it can be concluded that estimation of the ρ^* parameter is a complex process which requires thorough studies.

Several methods to estimate the ρ^* parameter were proposed by Noroozi and Mikheevskiy [64, 47]. Unfortunately, comprehensive analysis of these methods has revealed that none of the proposed ways to evaluate the ρ^* parameter can be used without significant changes. Thus, it was required to develop the new two-step method for the evaluation of the ρ^* parameter. The development of the new method was supported by the extensive investigation of the effect of the chosen value of the ρ^* parameter on the fatigue crack growth analysis.

4.1 Critical analysis of currently available methods for the evaluation of the ρ^* parameter

The first method to estimate the ρ^* parameter was formulated by Noroozi [64] in terms of requirements for the fatigue crack arrest. It was argued that, the stress experienced by the first material block ahead of the crack tip (see Figure 4.1) when threshold conditions are imposed on the cracked body can be found from the equation (4.1).

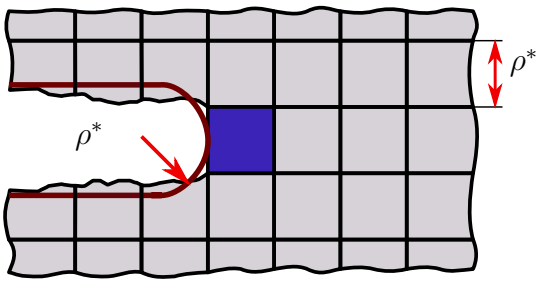

Figure 4.1: Depiction of the first material block ahead of the crack tip

$$\Delta\widetilde{\sigma}_{th} = \frac{\Delta K_{th} \times 1.633}{\sqrt{2\pi\rho^*}} \tag{4.1}$$

Respectively, if parameters ΔK_{th} and $\Delta\sigma^a_{th}$ are known, then equation (4.1) shall be rearranged, so the ρ^* parameter can be found as:

$$\rho^* = \frac{1.633^2}{2\pi}\left(\frac{\Delta K_{th}}{\Delta\sigma^a_{th}}\right)^2 \tag{4.2}$$

The main disadvantage of this method is that it requires precisely measured threshold stress intensity factor range ΔK_{th} and the fatigue limit $\Delta\sigma^a_{th}$. These two material parameters have to be obtained under the same R ratio and aren't always available in practice. Also, no studies have been carried out on whether the ρ^* value obtained from ΔK_{th} and $\Delta\sigma^a_{th}$ measured at different R ratios will produce the same result.

Another method to estimate the ρ^* parameter was formulated by Mikheevskiy in 2009 [47]. The proposed procedure had a direct impact on the fatigue crack growth analysis and came as a result of two observations. The first observation was that the total driving force, $\Delta\kappa$ can be formulated as a function of the parameter ρ^*as depicted below:

$$\begin{aligned}
&\Delta\kappa\left(\rho^*\right) = K^p_{max,tot}\Delta K^{1-p}_{tot} = \\
&= \left(K_{max,appl} + K_r\right)^p \cdot \left(\Delta K_{appl} + K_r\right)^{1-p} = \\
&= \left(K_{max,appl} + \int_0^a \sigma_r\left(x|\rho^*\right) m\left(x,a\right) dx\right)^p \cdot \\
&\left(\Delta K_{appl} + \int_0^a \sigma_r\left(x|\rho^*\right) m\left(x,a\right) dx\right)^{1-p}
\end{aligned} \tag{4.3}$$

Such formulation means that transformation of the original experimental fatigue crack growth data of the $[\Delta K, (da/dN)]$ form into the collapsed data of the $[\Delta\kappa, (da/dN)]$ form depends on the chosen value of parameter ρ^*. The second observation was that transformed experimental fatigue crack growth data $[\Delta\kappa, da/dN]$ obtained at various stress R ratios were always collapsed into a single curve (as shown in Figure 4.2b) when the correctly

chosen ρ^* parameter was used. Unfortunately, equation (4.3) doesn't have an analytical solution because the residual stress distribution $\sigma_r\left(x|\rho^*\right)$ can only be obtained in a numerical form. Therefore, special procedure for finding the ρ^* parameter had to be developed.

In order to develop the procedure for evaluation of the ρ^* parameter it was important to analyze why the scatter of the transformed fatigue crack growth data was significantly reduced. The following explanation was proposed by Mikheevskiy [8]. First it was argued, that the total driving force, $\Delta\kappa$ was derived using the Smith-Watson-Topper mean stress correction model [34]. Therefore it was assumed that $\Delta\kappa$ indirectly accounts for the mean stress effect. Then it was noted, that the scatter of the original experimental fatigue crack growth data of form $[\Delta K, (da/dN)]$ obtained at various stress R ratios (see Figure 4.2a) is often attributed to the mean stress effect. Therefore, transformation of the ΔK values obtained at the same da/dN level theoretically should yield the same $\Delta\kappa$ value when the actual value of the ρ^* parameter is used. Finally, the proposed "*transformation method*" was summarized in following three steps:

1. Select the list of potential values of the ρ^* parameter
2. For each value of the ρ^* parameter transform the available fatigue crack growth data from the $[\Delta K, (da/dN)]$ form into the $[\Delta\kappa, (da/dN)]$ form
3. Identify "*the best collapse of fatigue crack growth data*" [47] and choose the corresponding value of the ρ^* parameter

The main advantage of this method is that it is not only enables evaluation of the ρ^* parameter but also results in the experimental data of $[\Delta\kappa, (da/dN)]$ form. The latter is then has to be split into linear segments and used in the UniGrow fatigue crack growth prediction in form of the $[C_i, \gamma_i]$ coefficients.

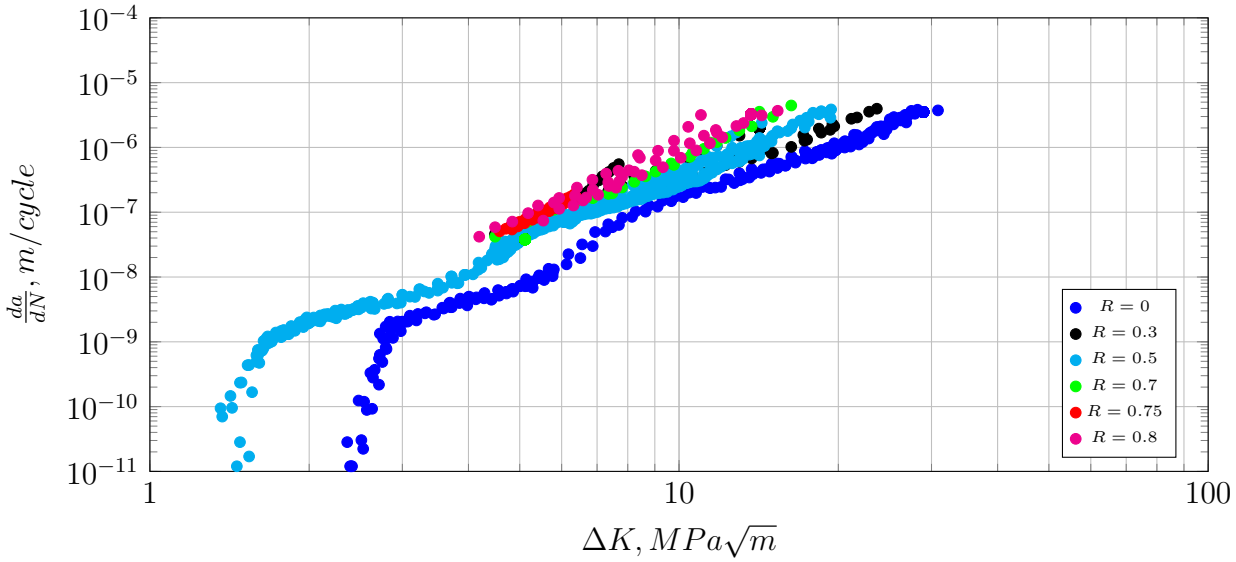

(a) Original fatigue crack growth data

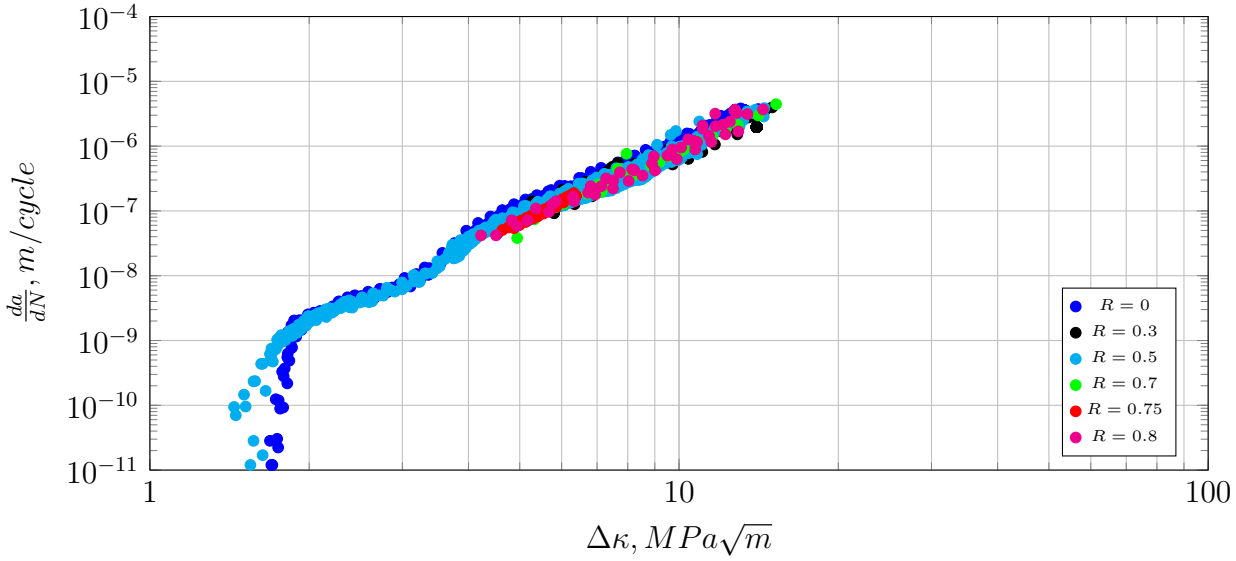

(b) Collapsed fatigue crack growth data

Figure 4.2: Collapse of the fatigue crack growth data obtained at different R ratios for the Al 7075-T6 aluminum alloy [66]

Despite the fact that this method was very important for further fatigue crack growth analysis it also had several drawbacks. The first deficiency of the "*transformation method*" was that list of potential values of the ρ^* parameter hasn't been constrained and was very subjective. This led to the results when equally good collapses could be identified for completely distinct ρ^* values. The second deficiency of the "*transformation method*" was that no explicit definition on what should be considered as "*the best collapse*" was given by Mikheevskiy. It means that two distinct values of the ρ^* parameter could produce collapses which would be visually indistinguishable.

Let's consider two distinct values of the ρ^* parameter: $3.9E-07$ $[m]$ and $3.9E-05$ $[m]$. These values are in an order magnitude from the actual value of the ρ^* parameter for the Al 7075-T6 aluminum alloy, which is $3.9E-06$ $[m]$. At first, by using the two mentioned above ρ^* values, raw experimental fatigue crack growth data $[\Delta K, (da/dN)]$ obtained for Al 7075-T6 aluminum alloy was transformed into the required for the fatigue crack growth analysis form of $[\Delta\kappa, (da/dN)]$. Then, transformed fatigue crack growth data sets were linearized by using the regression analysis. As a result, two sets of $[C_i, \gamma_i]$ coefficients were obtained. The result presented in Figure 4.3 shows that values of the those coefficients fitted to both sets of transformed data are significantly different. Consequently, results of fatigue live analysis with used values of the ρ^* parameter: $3.9e-07$ $[m]$ and $\rho^* = 3.9e-05$ $[m]$ will vary. Therefore, one has to be especially careful while performing the fatigue crack growth analysis with the UniGrow model since $[C_i, \gamma_i]$ coefficients shall always correspond to the value of the chosen ρ^* parameter. The aims of this exercise were to demonstrate the discussed above dependence of the $[C_i, \gamma_i]$ coefficients on the ρ^* parameter, but more importantly to show that quality of collapses obtained for the significantly ranging ρ^* values can't be distinguished without proper statistical analysis.

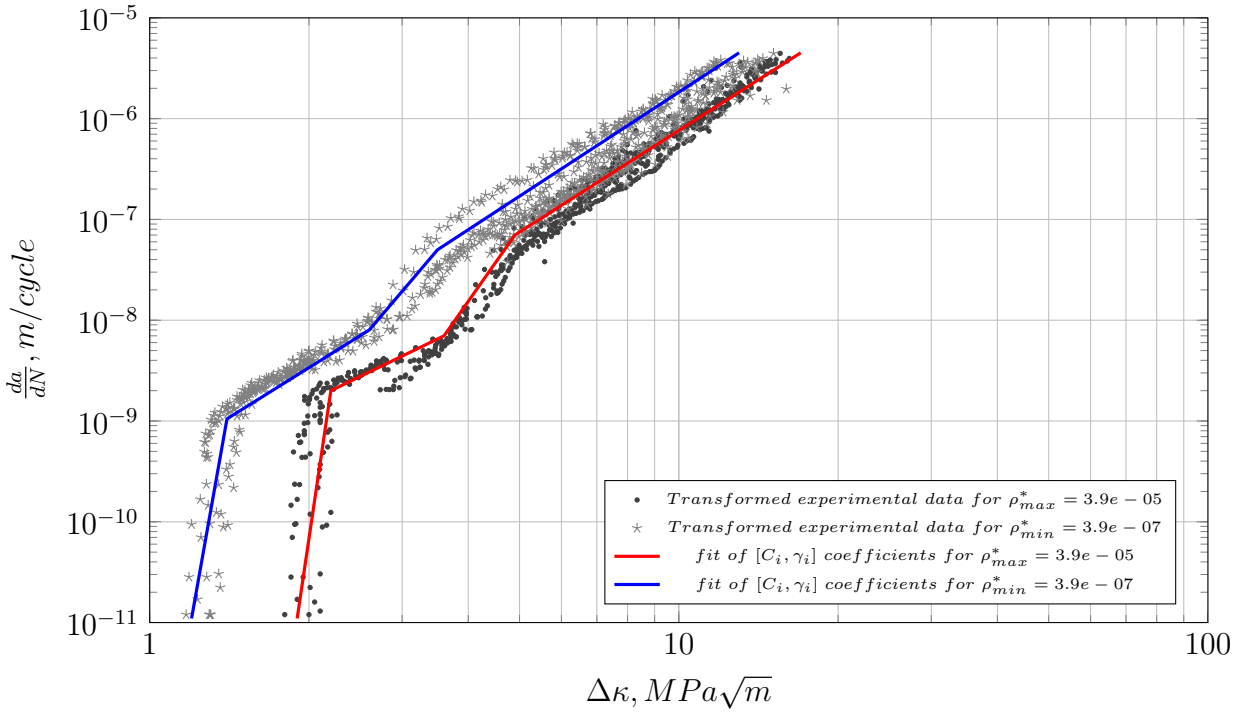

Figure 4.3: Collapsed fatigue crack growth data for Al 7075-T6 obtained at different R ratios [66]

To summarize, the analysis of the ρ^* parameter has revealed that in order to be consistent with the UniGrow model formulation, the procedure for the ρ^* parameter evaluation has to reflect its dual nature. Therefore, it was proposed to evaluate the ρ^* parameter by using a specifically designed two-step procedure. The first step of the developed procedure is used to approximate the value of the ρ^* parameter and to define the range of its potential values. During the second step, modified "*transformation method*" is used to find the actual value of the ρ^* parameter.

4.2 Proposed two-step method for estimation of the ρ^* parameter

The new method to evaluate the ρ^* parameter was proposed. This method consists of two steps. At the first step value of the ρ^* parameter shall be approximated as the value that represents the average material block size, ρ^*_{ini}. The second step is then used to find the true value of the ρ^* parameter within an order of magnitude around ρ^*_{ini}. The method's algorithm is presented in Figure 4.4

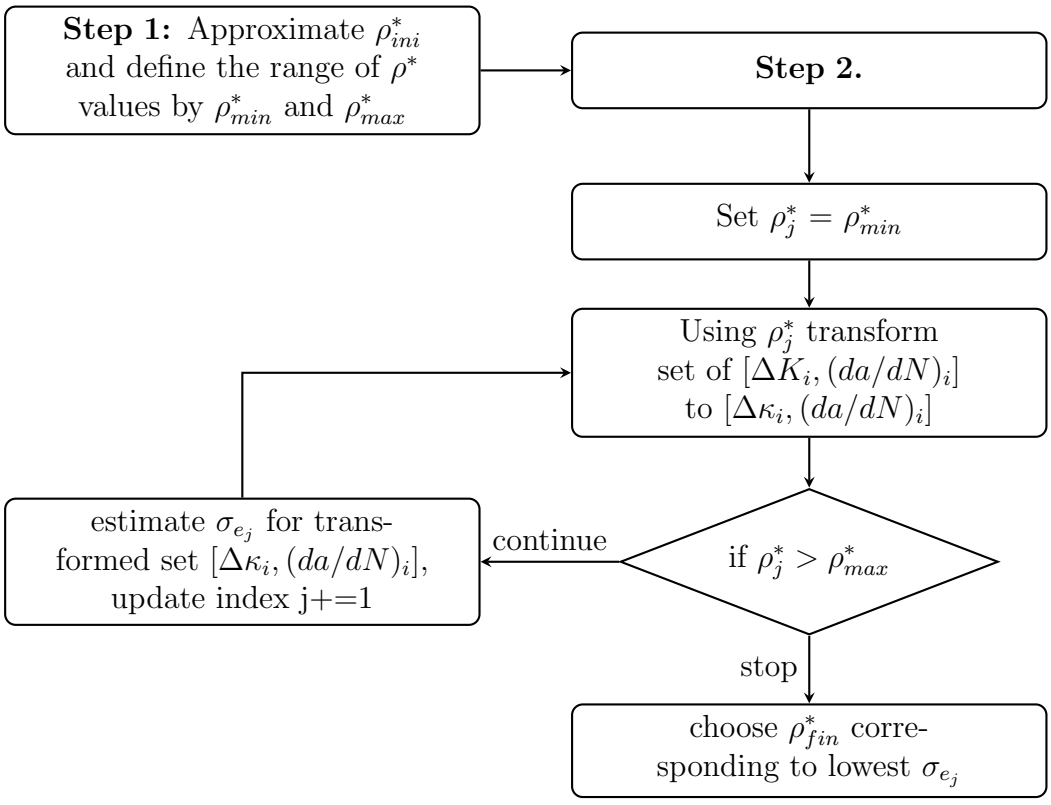

Figure 4.4: The iteration algorithm for determination of the ρ^* parameter.

As it can be seen from the algorithm depiction (Figure 4.4), the new two-step method covers the main deficiencies of the "*transformation method*". First, it narrows the range of potential values of the ρ^* parameter in a way that there is no contradiction with dual nature of this parameter. Second, it uses the statistical approach to evaluate the best collapse of the experimental fatigue crack growth data.

Let's consider now a set of $[\Delta K_i, da/dN_i]$ data points with stress intensity factor range values ΔK_i obtained at various R ratios but with da/dN_i being the same for each subset. As per "*transformation method*", ΔK_i values from the considered set of data theoretically are supposed to transform into the exactly same total driving force $\Delta\kappa_i$ if the ρ^* parameter was correctly identified. However, several practical considerations shall be taken into account:

- measurement precision during the fatigue crack growth experiment
- methods used for transformation from the measured a *vs.* N values to the fatigue crack growth data of form $[\Delta K, (da/dN)]$
- difference in orientation of the grains during the crack propagation

Therefore, it can be concluded that the resultant scatter of the transformed $[\Delta\kappa_i, (da/dN)_i]$ data points is unavoidable. Nevertheless, it is reasonable to assume that ρ^* value at which, the variance in $\Delta\kappa_i$ is minimized correspond to the actual ρ^* value. This assumption yields a criterion for evaluation of the true value of the ρ^* parameter and it is schematically shown in Figure 4.5. The *goodness of collapse*, proposed as a criterion for choosing the ρ^* value, has to be estimated by using the linear regression analysis in log-log scale of the transformed data set.

$$C = \frac{\sum(\Delta\kappa_i)^2 \sum(\frac{da}{dN}_i) - \sum(\Delta\kappa_i)\sum(\Delta\kappa_i \cdot \frac{da}{dN}_i)}{n \cdot \sum(\Delta\kappa_i)^2 - [\sum(\Delta\kappa_i)]^2} = \mu_C \tag{4.4}$$

$$\gamma = \frac{n \cdot \sum(\Delta\kappa_i \cdot \frac{da}{dN}_i) - \sum(\Delta\kappa_i)\sum(\frac{da}{dN}_i)}{n \cdot \sum(\Delta\kappa_i)^2 - [\sum(\Delta\kappa_i)]^2} = \gamma_C \tag{4.5}$$

$$\sigma_\varepsilon = \sqrt{\frac{\sum(\frac{da}{dN}_i)^2 - \mu_C \cdot \sum(\frac{da}{dN}_i) - \gamma_C \sum(\Delta\kappa_i \cdot \frac{da}{dN}_i)}{n-2}} \tag{4.6}$$

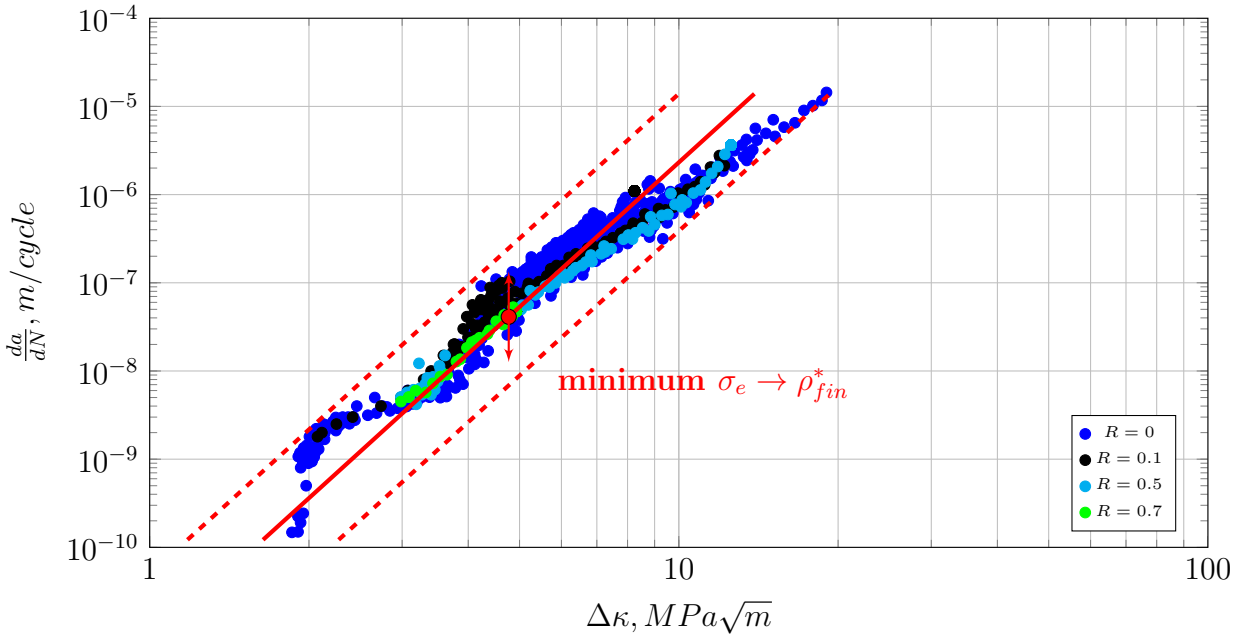

Figure 4.5: Criterion for choosing the ρ^* parameter as shown on the collapsed fatigue crack growth data for the Al 2024-T3 aluminum alloy [25].

4.2.1 Evaluation of the initial value of ρ^* parameter

The method proposed by Noroozi (4.2) was used for finding the initial value of the ρ^* parameter at the beginning of this study. Unfortunately, the lack of required experimental data for the vast amount of materials of interest (such as steel and aluminum alloys) has become a major roadblock for further investigation. Therefore, it was proposed to impose the fracture condition on the first material block ahead of the crack tip (see Figure 4.1) instead of used earlier fatigue crack arrest implication. To start with, theoretical strength of a first material block analogously to equation (4.1) was formulated as a function of the fracture toughness criterion, K_{IC}:

$$\widetilde{\sigma}_{theor} = \frac{K_{IC} \times 1.633}{\sqrt{2\pi\rho^*}} \tag{4.7}$$

Consequently, the initial value of the ρ^* parameter can be expressed as:

$$\rho^*_{ini} = \frac{1.633^2}{2\pi} \left(\frac{K_{IC}}{\widetilde{\sigma}_{theor}} \right)^2 \tag{4.8}$$

Due to the impurity of alloys used in the engineering practice, the value of the the theoretical strength of the material $\widetilde{\sigma}_{theor}$ can only be approximated with a certain degree of precision. For example, for steel alloys $\widetilde{\sigma}_{theor}$ is known to be about $0.1 \cdot E$ [67]. Therefore, this method alone can't be used to evaluate the ρ^* parameter for the fatigue crack growth analysis. Nevertheless, equation (4.8) has been proved very useful [68] for finding the approximate value of the material block size ρ^* since values of the fracture toughness, K_{IC} are known for variety variety of aluminum and steel alloys. Finally, it has been found that the value of the ρ^*_{ini} parameter is very close to the microstructural parameter derived by Kitagawa [69].

4.2.2 The algorithm for the search of the optimum value of the ρ^* parameter

After the value of the ρ^* parameter was approximated by equation (4.8), the optimum value of the parameter ρ^* has yet to be found. It was hypothesized that the true value of the ρ^* parameter can be found within a range spanning over an order of magnitude around ρ^*_{ini}. Therefore, the search range should be bounded by following values: $\rho^*_{min} = 0.1 \cdot \rho^*_{ini}$ and $\rho^*_{max} = 10 \cdot \rho^*_{ini}$. In order to find the actual value of the ρ^* parameter within the search range, it was proposed to use the modified "*transformation method*". As it was already discussed, equation (4.3) doesn't have an analytical solution. Therefore, description of how to transform original fatigue crack growth data $[\Delta K, (da/dN)]$ to the required for the fatigue crack growth analysis $[\Delta\kappa, (da/dN)]$ is of great importance. As per expression (2.22), the total driving force $\Delta\kappa$ can be calculated if the applied stress intensity factor range ΔK, the applied maximum stress intensity factor K_{max} and the residual stress intensity factor K_r are known. While evaluation of the ΔK and K_{max} is a straightforward process, the extrapolation of the residual stress intensity factor K_r is relatively complicated. This is due to difficulties with assessment of the residual stress field generated by the preceded cyclic loading for every given experimental point from the fatigue crack growth data. In general the residual stress intensity factor,K_r can be found by using the weight function method (2.23). While the universal one dimensional weight function $m(x,a)$ has a general form given by equation (4.9), it was shown recently [47] that geometry factors M_1, M_2 and M_3 can be omitted while calculating the residual stress intensity factor, K_r.

$$m(x,a) = \frac{2P}{\sqrt{2\pi(a-x)}}\left[1 + M_1\left(1-\frac{x}{a}\right)^{1/2} + M_2\left(1-\frac{x}{a}\right)^{1} + M_3\left(1-\frac{x}{a}\right)^{3/2}\right] \qquad (4.9)$$

Therefore, equation (2.23) yields to:

$$K_r = \int_0^a \frac{2P}{\sqrt{2\pi\,(a-x)}}\sigma_r dx \tag{4.10}$$

The integral (4.10) is then can be evaluated by using the special procedure described in reference [16]. The resultant residual stress distribution during the fatigue crack growth analysis is estimated on a cycle-by-cycle basis by using the memory rules described in the literature review. On contrary for the evaluation of the ρ^* parameter, information about the effective residual stress profile has to be recovered from the already available experimental data. Thus, it is logical to assume that since distribution of the actual residual stress profiles under the plane-stress and plane-strain conditions are significantly different (as schematically illustrated in Figures 4.6a and 4.6a), then residual stress profiles obtained from thick and thin specimens will also be different.

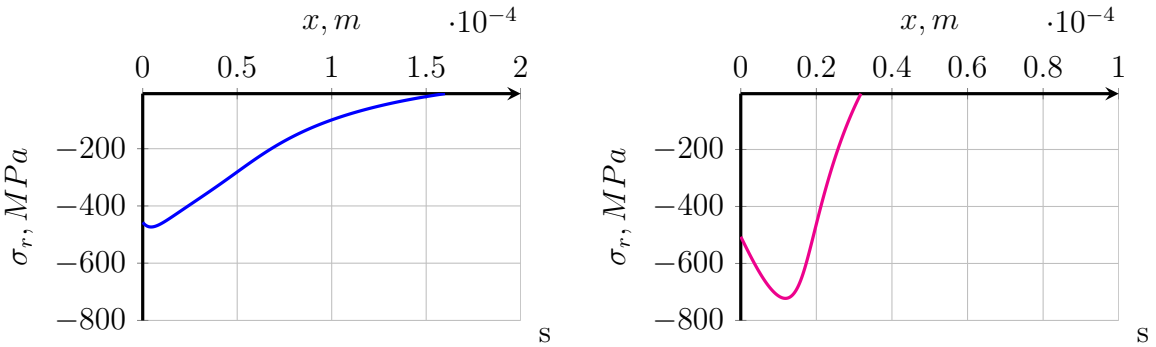

(a) Plane-stress (b) Plane-strain

Figure 4.6: Residual stress distribution under (a) plane-stress or (b) plane-strain condition.

The total residual stress profile as a combination of the single curves can be re-created (see Figure 4.7) if the fatigue crack growth rate $\Delta a/\Delta N$ is known from experimental data. The integration region over which the fatigue crack growth analysis is performed by using

the UniGrow model is defined by the distance X_f. Therefore, integral from equation (4.10) has to be determined over the region of $(a - X_f) \leq x \leq a$.

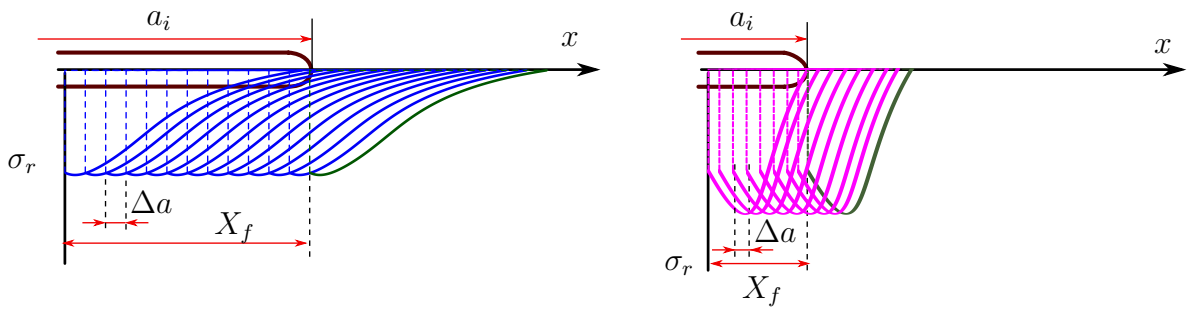

(a) Plane-stress (b) Plane-strain

Figure 4.7: Superposition of residual stress distributions created at the crack tip by subsequent loading cycles ($K_{max} = const$, $\Delta K = const$)

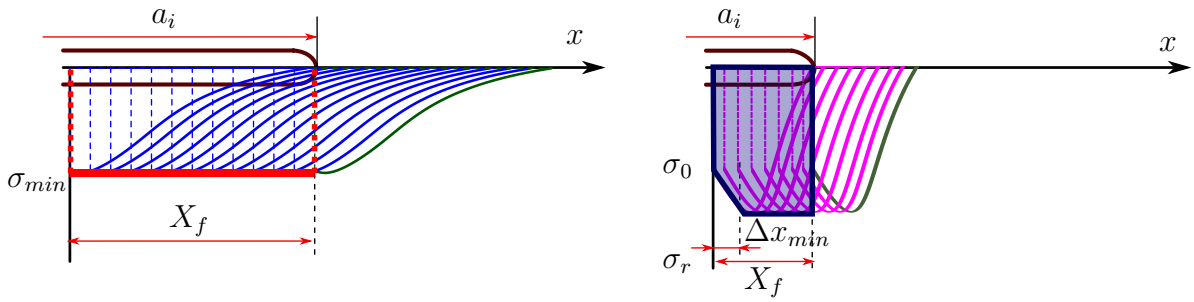

(a) Plane-stress (b) Plane-strain

Figure 4.8: The residual stress profile used for calculating the residual stress intensity factor K_r under (a) the plane-stress and (b) the plane-strain condition.

Studies of available fatigue crack growth data have shown that ratio of $\Delta a/X_f$ can be regarded as infinitesimal. Therefore, integration paths for the specimens under the plane-strain and plane-stress condition can be approximated as shown in Figures 4.8a and 4.8b accordingly.

For the plane-stress condition, residual stress distribution shall be represented by a single red line with the zero slope and intercept being equal to σ_{min} (see Figure 4.8a). Therefore, equation (4.10) can be simplified as:

$$K_r = \int_{a-X_f}^{a} \sigma_{min} \frac{2}{\sqrt{2\pi\,(a-x)}} dx \tag{4.11}$$

After integration, the residual stress intensity factor, K_r yields the following form:

$$K_r = 2\sqrt{\frac{2X_f}{\pi}}\sigma_{min} \tag{4.12}$$

If the basic fatigue crack growth data was obtained from thick specimens with prevailing plane-strain condition near the crack tip, then equation (4.12) won't be exactly applicable for the estimation of the residual stress intensity factor, K_r. Since the ratio of $\Delta a/X_f$ can still be regarded as infinitesimal, the integration path shall be represented by two linear regions (as shown in the Figure 4.8b). The first region is defined by the line with a slope zero and intercept at σ_{min} over the distance from $(a - X_f + \Delta x_{min})$ till a. The Δx_{min} is the distance from the crack tip to the point in the crack body where residual stress reaches the lowest value σ_{min}. The second line have a slope different from zero and can be defined by points $[a - X_f, \sigma_0]$ and $[a - X_f + \Delta x_{min}, \sigma_{min}]$:

$$y = \frac{\sigma_0 - \sigma_{min}}{\Delta x_{min}} \times x + \left[\sigma_0 - \frac{\sigma_0 - \sigma_{min}}{\Delta x_{min}} \times (a - X_f)\right] \tag{4.13}$$

Therefore, the integral for the residual stress intensity factor, K_r in the case of thick specimens with prevailing plane-strain condition near the crack tip was split into two parts:

$$K_r = K_{r,1} + K_{r,2} \tag{4.14}$$

where

$$\begin{aligned} K_{r,1} = &\int_{a-X_f+\Delta x_{min}}^{a} \left[\sigma_{min} \frac{2}{\sqrt{2\pi\,(a-x)}} \frac{\sigma_0 - \sigma_{min}}{\Delta x_{min}} \times x \right] dx + \\ &+ \int_{a-X_f+\Delta x_{min}}^{a} \left[\sigma_0 - \frac{\sigma_0 - \sigma_{min}}{\Delta x_{min}} \times (a - X_f) \right] dx \end{aligned} \tag{4.15}$$

and

$$K_{r,2} = \int_{a-X_f}^{a-X_f+\Delta x_{min}} 2\sqrt{\frac{2X_f}{\pi}} dx \tag{4.16}$$

After solving integrals (4.15) and (4.16) and combining them as stated in equation (4.14), the residual stress intensity factor K_r can be represented as:

$$\begin{aligned} K_r = &2\sqrt{\frac{2(X_f - \Delta x_{min})}{\pi}} \sigma_{min} + \\ &+ \sqrt{\frac{2}{\pi}} \left(X_f \left(A + 2\sigma_0 \right) - \sqrt{3} \times \left(A + \frac{4}{3}\sigma_0 + \frac{1}{3}\sigma_{min} \right) \right) \end{aligned} \tag{4.17}$$

where

$$A = \frac{4X_f \left(\sigma_{min} - \sigma_0 \right)}{3\Delta x_{min}} \tag{4.18}$$

The available from literature da/dN vs. ΔK data can be at this point transformed to the desired da/dN vs. $\Delta\kappa$ form given the ρ^* value. While difference between residual stress profiles obtained under plane-strain and plane-stress conditions is visually clear, the distinction between corresponding residual stress intensity factors, K_r had to be evaluated. Typical residual stress profile obtained in plane-strain condition has the absolute minimum stress approximately two times greater than the one in plane-stress: $|\sigma_{min,p-\sigma}|$ $|\sigma_{min,p-\varepsilon}|$. However, the X_f intercept in plane-stress is much larger than the X_f intercept in the plane-strain condition. Therefore, the relationship between the applied loading given by the stress intensity factor range ΔK and the corresponding residual stress intensity factor, K_r is of great interest. The difficulty with such an analysis is that the solution for the residual stress profile and consequently for the residual stress intensity factor K_r value depends on the assumed radius of the crack tip, ρ^*. For this reason, a large number of plots, such as the one presented in Figure 4.9 for the aluminum alloy Al 2024-T3 and $\rho^* = 1.2e-05$ $[m]$, were constructed. The data revealed, that the difference between the residual stress intensity factor K_r obtained under the plane-stress and plane-strain conditions didn't exceed 15%. That proves that the concept of the ρ^* as a material parameter holds relatively well, since the value of this parameter does not depend on the loading conditions nor the thickness of the specimen.

4.3 The effect of the chosen value of the ρ^* parameter on the fatigue crack growth analysis

The two-step procedure for the evaluation of the ρ^* parameter described above is computationally tedious and time consuming. That is why, it was implemented into the special software package called "*The ρ^* program*" (see Figure 4.10).

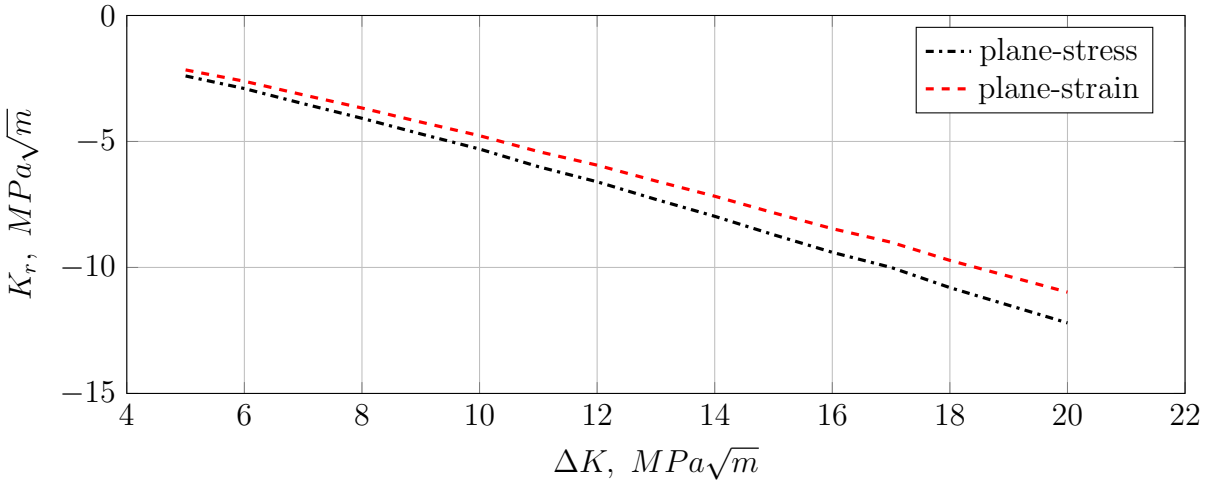

Figure 4.9: The $\Delta K - K_r$ relationship for plane-strain and plane-stress formulations obtained for Al 2024-T3 aluminum alloy ($R = 0$).

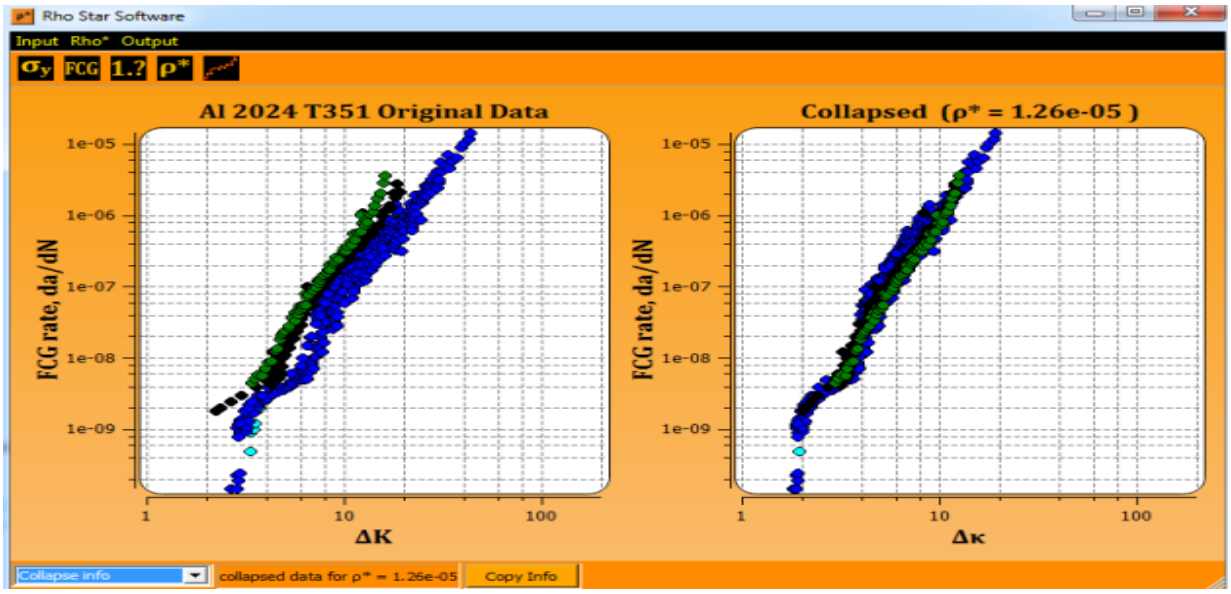

Figure 4.10: Graphic User Interface of "*The ρ^* program*"

The ρ^* computer program takes as a first input data set, the required material data such as Young's modulus, E, Poisson's ratio, ν, the yield stress, σ_{ys} and Ramberg-Osgood coefficients $K^{'}$ and $n^{'}$. With the second input data set, the program requires upload of the set of experimental fatigue crack growth data of $[\Delta K, (da/dN)]$ form obtained at various stress ratios R. Once the data is supplied, the program is able to perform the two-step procedure described earlier and to determine the value of the ρ^* parameter.

A number of values of the ρ^* parameter obtained for variety of materials is given in Table 4.1. These ρ^* values were successfully used for the fatigue crack growth analysis and for the model validation purposes.

Table 4.1: Values of the ρ^* parameter for a variety of materials

Material	$\rho^*,\ m$	E, MPa	ν	$\sigma_{ys},\ MPa$	$K^{'},\ MPa$	$n^{'}$
Al 2024	$1.26E-05$	73100	0.33	428	662	0.070
Al 2219	$9.00E-05$	71000	0.33	350	709	0.121
Al 2324	$2.02E-06$	74400	0.33	425	745	0.090
Al 7050	$1.23E-05$	71000	0.33	329	510	0.071
Al 7075	$9.70E-06$	71000	0.33	504	899	0.093
Al 7475	$3.20E-05$	71000	0.33	460	675	0.059
Hy Tuf Steel	$1.36E-05$	202600	0.3	1270	2850	0.13
A36 steel	$4.00E-05$	190786	0.3	324	991	0.18

4.3.1 Evaluation of $[C_i, \gamma_i]$ parameters

After the ρ^* program completes the iterative process, in addition to the found ρ^*_{fin} value, the corresponding set of $[\Delta\kappa, (da/dN)]$ appears in the program interface. The purpose of it is two-fold: first, it is done, so the user could confirm that there are no discrepancies and second, more importantly, so the $[C_i, \gamma_i]$ parameters can be estimated from the collapsed data. The fatigue crack growth coefficients $[C_i, \gamma_i]$ are nothing but piecewise linear approximation of the $\frac{da}{dN} - \Delta\kappa$ relationship in the log-log scale and they are essential for any further fatigue crack growth analysis. With the next step, the program authorizes user to define for how many linear pieces the data set have to be "*cut*" (see Figure 4.11). Then, by using the linear regression method (4.4), (4.5), set of the $[C_i, \gamma_i]$ parameters are being evaluated. As an example, the result of transformed fatigue crack growth data obtained from Al 2024-T3 aluminum alloy is presented in Figure 4.12.

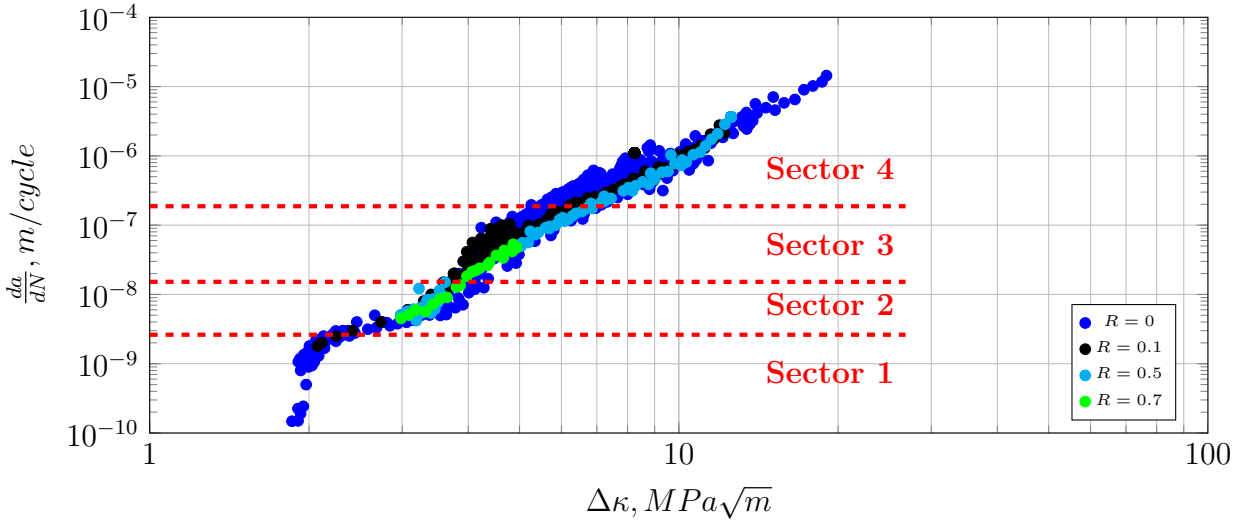

Figure 4.11: Segmentation of the collapsed fatigue crack growth data set obtained for the Al 2024-T3 aluminum alloy [25].

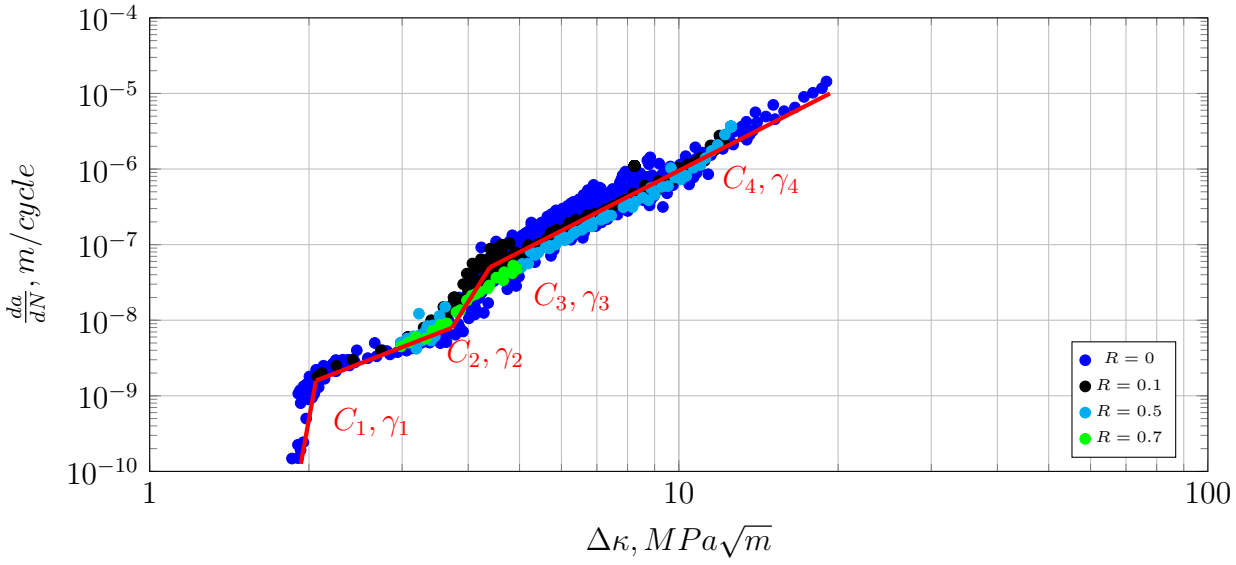

Figure 4.12: Segmentation of the collapsed fatigue crack growth data set obtained for the Al 2024-T3 aluminum alloy [25] and fitted $da/dN - \Delta\kappa$ curves.

4.3.2 The significance of the ρ^* parameter

Once the procedure for evaluation of the ρ^* parameter was established, it was of interest to analyze the effect of the chosen ρ^* value on the fatigue crack growth simulations. Since relationship between value of the ρ^* parameter and results of fatigue crack growth predictions is quite complex, following considerations have preceded numerical studies. From one side, it was obvious that the profile of residual stress distribution will depend on the chosen value of the crack tip or the ρ^* value. From other side, fatigue crack growth coefficients $[C_i, \gamma_i]$, are also dependent on the chosen value of the ρ^* parameter. The test of how sensitive fatigue crack growth analysis on the value of the ρ^* parameter was performed on variety of materials such as Al 2024-T3 and Al 7075-T6 aluminum alloys, St4130 and A36

steel alloys and etc. For demonstration purposes experimental fatigue crack growth data obtained from Al 2024-T3 aluminum alloy [5] (see Figure 4.15a) will be used. The value of the ρ^* parameter for Al 2024-T3 was found from "*The ρ^* program*": $\rho^*_{fin} = 1.26e-05$. To test how sensitive the fatigue crack growth predictions will be it was proposed to use 200 evenly spaced values of the ρ^* parameter within the $\pm 50\%$ range around $\rho^*_{fin} = 1.26e-05$.

To start with, the dependance of the residual stress distribution profile on chosen values of the ρ^* parameter is demonstrated in Figure 4.13. In this figure residual stress distributions ahead of the crack tip were obtained for Al 2024-T3 aluminum alloy under imposed plane-stress condition by using the ESED method. It should be noted that the data plotted in Figure 4.13 was obtained from the stress analysis program (see Figure 3.7).

In order to demonstrate the dependency of C_i value on the value of the ρ^* parameter, the same range of the ρ^* values was considered. For 200 evenly spaced values of the ρ^* parameter within this range, the transformation procedure described above was applied for the fatigue crack growth data obtained at various R ratio from Al 2024-T3 aluminum alloy specimens. Thereafter, 200 sets of $[C_i, \gamma_i]$ parameters were evaluated. Finally, the dependency of C_i value on the value of the ρ^* parameter in form of a histogram of C_3 values is presented in Figure 4.14.

When 200 sets of $[C_i, \gamma_i]$ parameters corresponding to the 200 values of the ρ^* parameter were available, it became possible to perform numerical studies, i.e. to run 200 fatigue crack growth simulations using the UniGrow model. The results then were stored and subjected to the graphical analysis. Figure 4.15 represents a typical outcome of such analysis. Such studies were done for variety of the aluminum and steel alloys and the general conclusion is that ρ^* value has no or very little impact on fatigue crack growth predictions. It can be also concluded that proposed two-step procedure for estimation of the ρ^* parameter is very effective.

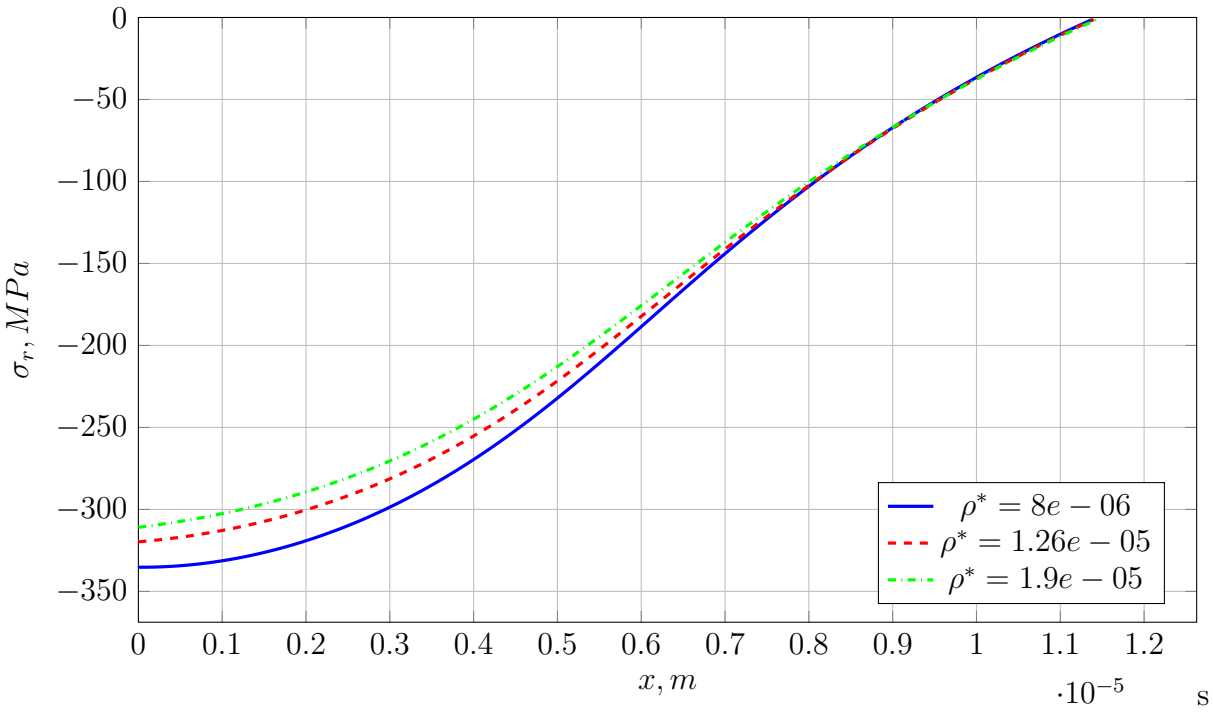

Figure 4.13: Residual stress distribution obtained for various ρ^* values

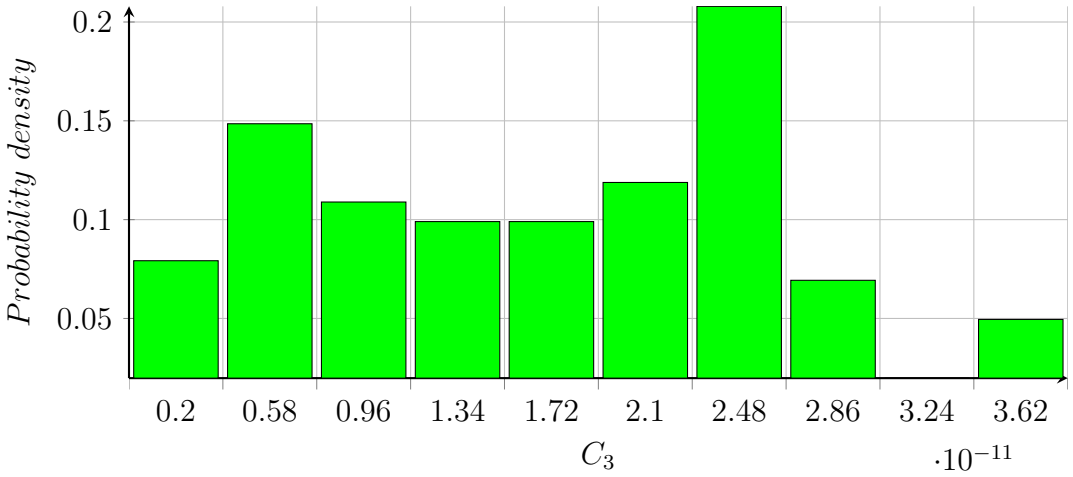

Figure 4.14: Spread of C_3 values obtained for the analyzed range of ρ^* values

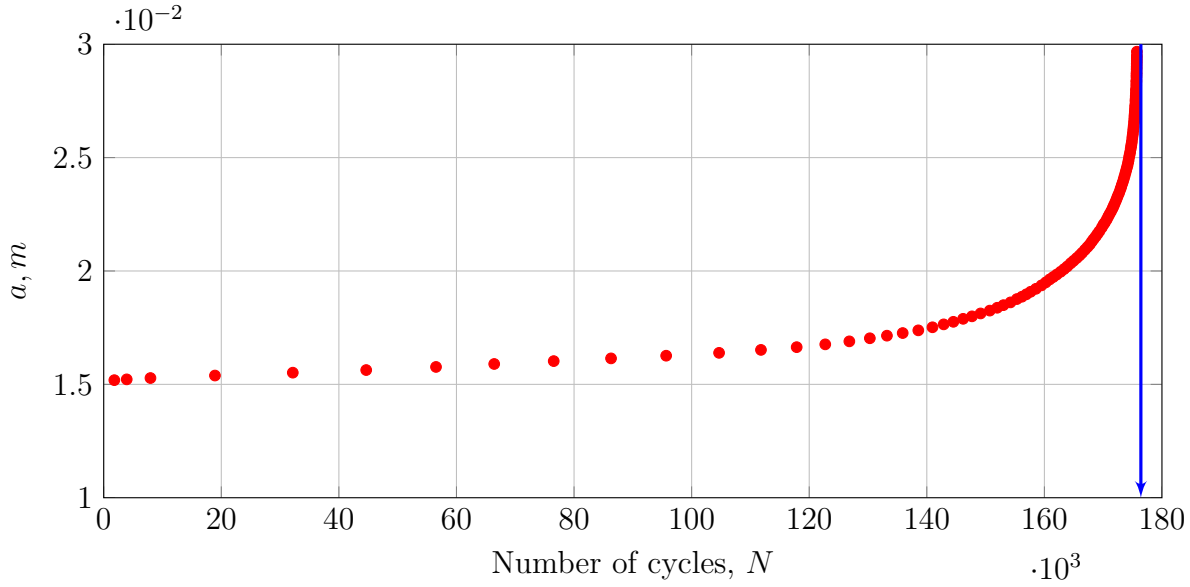

(a)

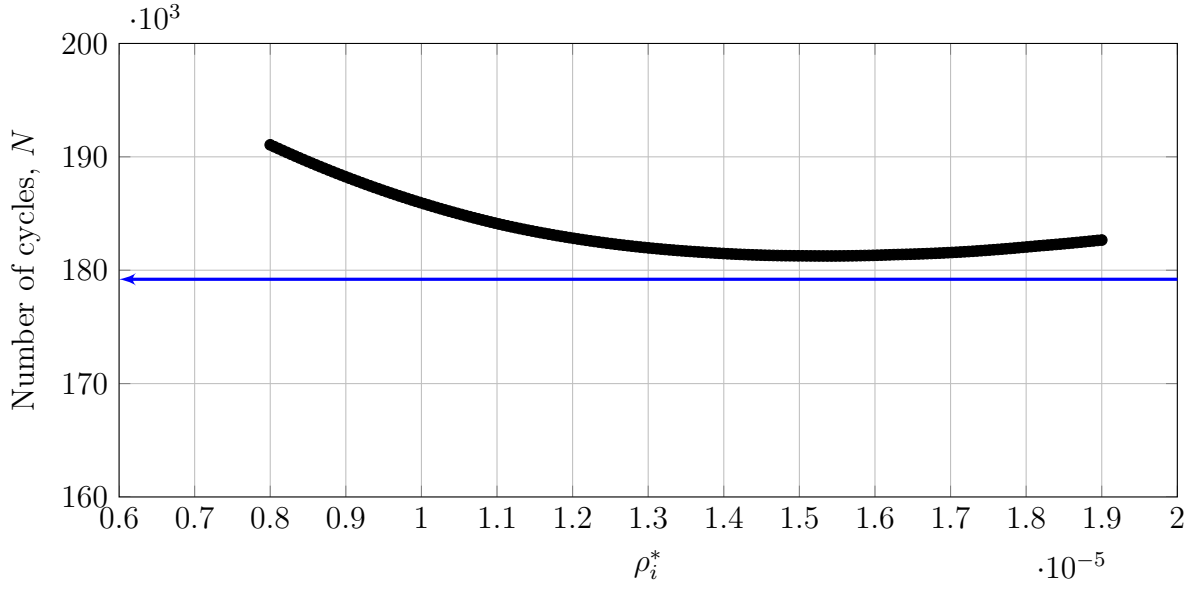

(b)

Figure 4.15: Fatigue lives (b) as a function of the effective crack tip radius, ρ^*obtained for experimental fatigue crack growth data of Al 2024-T3 aluminum alloy (a) [5]

Chapter 5

Probabilistic analysis of the fatigue crack growth

A lot of efforts have been put into improvement of the UniGrow fatigue crack growth model. Nevertheless, in spite of all the changes and modifications, the UniGrow as well as any other deterministic fatigue crack growth model will still fail to make a "*ideal*" prediction of the fatigue live without some degree of luck. The reason for that is as follows. Every available fatigue crack growth model relies on experimental data of the $da/dN = f(\Delta K, K_{max})$ form. Such data, in turn, is known [5] to contain a significant amount of scatter (see for example Figure 4.2b). Therefore, the fatigue life forecast accuracy depends not only on how good the fatigue crack growth model is, but also on the model ability to account for the scatter of experimental data. The scatter inherent to the crack propagation can be further categorized into the scatter resultant from a single experiment and scatter from a series of identical tests. The former can be defined as deviation of the crack path from a smooth line during the fatigue crack growth experiment and the latter is represented by completely different fatigue lives of two or many identical specimens (see examples of both in Figure 5.1).

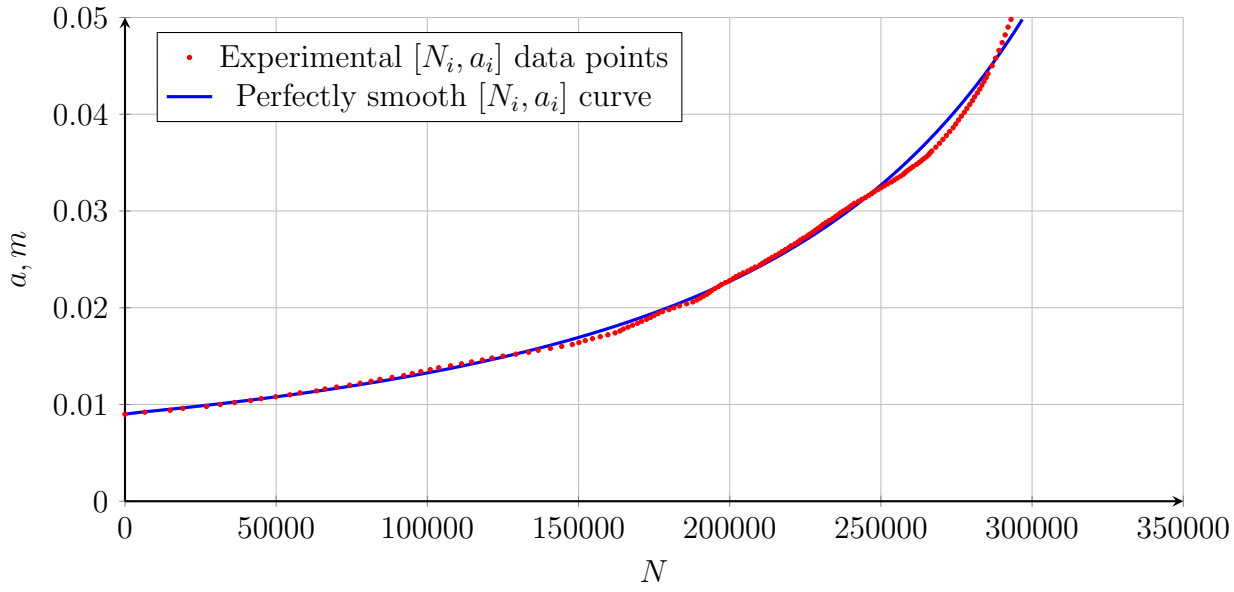

(a) Illustration of the intraspecimen scatter

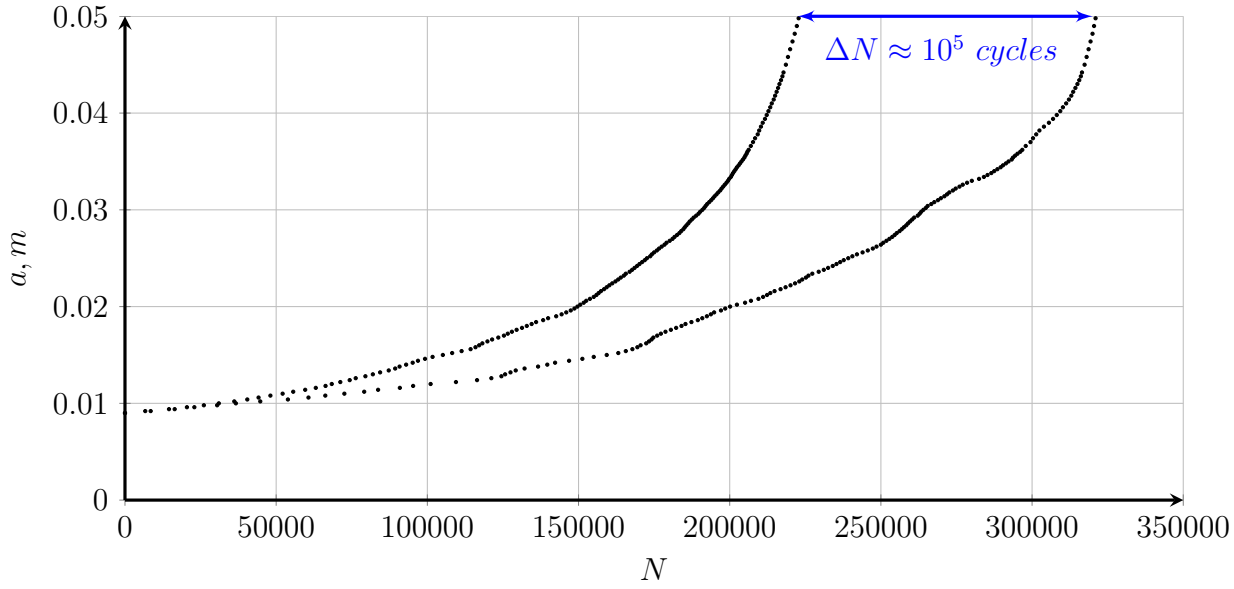

(b) Illustration of the interspecimen scatter

Figure 5.1: Examples of the intraspecimen and interspecimen variability of fatigue crack growth data obtained for Al 2024-T3 aluminum alloy [4]

5.1 Impracticality of the Random Process approach to fatigue crack growth modeling

Two methodologies are known for predicting of the random nature of the fatigue crack growth. The first one is called the random process method and the second one is called the random variables method. These methodologies are conceptually different, and therefore the choice of one over another has to be justified. The main advantage of the random process approach is that it is able to account for interspecimen variability by reproducing the erratic behavior of propagating cracks. Superiority of the random variables method is due to fact that models based on this approach:

- are able to account for variability of all input parameters (material, geometry, etc.);
- depend on the input distributions which are relatively easy to obtain;
- have a reduced complexity.

In spite of the apparent advantage of random variables approach, variety of stochastic fatigue crack growth models based on random process formulations have been proposed in recent years. Such random process models [70, 71, 72, 73] are usually based on complicated statistical formulations in combination with the "*Paris law*" (2.1). Unfortunately, the material fatigue crack growth model proposed by Paris [74] is known to be a simplification and consequently it is insufficient for some engineering applications. Therefore it is not obvious why to use complicated statistical formulations in combination with a "*weak*" material model, which is not able to provide adequate results.

Choice of the random process approach over the random variables one can only be justified for cases when it is important to account for the scatter within a single specimen. Therefore, assessment of the intraspecimen variability for the representative set of fatigue crack growth experimental data had to be done. To start with, let us define the intraspecimen variability. The intraspecimen variability is an average deviation of experimental fatigue crack growth data points around the smooth curve. This smooth curve represents the crack propagation in homogeneous media and can be obtained through fatigue crack growth modeling or from fit of experimental data to equation (5.1):

$$y = A + \frac{B}{x} + C \cdot \ln(x) \tag{5.1}$$

where $y = (N_i - N_1)/1000$, $x = a_i/a_1$ and A, B and C are fit coefficients. The formulation above was derived by McCartney et al. [75] in 1971 as an equation for the crack propagation in a homogeneous media. In order to demonstrate, how equation (5.1) can be used, let's consider fatigue crack growth data set, $[N_i, a_i]$ obtained from a constant amplitude fatigue crack growth experiment [3] and presented in Figure 5.2. The material tested was the Al 7075-T6 aluminum alloy. A fit of experimental $[N_i, a_i]$ data was obtained by using the multiple regression analysis and it is also presented in Figure 5.2. Coefficients of equation (5.1) according to this fit were $A = 69.03$, $B = -67.91$ and $C = -2.50$. It is important to note that the fitted curve in this analysis can be viewed as representation of the perfect prediction of the fatigue crack growth experiment. From the visual analysis of the data (Figure 5.2) it can be concluded that distinction between fitted curve and experimental points is imperceptible. Nevertheless, there are no prove yet that interspecimen variability doesn't need to be accounted for.

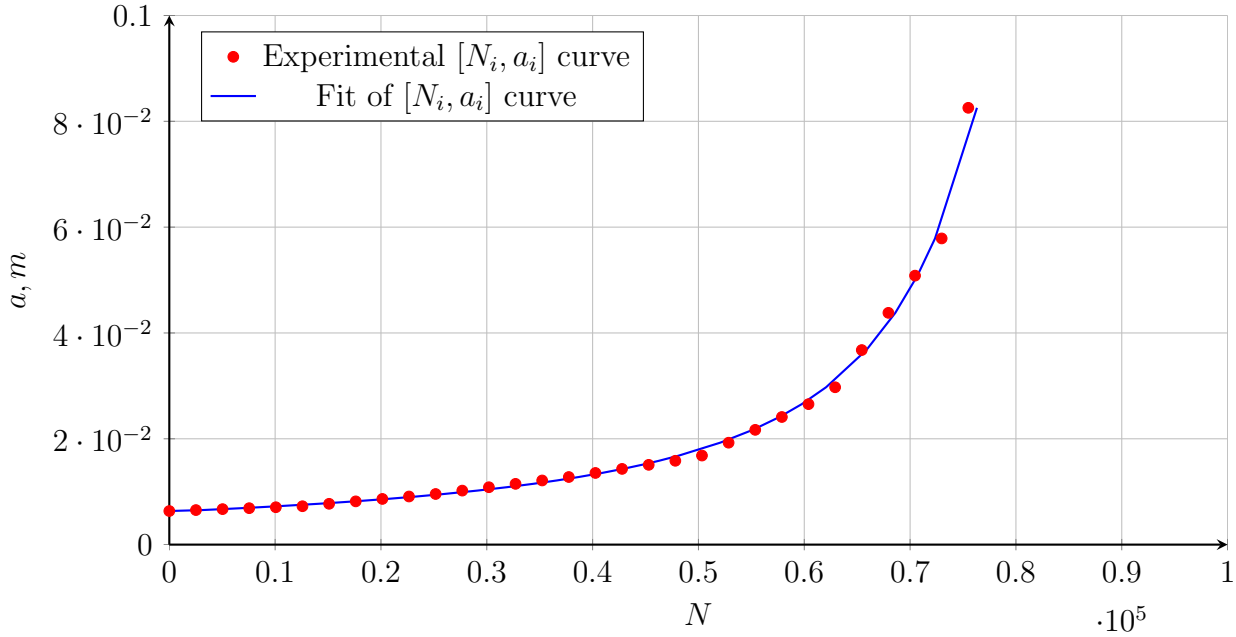

Figure 5.2: Experimental fatigue crack growth data [3] for Al 7075-T6 aluminum alloy and the corresponding curve fit (5.1).

The next step was to test the significance of the interspecimen variability on the basis of representative fatigue crack growth data set. The chosen set consisted of a large amount of experimental fatigue crack growth data obtained for aluminum [4, 3, 6] and steel [5] alloys. The analysis has started from fitting of the equation (5.1) into every experimental fatigue crack growth curve of $[N_i, a_i]$ form. Then, collection of residuals (difference between the number of elapsed cycles N_i coming from the experiment and fitted curve):

$$N_{i,res} = |N_{i,exp} - N_{i,fit}| \tag{5.2}$$

was aggregated for every given fatigue crack growth curve. After that, average value of residuals for every single fatigue crack growth experiment, $\mu N_{i,res}$ was calculated and

stored. The resultant collection of $\mu N_{i,res}$ values was used for assessment of the intraspecimen variability importance. As an example, result of analysis for the Al 2024-T3 aluminum alloy [4] is presented in Figure 5.3. The histogram shown in this Figure represents the typical distribution of $\mu N_{i,res}$ values.

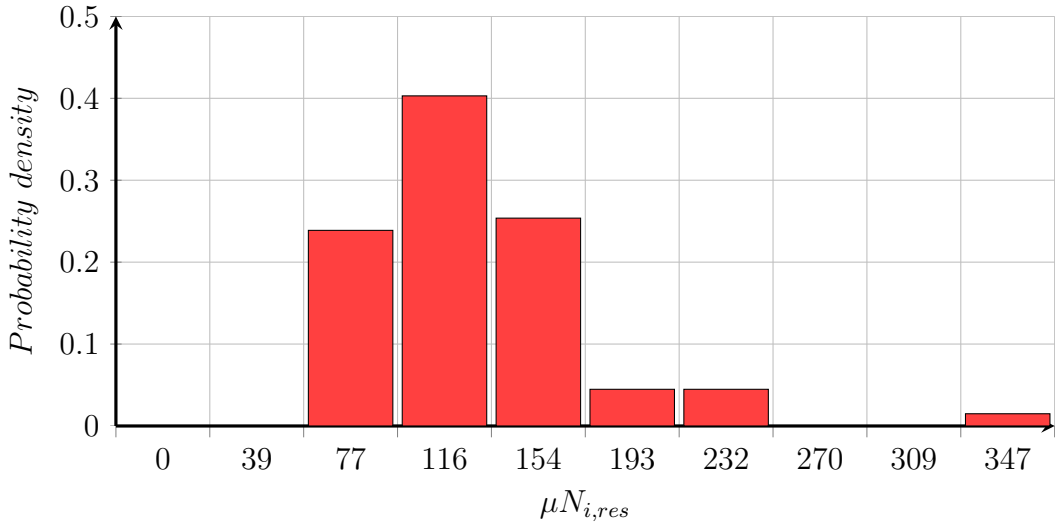

Figure 5.3: Histogram of the $\mu_{N_{i,res}}$ values for Virkler data [4]

Mean values of distributions similar to the one shown in Figure 5.3 were used to assess whether it is important or not to account for the "*within the specimen*" variability in fatigue crack growth modeling. These mean values obtained for aluminum alloys were estimated to be less than 1000 cycles for and less than 650 cycles for steel alloys. Since typical span of fatigue crack growth results for the mean life of 250×10^3 cycles can reach 100×10^3 cycles, the intraspecimen variability can be regarded as negligible. It can be concluded that the intraspecimen variability has little influence on the goodness of the fatigue crack growth predictions and can be neglected in the statistical modeling of the fatigue crack growth. Therefore, it was concluded that random variables modeling is preferable for the probabilistic fatigue life analysis.

5.2 Studies of the UniGrow model bias

The use of random variables approach has been justified at this point of studies. Nevertheless, before the UniGrow fatigue crack growth model could be turned into the random variables model, it had to be tested for the bias. To begin with, it is important to define what constitutes the bias for an arbitrarily chosen deterministic fatigue crack growth model. In general, the bias is defined as an inclination or prejudice for or against one thing or person. In the context of fatigue life analysis the presence of bias implies that predictions of the number of cycles to failure, N_f are predominantly over or under predicted. The first parameter proposed for the assessment of chosen fatigue crack growth model bias was the difference between experimental and predicted values of number of cycles to failure, ΔN_f. The downside of this descriptor is that it uses absolute values. This means that $\Delta N_f \approx 10^3$ cycles might be considered as the large difference in case of relatively short total fatigue life of let's say $N_f = 10^4$. In the same time $\Delta N_f \approx 10^3$ for the fatigue life of $N_f = 10^6$ cycles can be regarded as infinitesimal. Therefore, it was proposed to use the ratio of $\Delta N_f / N_{f,exf}$ for the bias assessment, where the value of $N_{f,exp}$ in a modified descriptor is a number of cycles to failure obtained from the fatigue crack growth experiment.

There are many factors which might impact the fatigue crack growth analysis and consequently interfere with evaluation of the UniGrow model bias. The highest impact is known to come from the variability of material resistance to fatigue crack growth from specimen to specimen [4]. In order to minimize such interference, it was proposed to use the "*closed*" cycle for assessment of the bias. The closed cycle analysis consists of following four steps:

1. Transform available fatigue crack growth data from $[N_i, a_i]$ to $[\Delta\kappa_i, (da/dN)_i]$ form
2. Use the $[\Delta\kappa_i, (da/dN)_i]$ data to estimate the specimen-specific $[C_i, \gamma_i]$ parameters
3. Perform fatigue life analysis using the evaluated $[C_i, \gamma_i]$ parameters
4. Compare the result against original $[N_i, a_i]$ data set

Such analysis is obviously not practical for design purposes but it is sufficient for determination of whether the UniGrow model is biased. Since aluminum and steel alloys are known to exhibit slightly different fatigue crack growth behavior, it was decided to use both types of material for validation purposes. Sets of experimental fatigue data obtained from round-robin studies [5] for the St 4130 steel and 2024-T3 aluminum alloys were chosen for the analysis of UniGrow bias. As a result, the ratio $\Delta N_f/N_{f,exp}$ was assembled into the histogram shown in Figure 5.4. The difference between experimental and predicted values of number of cycles to failure, ΔN_f is negative for cases when UniGrow model under-predicted the results of experiments and positive otherwise.

It can be concluded from the performed analysis that by using the closed cycle UniGrow model is able to reproduce the fatigue crack growth experiment with an average of $\Delta N_f/N_{f,exp} \approx -2\%$. It means that fatigue crack growth experiments are on average slightly under-predicted but descriptor values aren't significant to consider the UniGrow model as biased. Therefore, there is no need to implement a bias correction for the combination of deterministic fatigue crack growth model UniGrow with the "Monte-Carlo" simulation method.

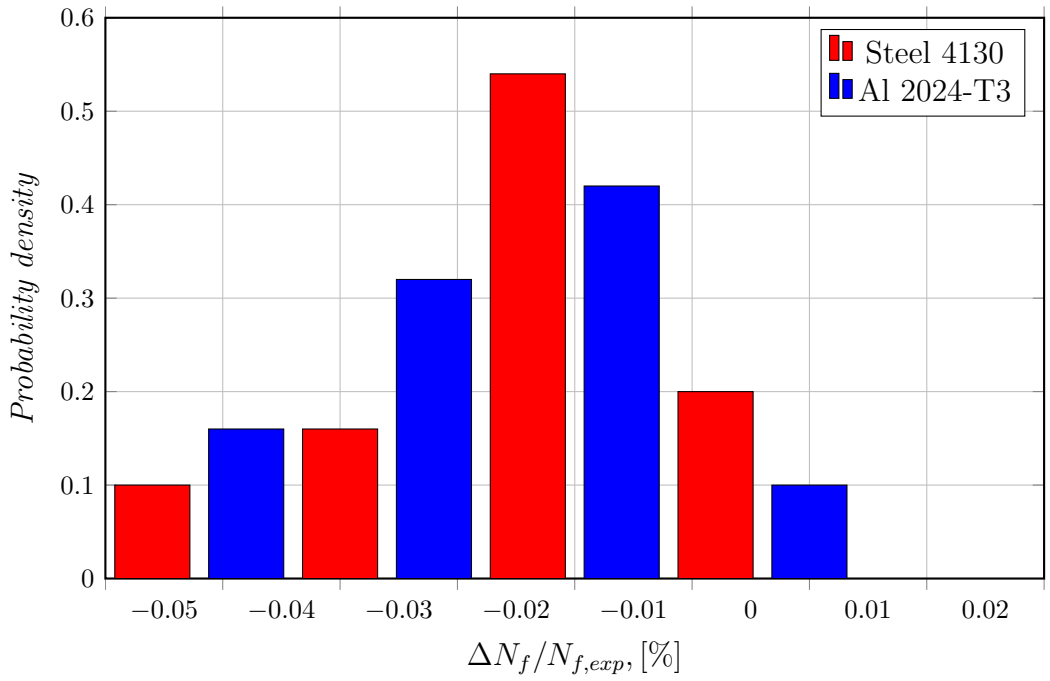

Figure 5.4: Histograms of the $\Delta N_f/N_{f,exp}$ values for the St 4130 steel and Al 2024-T3 aluminum alloys.

5.3 Combination of the "Monte-Carlo" method with the UniGrow fatigue crack growth model

After the UniGrow model was shown to be unbiased, it became ready for turning itself into the random variables model through combination with the "Monte-Carlo" simulation method. The "Monte-Carlo" simulation method is a multipurpose statistical tool which can be used to solve different problems. In the case of statistical fatigue crack growth modeling it can be used to perform multiple numerical experiments and obtain required information for subsequent reliability analysis. The desired information is usually gathered by continuous repetition of following steps:

1. Sample the input parameter value from its probability distribution

2. Pass the sampled number to the deterministic model

3. Apply the deterministic model and generate the target answer

4. Save the result and repeat the procedure

The "Monte-Carlo" simulation method essentially enables the replacement of the deterministic value of the input parameter by its probability distribution. Therefore, it can be concluded that success in implementation of the "Monte-Carlo" simulation method depends on: input parameters chosen for sampling and established sampling procedure. Let's start from review of the input required for the fatigue crack growth analysis based on the deterministic UniGrow model. The necessary input can be broken down to three categories schematically shown in Figure 5.5: material properties, loading history and geometry.

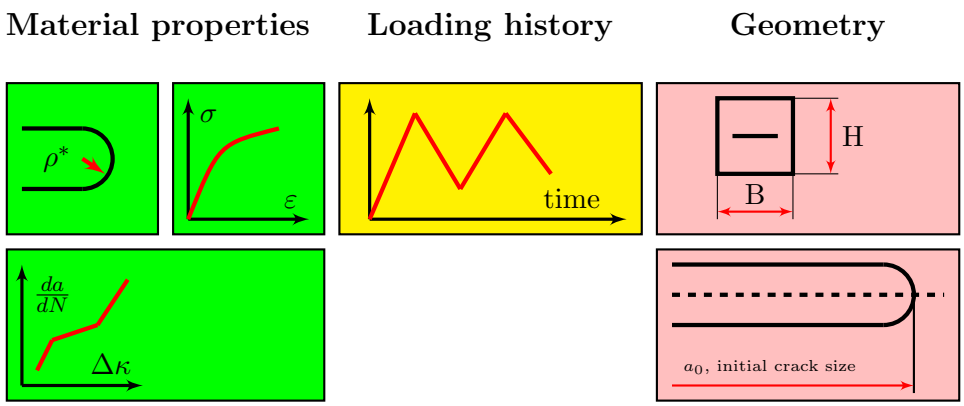

Figure 5.5: Summary of the input data needed for the fatigue crack growth analysis

The first category can be subsequently split into a set of fatigue crack growth coefficients: $[C_i, \gamma_i]$, the material block size, ρ^* and parameters of the Ramberg-Osgood cyclic stress-strain curve: $E, \nu, \sigma_{ys}, K^{'}, n^{'}$. The second category is represented by a continuous set of loading pairs $\{\Delta S_i, S_{max,i}\}$. The third category, consists of initial crack size a_0 and set of the global geometry parameters, such as thickness and width. Using the random variables approach it is possible to change every parameter with its probability distribution. Nevertheless, implementation of every single input variable as a probability distribution can result in unnecessary complicated model which will be impossible to validate. Therefore, only two types of parameters were considered for randomization. The first one is the set of the C_i values from $[C_i, \gamma_i]$ fatigue crack growth coefficients. The second is the initial crack size a_0. All other necessary for fatigue crack growth modeling input parameters were kept deterministic.

Implementation of the loading history in form of the random process won't be considered because it doesn't impact the essence of the UniGrow fatigue crack growth model formulation. It can be added later, if needed, on top of the existing combination of the UniGrow model with the "Monte-Carlo" simulation method. Scatter of Ramberg-Osgood parameters is insignificant and therefore can be disregarded. The only parameter left for discussion is the material block size, ρ^*. It was shown in previous chapter that set of $[C_i, \gamma_i]$ coefficients depends on the value of the ρ^* parameter. Therefore, assumption of the ρ^* parameter as a random variable will make a modeling unnecessary complex. It was also shown (see Figure 4.15b) that dependence of the fatigue crack growth prediction on the value of ρ^* parameter is insignificant. Therefore, it was decided to keep the value of the ρ^* parameter deterministic.

5.3.1 Uncertainty of the material data

Series of statistical fatigue crack growth experiments performed by Virkler and Ghonem [4, 6] have revealed that no matter how precise the experimental measurements are, the number of cycles, N_f required for crack to propagate from the precisely determined initial length, a_0 to the final crack size, a_f will vary significantly. The desired outcome of random variables modeling for case when the initial crack size is precisely determined should look as shown in Figure 5.6.

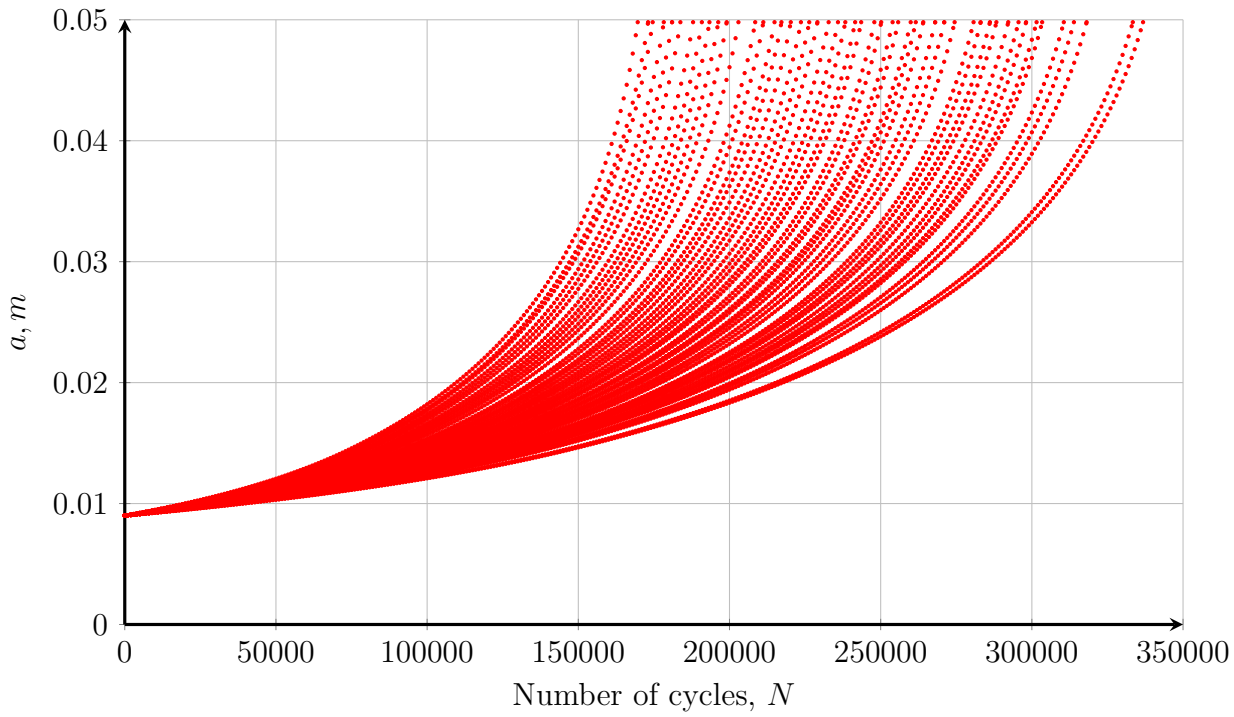

Figure 5.6: Simulation results based on the combination of the UniGrow model with the "Monte-Carlo" simulation method of Virkler experimental data [4].

The UniGrow deterministic procedure for predicting fatigue crack growth lives is based on the fatigue crack growth expression given in the form:

$$\begin{aligned}\frac{da}{dN} =& C_i \left(\Delta\kappa\right)^{\gamma_i} = C_i \left[K^p_{max,tot} \times \Delta K^{1-p}_{tot}\right]^{\gamma_i} = \\ =& C_i \left[\left(K_{app,tot} + K_r\right)^p \times \left(\Delta K_{app} + K_r\right)^{1-p}\right]^{\gamma_i}\end{aligned} \tag{5.3}$$

The set of $[C_i, \gamma_i]$ coefficients in the UniGrow model represents the scattered fatigue crack growth data in the form $[\Delta\kappa, (da/dN)]$. It was hypothesized that the intraspecimen variability can be described by the probability distributions of $[C_i, \gamma_i]$ parameters. In the previous chapter it was shown how to obtain set of these coefficients given the collapsed experimental fatigue crack growth data of $[\Delta\kappa, (da/dN)]$ form. Statistical analysis of various sets of constant amplitude fatigue crack growth data also indicated that the scatter of the γ_i exponent was small in comparison with the scatter of the C_i parameter. Therefore, it was concluded that since γ_i parameter does not vary, scatter of predicted fatigue crack growth propagation lives depends predominantly on the scatter of the C_i parameters. This assumption was validated based on the available experimental statistical fatigue crack growth data [4, 6].

It is well-known that the amount of crack extension per number of applied stress cycles, da/dN, fluctuates around the least-squares regression line. However, in most cases three or four pairs of $[C_i, \gamma_i]$ coefficients are needed to fit the experimental data accurately (see Figure 5.7). In order to obtain the desired probability distributions of C_i parameters two types of data can be used. The first type is the statistical fatigue crack growth data such as was obtained by Virkler [4] and Ghonem [6]. The second type is fatigue crack growth data obtained under different stress R ratios from various laboratories. Let's review the difference between two. To start with, availability of the experimental data in

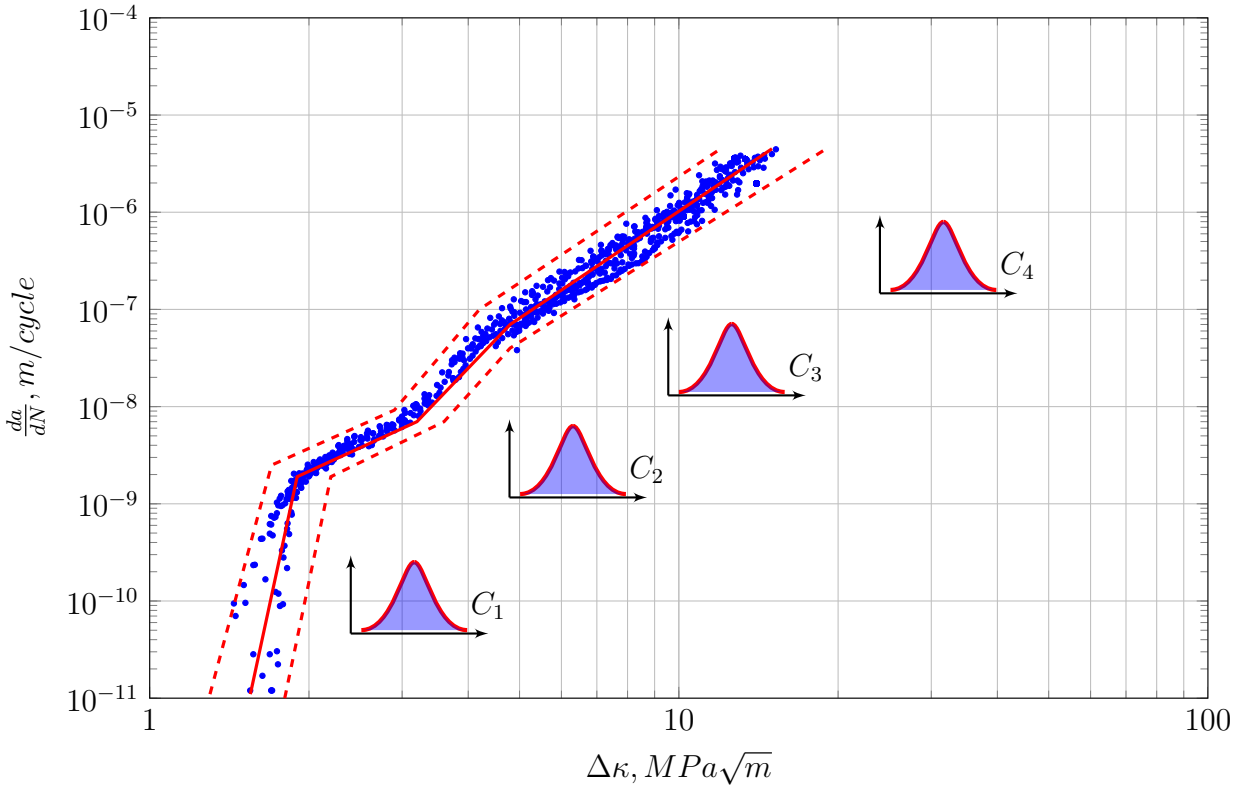

Figure 5.7: Schematic representation of the material scatter on the basis of available fatigue crack growth data obtained from Al 7075-T6 aluminum alloy

open sources of information is significantly different. The data of second type is widely available. Statistical fatigue crack growth data, in turn, is rare and thus has to be obtained from the new tests, which are costly and time consuming. Another limitation of available statistical fatigue crack growth data [4, 6] is the fact that material tested comes from a single production batch of analyzed material. In practice, material used by manufacturers comes continuously from different working shifts and suppliers. Therefore, the resistance of material to fatigue crack propagation will vary from batch to batch. On contrary, the same by nomenclature material tested in different laboratories by using a standard experimental

setup comes from variety of suppliers and therefore, it is more representative in terms of batch to batch variability.

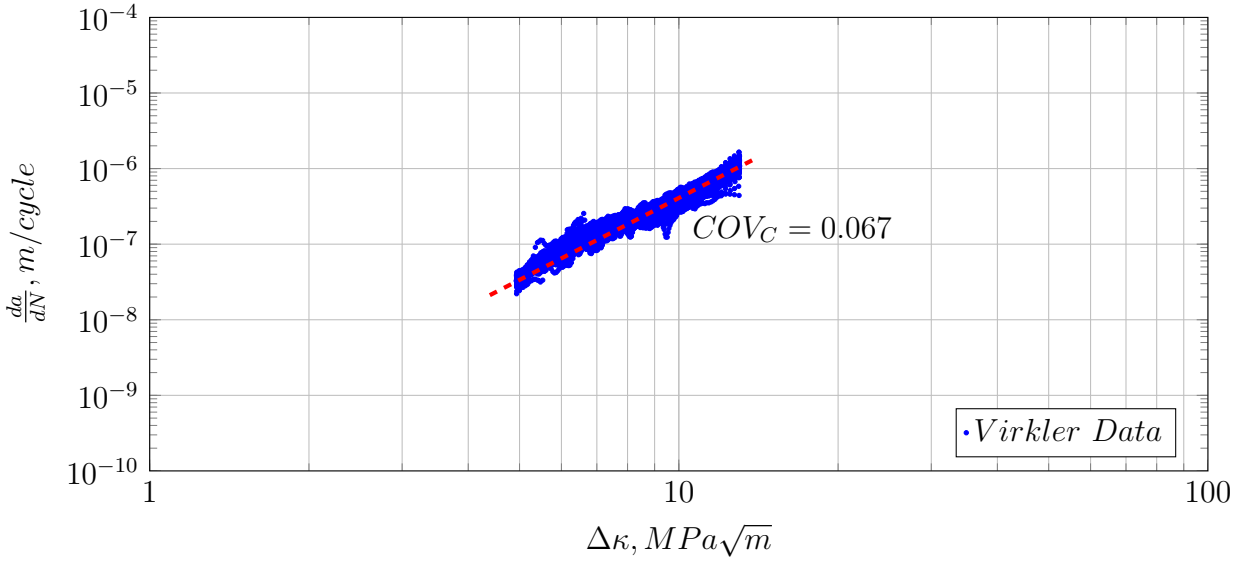

Figure 5.8: Transformed fatigue crack growth data from Virkler studies [4]

Comparison of fatigue crack growth constants obtained from the Ghonem and Virkler data alone with the fatigue crack growth constants obtained from the variety of laboratories has revealed that there is no significant difference. The coefficient of variation of the fatigue crack growth constant, σ_{C_i}/μ_{C_i}, for the Virkler data, Al 2024-T3, (see Figure 5.8) was 0.067 while the data obtained from the different fatigue crack growth studies (see Figure 5.9) was about 0.09. Since mean values of C_i parameter are approximately of the same value for both cases, this increase in the spread could be characterized as data being slightly more dispersed. It is impossible to compare coefficients of variation in other regions of the fatigue crack growth curve, therefore even if the above assumption holds, the results of the crack growth simulations in the threshold region should be treated with care. Since there is no significant difference between the scatter of fatigue crack growth parameters obtained

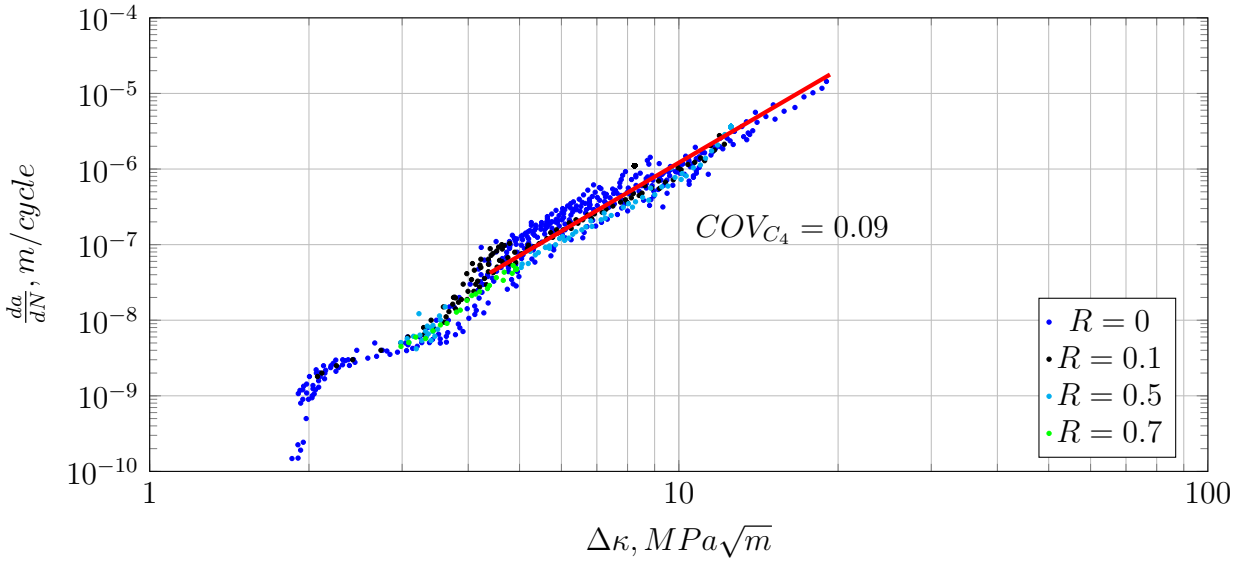

Figure 5.9: Collapsed fatigue crack growth data from different laboratories [25]

from statistical studies [4, 6] and the ones obtained from different laboratories [5, 66, 25], it is of interest then to use the latter for predictions. The fatigue crack growth parameters $[C_i, \gamma_i]$ being used in the studies are summarized in the Table 5.1.

5.3.2 Scatter of the initial crack size a_0

Measurement of the initial crack size a_0 is essential for the standard fatigue crack growth experiment [15]. In reality evaluation of flaws in structures is complicated and has a lot of limitations. The crack in the structure can be detected by using one of available non-destructive evaluation methods: ultra-sonic, magnetic-particle, radiographic, eddy current or with the use of liquid penetrant [76]. Each non-destructive evaluation method has a lower limit of size of crack which can be detected (see Table 6.1). Therefore, reliability of these methods should also be considered. Some information about the probability of

Table 5.1: Fatigue crack growth coefficients for various materials

	Materials	**Al 2024**	**Al 2219**	**Al 2324**	**Al 7050**
Sector 1	C_1	4.18e-15	4.28e-16	1.34e-16	1.87e-11
	γ_1	17.81	13.07	19.06	9.37
	COV_1	0.397	0.284	0.47	0.55
Sector 2	C_2	3.57e-10	7.06e-13	5.91e-11	2.02e-10
	γ_2	2.38	6.55	3.81	3.86
	COV_2	0.07	0.11	0.19	0.04
Sector 3	C_3	5.65e-13	6.65e-11	3.61e-12	3.62e-11
	γ_3	7.55	3.77	5.86	5.71
	COV_3	0.05	0.07	0.23	0.08
Sector 4	C_4	2.58e-10	×	×	1.93e-09
	γ_4	3.61	×	×	2.88
	COV_4	0.09	×	×	0.04
	Materials	**Al 7075**	**Al 7475**	**Hy Tuf Steel**	**A36 Steel**
Sector 1	C_1	2.39e-15	2.33e-11	4.22e-15	1.39e-18
	γ_1	21.4	5.42	10.23	8.73
	COV_1	0.31	0.09	0.1	0.06
Sector 2	C_2	2.66e-10	5.5e-10	7.36e-12	3.38e-13
	γ_2	3.04	3.19	3.25	3.97
	COV_2	0.04	0.04	0.16	0.05
Sector 3	C_3	7.58e-12	7.49e-11	3.27e-26	×
	γ_3	6.09	4.05	10.53	×
	COV_3	0.06	0.06	0.37	×
Sector 4	C_4	2.12e-10	×	×	×
	γ_4	3.67	×	×	×
	COV_4	0.05	×	×	×

detection can be found in reference [77].

Initial crack-like defects in general can be classified into the inherent material defects, such as inclusions and porosity and flaws resulting from the drilling, corrosion, etc. Former are known to be in the range of $1 - 50\mu m$ [78] and latter vary around $50 - 200\mu m$ [79]. Unfortunately, these dimensions are approximately 1000 times less than those which can be reliably detected. It is also known and it was experimentally confirmed [80] that from the variety of initial voids and inclusions only a few will develop into the long cracks leading to the final failure. Therefore, only analysis of the microstructure is not sufficient for fatigue live assessment.

It is also known, that the total fatigue live of a given structure is strongly dependent on the size of initial crack [55]. Therefore, implementation of the initial crack size a_0 in form of its probability distribution is of great importance. When implemented into the "Monte-Carlo" UniGrow analysis, the typical result of simulation will look like the one shown in Figure 5.10.

Table 5.2: Minimum detectable crack sizes [81]

Detection method	**Semi-elliptical crack dimensions, a / c [m]**
Ultrasonic	$\approx 0.43 \times 10^{-3}/2.21 \times 10^{-3}$
Magnetic Particle	$\approx 0.97 \times 10^{-3}/4.78 \times 10^{-3}$
Radiographic	$\approx 1.91 \times 10^{-3}/1.91 \times 10^{-3}$
Eddy current	$\approx 0.51 \times 10^{-3}/2.54 \times 10^{-3}$
Liquid penetrant	$\approx 0.64 \times 10^{-3}/3.18 \times 10^{-3}$

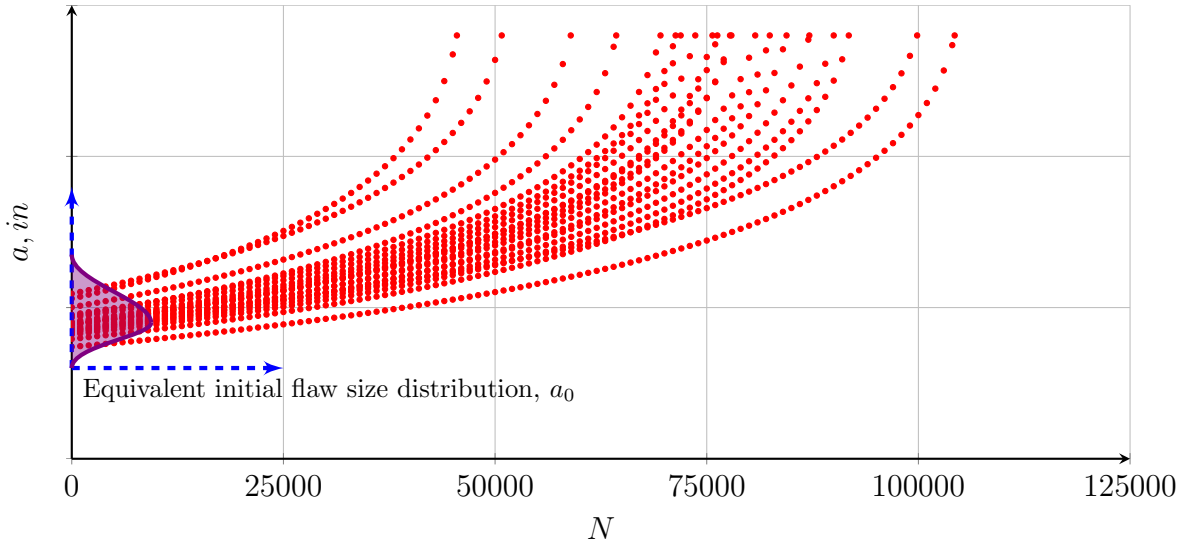

Figure 5.10: Fatigue life analysis of experimental fatigue crack growth data from reference [82] with randomly sampled initial crack length a_0

The question of how to estimate the probability distribution of the initial crack size in order to apply the fatigue crack growth modeling for estimation of the total life of the structure is of great importance. In order to avoid rigorous and expensive fractographic testing, Rudd and Gray have introduced the concept of equivalent initial flaw size [83]. The crack size represented by this concept is a projection of similar crack "*backward-extrapolated*" from the available fatigue crack growth data. The correlation between the equivalent initial flaw size and real crack length is known to be loose and dependent on the stress-level at which the former was obtained. Therefore, one has to be careful with transferring the crack size distributions obtained using the equivalent initial flaw size approach to different structural configurations and loading spectra. Significant amount of equivalent initial flaw size data was obtained and presented in a report "*Fastener Hole Quality*" by Norohna et.al [79]. Data from this report can be used for variety of applications. The method of how to determine distributions of initial flaw size can be found in the work by Manning [84].

Let's review how the equivalent initial flaw size was originally obtained. First, available fatigue crack growth data of the (N_i, a_i) form has to be obtained by applying the load to the smooth specimen. Obviously information about crack size can be only recorded from the time when the crack can be detected. Then, (N_i, a_i) data is fitted by a polynomial. Finally the crack size at $N = 0$ is denoted as an equivalent initial flaw size. The process is schematically illustrated in Figure 5.11.

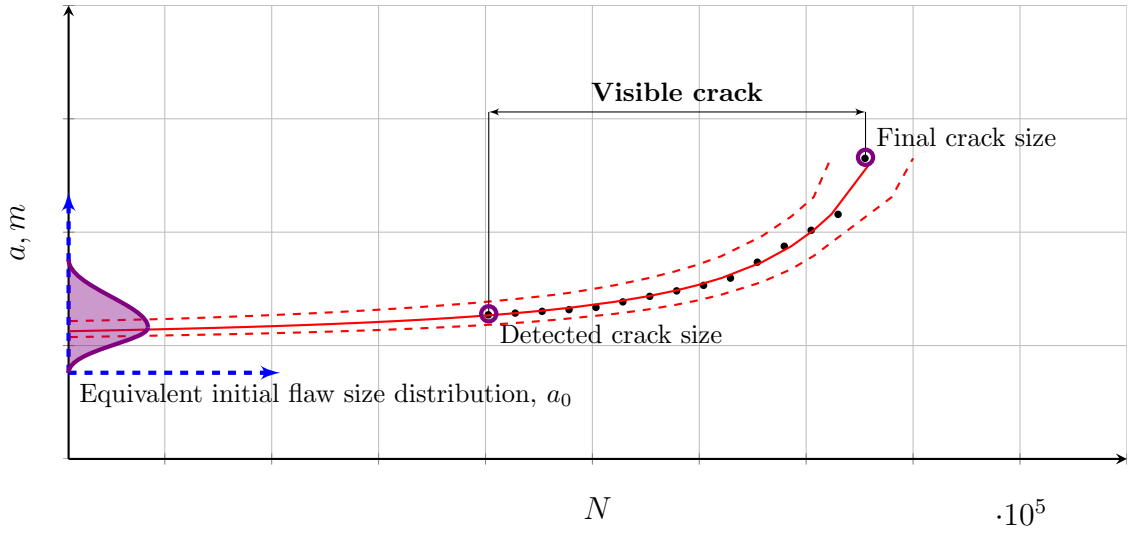

Figure 5.11: Estimation of the equivalent initial flaw size from available fatigue crack growth data

Another method to evaluate the equivalent initial flaw size was proposed by Fawaz [85]. Instead of fitting of a polynomial into the available a vs. N data, the "*hit or miss*" method is employed. In Figure 5.12 it is schematically shown how AFGROW and FASTRAN deterministic fatigue crack growth models are used to obtain the equivalent initial flaw size. The principle is based on the trial and error concept. Given the detected crack size and elapsed number of cycles it is possible to vary the initial crack size a_0 and run FASTRAN or AFGROW several times until the desired final crack length is reached at the desired number

of cycles, N_f with a certain degree of accuracy. In the proposed method, the evaluated equivalent initial flaw size depends on the chosen fatigue crack growth model. Therefore, in order to evaluate the equivalent initial flaw size in our case, the UniGrow fatigue crack growth model has to be utilized. The main deficiency of the "*hit or miss*" method proposed by Fawaz [85] is that it doesn't consider the random nature of material properties. In order to overcome that limitation it was proposed to use the "*backward*" fatigue crack growth analysis. The UniGrow fatigue crack growth model was modified in a such a way that it was able to perform the analysis in the reversed direction (from final crack size to the initial one). Using the scatter of the material properties in the form of C_i fatigue crack growth coefficients described above and the "Monte-Carlo" simulation method it was possible to assess the equivalent initial flaw size. Consequently, the proposed method enables assessment of the the equivalent initial flaw size probability distribution (as shown in Figure 5.13) from available stress-life data.

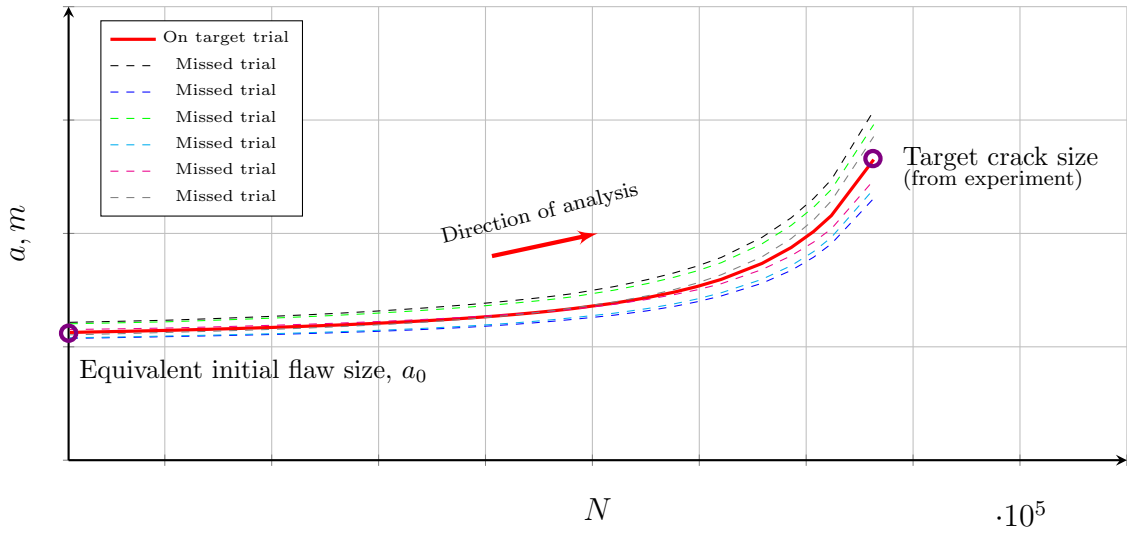

Figure 5.12: The FASTRAN [44] and AFGROW [41] methods for estimation of the equivalent initial flaw size from available fatigue crack growth data [85]

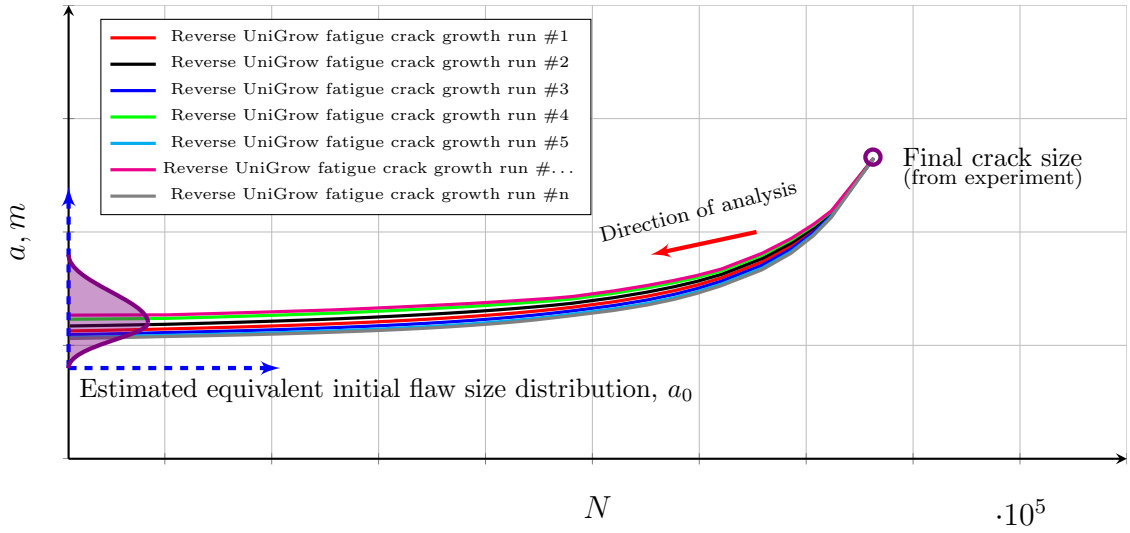

Figure 5.13: Estimation of the equivalent initial flaw size from available fatigue crack growth data

5.3.3 The "Monte-Carlo" simulation method

Random variables modeling, as it was stated earlier, requires the replacement of deterministic single value parameters with their probabilistic distributions. Respectively, the choice of a statistical distribution type has a strong influence on results of "Monte-Carlo" simulations. The most popular distributions used in the fatigue life analysis are the Weibull and the Log-Normal distributions. The primary advantage of the former is the ability to provide reasonably good failure forecast based on the small amount of data. The Log-Normal distribution in turn was shown to be the most suited for fatigue crack growth analysis [50, 4].

Probability density functions of random variable X (where X represents the fatigue crack growth coefficient C_i or the initial crack size a_0) based on the Weibull and Log-Normal distributions are given by equations (5.4) and (5.5) accordingly:

$$f(X) = \frac{k}{\lambda}\left(\frac{x}{\lambda}\right)^{k-1} e^{-(x/\lambda)^k} \tag{5.4}$$

$$f(X) = \frac{1}{X\zeta_x\sqrt{2\pi}} e^{-\frac{1}{2}\left(\frac{\ln(X)-\lambda_x}{\zeta_x}\right)^2} \tag{5.5}$$

Cumulative distribution functions of random variable X based on the Weibull and Log-Normal distributions are given by equations (5.6) and (5.7) accordingly:

$$F(X) = 1 - e^{-\left(\frac{x}{\lambda}\right)^k} \tag{5.6}$$

$$F(X) = \int_0^x \frac{1}{X\zeta_x\sqrt{2\pi}} e^{-\frac{1}{2}\left(\frac{\ln(X)-\lambda_x}{\zeta_x}\right)^2} dX \tag{5.7}$$

Both, Weibull and Log-Normal distributions are able to approximate well the distributions of the C_i and a_0 parameters. Since there is no preferable distribution, both options were chosen to be implemented for further analysis.

The next part of the studies was focused on implementation of sampling technique into the UniGrow fatigue crack growth model. Sampling method consists in general from two steps

1. Sample random number $U \in (0 \ldots 1)$ which follows the uniform distribution
2. Transform sampled number U into corresponding value X from the distribution of interest

Since quality of the prediction based on the "Monte-Carlo" method depends on the number of how many times simulation has been carried out, methods to obtain large sequence of U

values are very important. While it is possible to get the "*real*" random numbers U from thermal noise, nuclear decay or other sources of randomness, in most of the cases such approach is far from being practical. Therefore, pseudo-random number generators are being used in many stochastic computational algorithms. The linear congruential generator as the oldest and still the most popular mechanism for production of pseudo-random numbers was considered first. In order to get pseudo-random numbers, recursive relation presented by equation (5.8) has to be used.

$$U_{i+1} = (aU_i + c)\,(mod\ m) \tag{5.8}$$

The main disadvantage of this method is that the sequence length is dependent on the seed (U_0 value) and in most cases it is not long enough for fatigue crack growth "Monte-Carlo" simulations. Another algorithm for generating pseudo random numbers is based on the Mersenne prime. Accordingly, this method to obtain a pseudo-random number is called Mersenne Twister generator and it was proposed in 1998 by M. Matsumoto and T. Nishimura [86]. This algorithm has passed various statistical tests, its speed is compatible with other generators and it is able to produce unique sequences of (219937-1) length. Therefore, the Mersenne Twister algorithm (MT-19937) in the form of a C++ library from [87] was used.

With the second step, the "Monte-Carlo" method implementation requires uniformly distributed values U to be transformed into the values X corresponding to distribution of interest (Log-Normal, Weibull, etc.). For this purpose, variety of methods were proposed in the past [88]. These methods can be classified into general ones, such as inverse transform, rejection, etc. and specific, such as the Box-Mueller approach or Von-Neuman algorithm. While latter category is easier to implement, the former is of interest due to its universality.

The inverse transform method is based on the following proposition. Let $U \in (0 \ldots 1)$ be a random variable obtained from pseudo-random number generator and X be a random variable following the desired continuous distribution function F and defined as:

$$X = F^{-1}(U) \tag{5.9}$$

Then inverse function $F^{-1}(U)$ is equal to the value of x for which $F(x) = U$. In order to use this method an analytical solution for the inverse function should be known. The quantile cumulative distribution functions of interest (Weibull, Log-Normal) are well-known and thus, this method is often used in stochastic fatigue crack growth modeling.

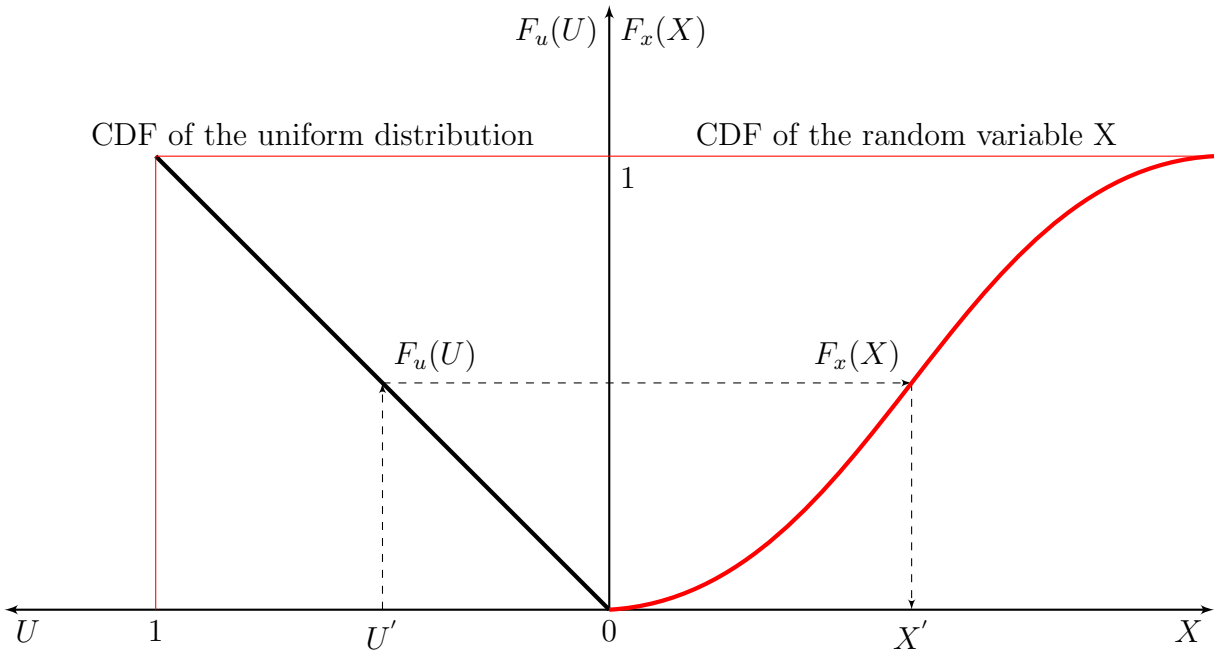

Figure 5.14: Inverse tranform sampling method

Another method to obtain random numbers from the desired probability distribution is called the rejection method. If simulation of a random variable following density func-

tion $g(x)$ is possible, then it can be used as the basis for simulating from the continuous distribution having density $f(x)$. The random variable from $g(x)$ has to be simulated and then accepted with a probability proportional to $f(Y)/g(Y)$. Let d be a constant such that $f(Y)/g(Y) \leq d$ for all Y. To simulate random variable having probability density $f(x)$, following steps have to be taken:

1. Simulate Y having a density $g(Y)$ and simulate a random number U
2. If $U \leq f(Y)/d \cdot g(Y)$ set X = Y. Otherwise return to Step 1.

The main disadvantage of the rejection method is that it is more computationally intense and relies heavily on the chosen initial probability density $g(x)$. Therefore, inverse transform method was chosen for the constructed random variables model.

5.4 The resultant fatigue life assessment methodology

The chapter shall be concluded with general depiction of the proposed fatigue life model. The proposed methodology can be split into four steps:

1. Collection of the "*raw*" data required for analysis
2. Preparation of the input data for fatigue life analysis
3. Execution of the "Monte-Carlo" UniGrow model
4. Assessment of obtained results

The first step of fatigue life analysis is aggregation of required data. The object of studies (component of structure or mechanism) has to be thoroughly pre-analyzed and information about stress-concentrators (geometry), material used and predicted service loading should be gathered. Then, following information has to be obtained either through additional testing or from open sources of information: first, the fatigue life tests of smooth specimens; second, fatigue crack growth data of the $[\Delta K, (da/dN)]$ form obtained at various stress ratios R for the material of interest; third, stress-strain material cyclic properties $E,\ \nu,\ \sigma_{ys},\ K^{'},\ n^{'}$. The first step shall be concluded with assumption of the loading sequence and component dimensions.

The second step of fatigue life analysis is preparation of the input data required to perform the probabilistic fatigue crack growth analysis. The effective crack tip radius ρ^* has to be assessed by using the described above ρ^* program. Another outcome of the ρ^* program required for further fatigue crack growth analysis is the data of $[\Delta\kappa, (da/dN)]$ form. This data has to be used to obtain set of corresponding $[C_i, \gamma_i]$ parameters and to evaluate probability distribution of the C_i values. The next step in preparation of the input data is assessment of equivalent initial flaw size distribution by using the developed "*backward*" fatigue crack growth routine in combination with fatigue life data from smooth notched specimens.

The third step of fatigue life analysis is execution of the "Monte-Carlo" UniGrow model. Preparation of special files required for the "Monte-Carlo" UniGrow program and assumption of the plane-strain or plane-stress and Neuber or ESED method for stress-strain analysis has to be done before the simulations will start. While no other actions are required, it should be noted that "Monte-Carlo" simulation process is very time consuming.

The final step is concerned with analysis of the simulated data. The proposed methodology in form of the combined "Monte-Carlo" method with the deterministic UniGrow model

enables estimation of two types of probability distributions. The first distribution represents the number of cycles or time required for a crack to reach a certain size, $P(N)$. The second distribution represents the spread of a crack sizes after certain number of cycles, $P(a)$. The first type can be used for the design purposes in order to model the structure in a way it will sustain a specific number of cycles, N_f with a certain degree of probability. Information of the second type should be used to assist with non-destructive evaluation. Illustration of how these distributions are obtained from the developed UniGrow software is schematically shown in Figure 5.15. Superiority of the "Monte-Carlo" method comes from the fact that probability distributions obtained by using this method do not need to be fitted into the well-known classical probability distributions, such as Log-Normal and Weibull. The probability distributions of interest, $P(N)$ and $P(a)$ in the end of simulations in the "Monte-Carlo" UniGrow program are constructed into the histogram-like plots based on the simulation data. The example of such outcome is presented in Figure 5.16.

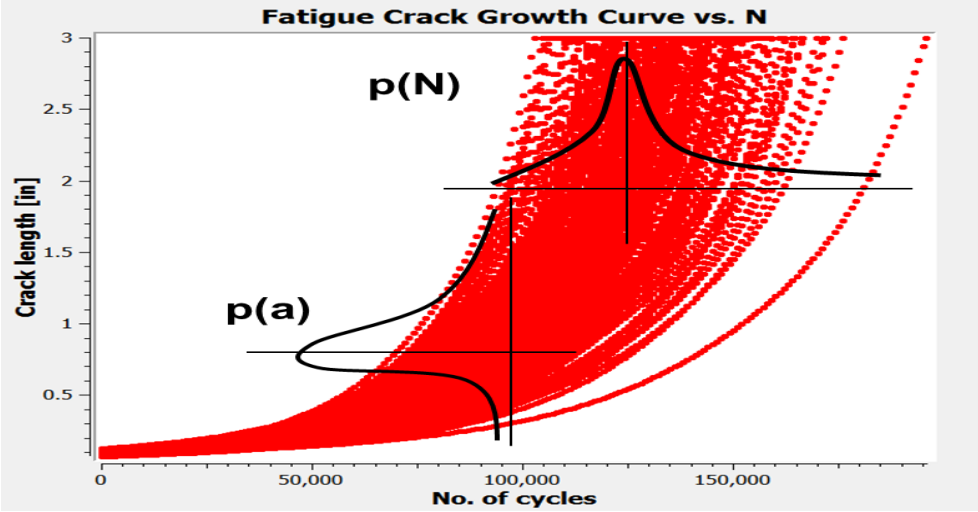

Figure 5.15: Evaluation of probability density functions P(N) and P(a) from the "Monte-Carlo" UniGrow simulation.

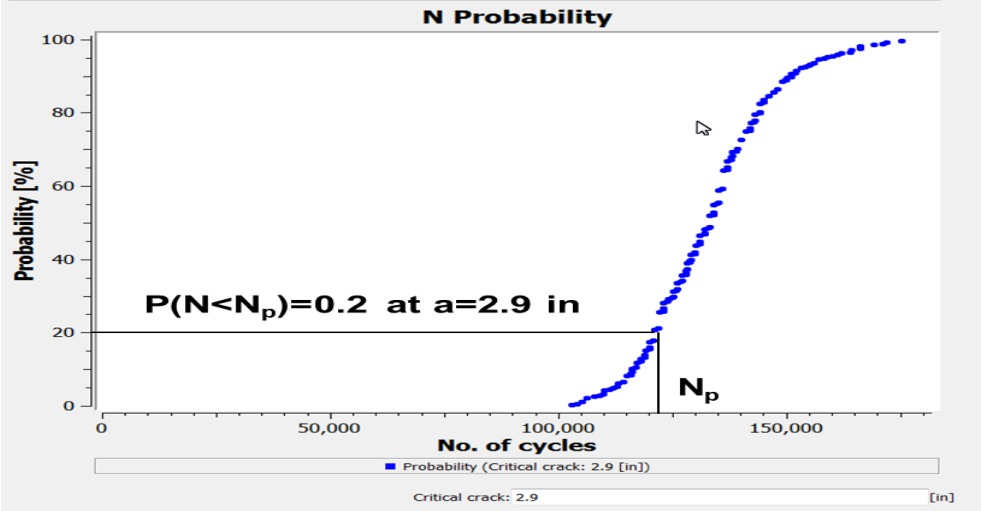

Figure 5.16: Example of the P(N) function obtained from the "Monte-Carlo" UniGrow simulation.

Chapter 6

Application of the proposed fatigue life analysis method

The typical design life cycle consists of the development, manufacturing and service life stages. In each of those stages, fatigue life assessment methodology can be used. The proposed fatigue life analysis can be used at the design stage in order to ensure that product will reach the end of its life-cycle with a certain degree of safety or probability of failure. Fatigue life analysis in combination with non destructive evaluation methods can be used during the production stage for quality control purposes and risk analysis. Methods to estimate the crack propagation are extensively used throughout the service life for establishing the periodicity of maintenance and inspection intervals. Finally, fatigue crack growth analysis in combination with "Monte-Carlo" simulation method can be used at the end of the designed life-cycle to justify the service life extension for the machine or mechanism. Despite the fact that there are many ways to apply the proposed method of fatigue life analysis, it is rather impossible to find a reliable data sets from development and manufacturing stages in order to run any validation tests. Therefore, in order to validate the proposed random variables model, four sets of available statistical fatigue crack growth data

generated by Virkler [4] and Ghonem [6] were used. While these data sets are sufficient to validate the "Monte-Carlo"-UniGrow model ability to account for the variability in material properties, the scatter of the initial crack size a_0 was out of scope in these experiments. Therefore, additional fatigue crack growth data set generated by the Northroop Grumman corporation [59] was used for the verification of the proposed random variables model. It is important to note that only aluminum alloys were used in these validation studies and no similar data was found for steel alloys. However, several investigations [5, 50] indicate that steels exhibit less variability in the fatigue crack growth process and therefore use of aluminum alloys for validation shall be satisfactory.

6.1 Validation of the proposed model against available statistical fatigue crack growth data

Two major statistical fatigue crack growth studies are known and widely used for validation of various probabilistic fatigue life models such as those developed by Yang [52], Patankar [89] and others [51, 53]. Those studies were performed by Virkler [4] and Ghonem [6] on middle-tension specimens (such as shown in Figure) made of Al 2024-T3 and Al 7075-T6 aluminum alloys. The study performed by Virkler is represented by a single statistical set which consists of 68 identical fatigue crack growth experiment. The studies done by Ghonem are represented by three statistical sets, each made of 60 identical fatigue crack growth experiments. Therefore, in total, four comprehensive statistical fatigue crack growth data sets (see Figure 6.2) was used for validation of the random variables model based on the UniGrow fatigue crack growth concept. The scatter in fatigue lives measured as the ratio of the $N_{f,max}$ to $N_{f,min}$ is summarized in Table 6.1.

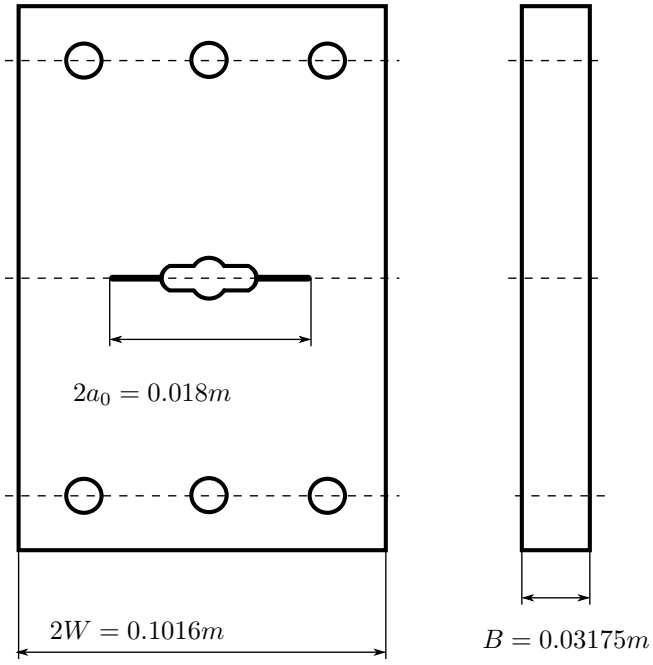

Figure 6.1: Middle-tension specimen used in the statistical studies done by Ghonem [6]

Table 6.1: Scatter of the experimental fatigue crack growth data

material	R	$\Delta N, cycles$	$N_{f,max}/N_{f,min}$
Al 2024-T3	0.2	$\approx 100 \cdot 10^3$	≈ 1.5
Al 7075-T6	0.4	$\approx 200 \cdot 10^3$	≈ 4
Al 7075-T6	0.5	$\approx 50 \cdot 10^3$	≈ 2
Al 7075-T6	0.6	$\approx 60 \cdot 10^3$	≈ 2

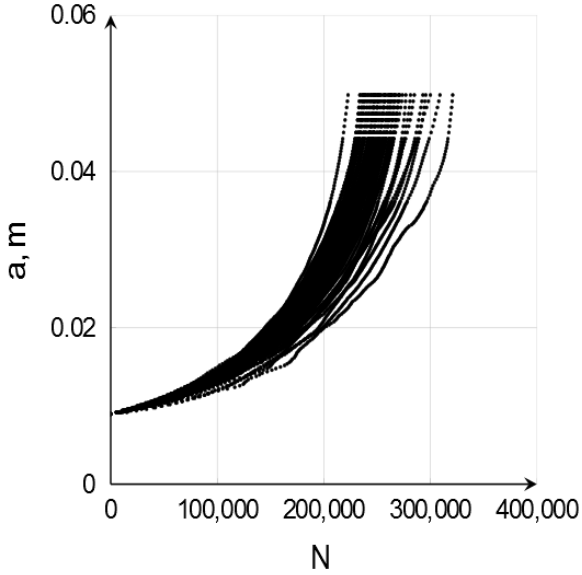

(a) Virkler

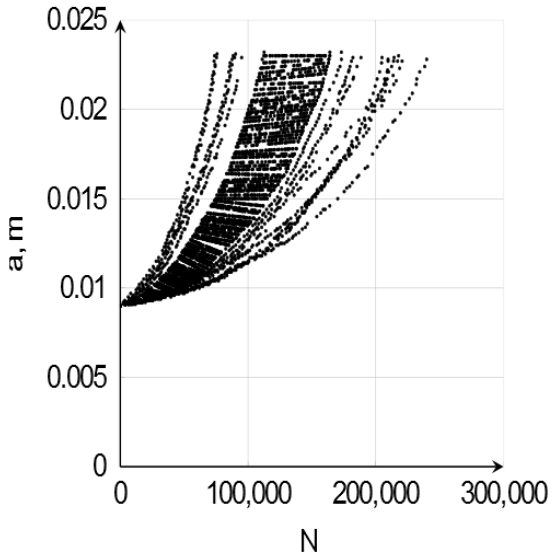

(b) Ghonem, $R = 0.4$ [6]

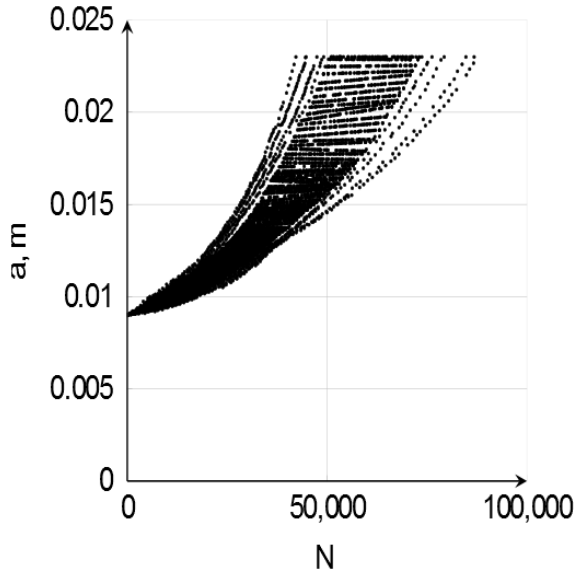

(c) Ghonem, $R = 0.5$ [6]

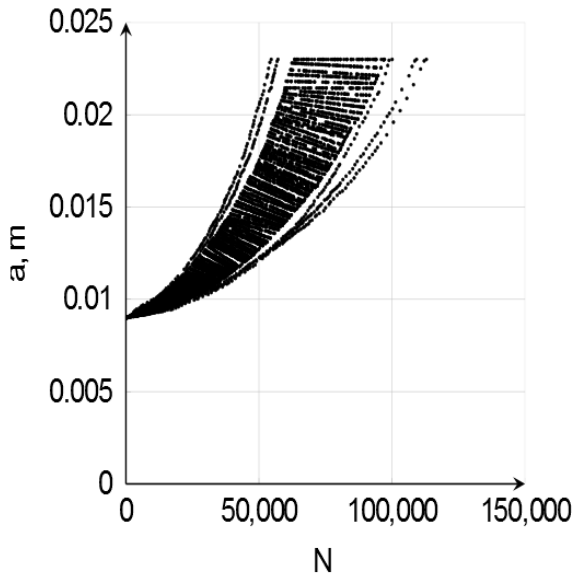

(d) Ghonem, $R = 0.6$ [6]

Figure 6.2: Four sets of statistical fatigue crack growth data [4, 6]

6.1.1 Preparation of the data required for fatigue crack growth analysis (geometry, loading and material)

In order to run numerical simulations based on the proposed model information about material, geometry and loading conditions used during the experimental studies have to be collected and analyzed. Let's review the material data first. Tested alloys were aluminum Al 2024-T3 [4] and Al 7075-T6 [6]. The UniGrow fatigue crack growth model requires specifically material properties such as Young's modulus, Poisson ratio and Ramberg-Osgood stress-strain relationship coefficients to perform analysis. All required cyclic stress-strain material data was obtained from reference [90] and they are given in Table 6.2.

Table 6.2: Material properties of Al 2024-T3 and Al 7075-T6 aluminum alloys [90]

	Al 2024-T3	Al 7076-T6
Young's modulus E,[MPa]	73100	71000
Poisson's ratio ν	0.33	0.33
Yield stress σ_{ys}, [MPa]	428	504.4
Ramberg-Osgood coefficient $K^{'}$, [MPa]	662	899
Ramberg-Osgood exponent $n^{'}$	0.07	0.093

Each statistical set was obtained under the constant amplitude loading condition imposed on the middle-tension specimen. While there are four sets of statistical fatigue crack growth data only two different specimen types were used. One for Al 2024-T3 aluminum alloy and another for Al 7075-T6. The specimen dimensions are summarized in Table 6.4. Loading parameters used during the experiments are summarized in Table 6.3.

Table 6.3: Test loading conditions [4, 6]

material	# of experiments	P_{max}, kN	P_{min}, kN	R
Al 2024-T3	68	23.35	4.67	0.2
Al 7075-T6	60	15.19	6.08	0.4
Al 7075-T6	60	22.25	11.13	0.5
Al 7075-T6	60	22.79	13.68	0.6

Table 6.4: Specimen dimensions [4, 6]

	Al 2024-T3	Al 7076-T6
initial crack size, a_0	9 mm	9 mm
final crack size, a_f	49.8 mm	23 mm
total width, 2W	152.4 mm	101.6 mm
thickness, B	2.54 mm	3.175 mm

In order to perform the fatigue crack growth analysis by using the UniGrow model, value of the material parameter ρ^* has to be known. The new ρ^* evaluation method presented in the chapter 4 was used to find values of the ρ^* parameter for Al 2024-T3 and Al 7075-T6 aluminum alloys. These values are $\rho^*_{al2024} = 1.26e-05$ and $\rho^*_{al7075} = 9.7e-06$ accordingly. Using these values of the ρ^* parameter, original experimental fatigue crack growth data obtained for Al 2024-T3 and Al 7075-T6 aluminum alloys (see Figure 2.5 and 4.2) was transformed into required for analysis form of $[\Delta\kappa, (da/dN)]$. With the next step transformed data was linearized into four segments and mean values of $[C_i, \gamma_i]$ coefficients were

estimated (see Figure 6.3). Proposed random variables model requires assessment of C_i parameters scatter. Statistical distributions of C_i parameters were approximated by the log-normal distribution and they were found by using the maximum likelihood estimation method [91]. Probability density functions of C_1, C_2, C_3 and C_4 parameters are shown in Figure 6.4. Corresponding cumulative distribution functions are presented in Figure 6.5.

Important feature of described statistical fatigue crack growth experimental investigations is that in every one of them, initial flaw size a_0 was precisely measured. Therefore, only distribution of the number of cycles required for crack to reach a specified length is out of particular interest. Using the experimental data, number of cycles or time required to propagate the crack from the initial a_0 to the final a_f crack size, N_f can be aggregated into the specific histogram (such as shown in Figure 2.24). It is of great interest to compare such histogram with the probability distribution of N_f values obtained from the "Monte-Carlo" simulations. It is also of particular interest to compare the distributions of number of cycles required to propagate crack from a_0 to some intermediate value of a_i (N_{a_i}).

6.1.2 Validation results

Based on the performed preliminary data analysis, four projects were prepared for further "Monte-Carlo" simulations. Multiple runs with various numbers of iterations (from 1000 to 10000) were carried out and extensive data for post-simulation analysis has been generated. The main task was to compare the scatter of number of cycles required to propagate crack from certain initial size a_0 to the given crack size a_i. For this comparison experimental fatigue crack growth data obtained by Virkler [4] was "*cut*" as shown in Figure 6.6 at $a_i = 0.017\ m,\ a_i = 0.035\ m$ and $a_f = 0.0498\ m$.

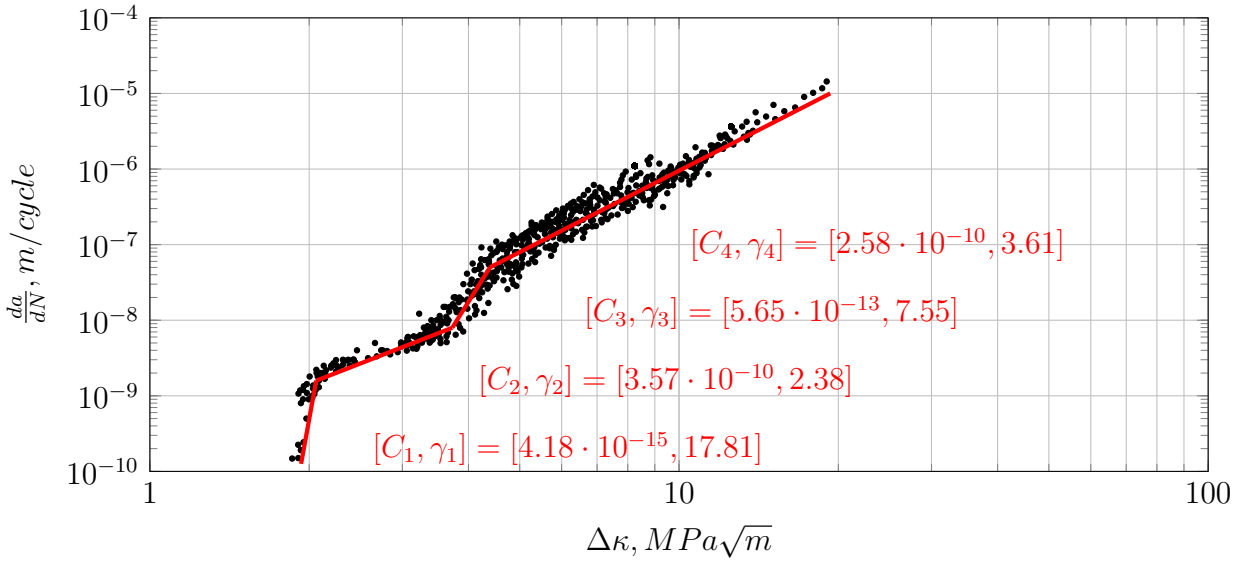

(a)

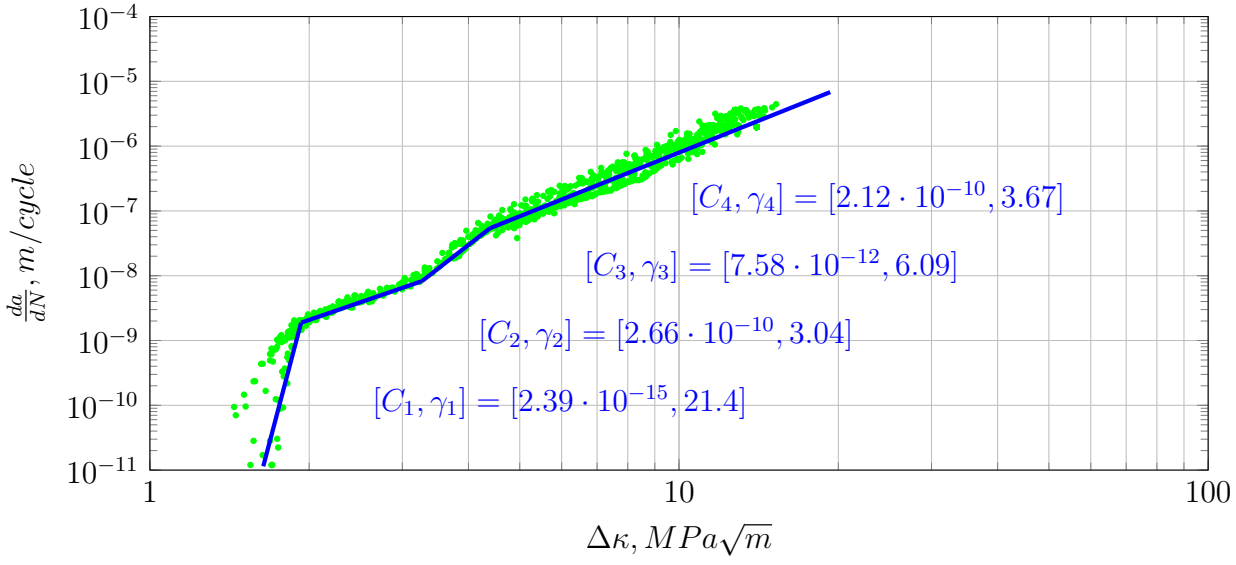

(b)

Figure 6.3: Transformed fatigue crack growth data for the Al 2024-T3 (a) and Al 7075-T6 (b) aluminum alloys used for the estimation of C_i distributions

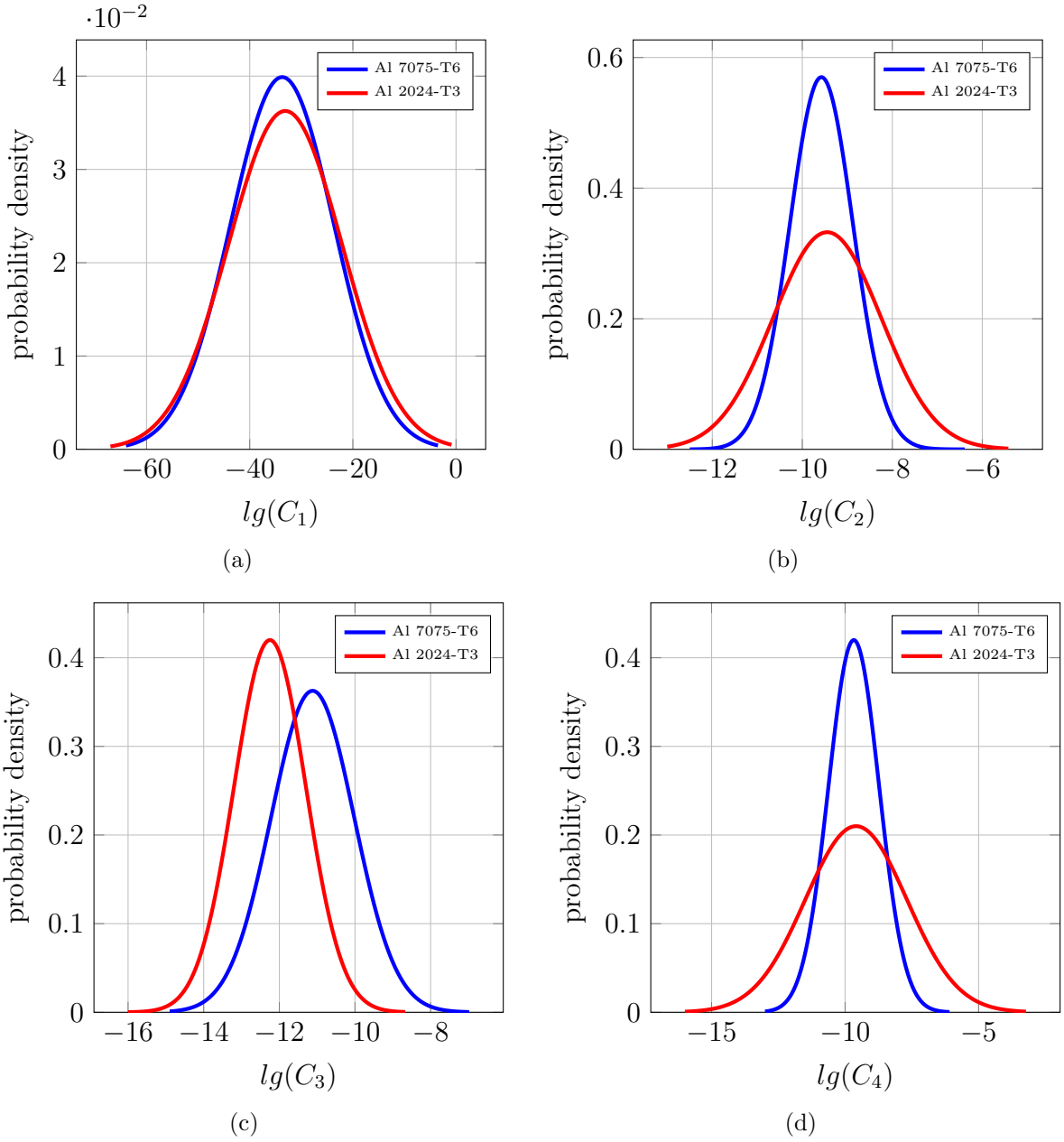

Figure 6.4: Probability density functions of C_1 (a), C_2 (b), C_3 (c) and C_4 (d) parameters of Al 2024-T3 and Al 7075-T3 aluminum alloys

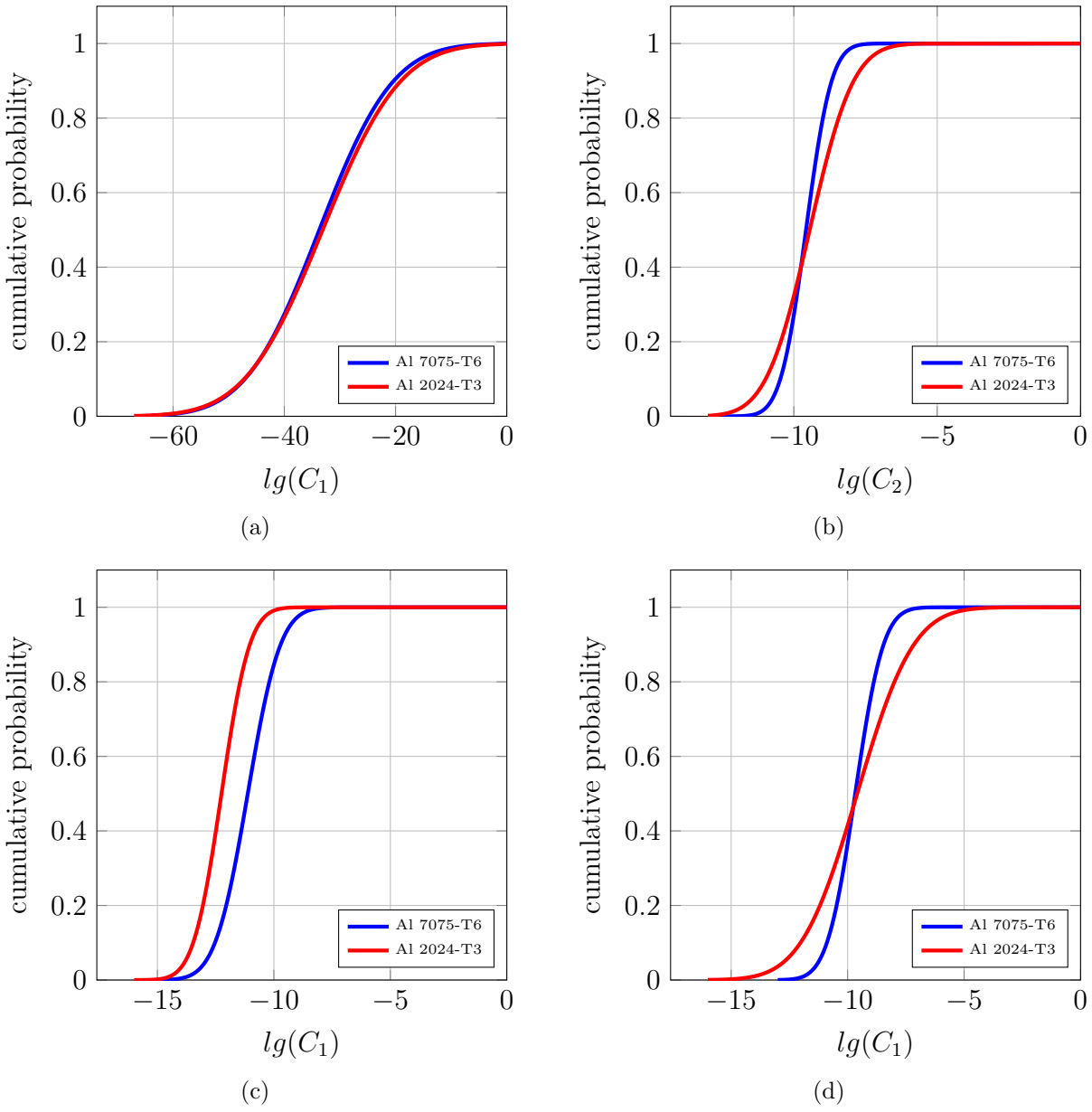

Figure 6.5: Cumulative distribution functions of C_1 (a), C_2 (b), C_3 (c) and C_4 (d) parameters of Al 2024-T3 and Al 7075-T6 aluminum alloys

Histograms showing the experimental and simulated data distributions of fatigue lives corresponding to various crack sizes $ln(N_{0.017m})$, $ln(N_{0.035m})$ and $ln(N_f)$ are presented in Figures 6.7 6.8 and 6.9. It can be seen from the graphs that, the shape of the distribution does not change for P(N) obtained at different crack sises, N_{a_i} and it follows the bell-shaped curve.

Another important observation was that the simulation outcome from combination of the "Monte-Carlo" with the UniGrow fatigue crack growth model closely resemble the distribution of the chosen variability measure based on the experimental results. Experimental and simulation set of values of the number of cycles N_f required to propagate crack from a_0 to a_f for every set of statistical fatigue crack growth data were used to fit the lognormal probability distribution function. As a result shape and scale parameters (λ, ζ) were obtained and summarized in Table 6.5. The scatter of "Monte-Carlo" simulation results is schematically shown on "*top*" of the experimental fatigue crack growth data in Figures 6.10, 6.11, 6.12 and 6.13.

Table 6.5: Log-normal parameters. Experiment and simulation data.

material	R ratio	Experiment		Simulations	
		λ	ζ	λ	ζ
Al 2024-T3	0.2	12.45	0.067	12.4	0.072
Al 7075-T6	0.4	11.73	0.065	11.61	0.068
Al 7075-T6	0.5	11.01	0.062	10.96	0.066
Al 7075-T6	0.6	11.23	0.063	11.18	0.065

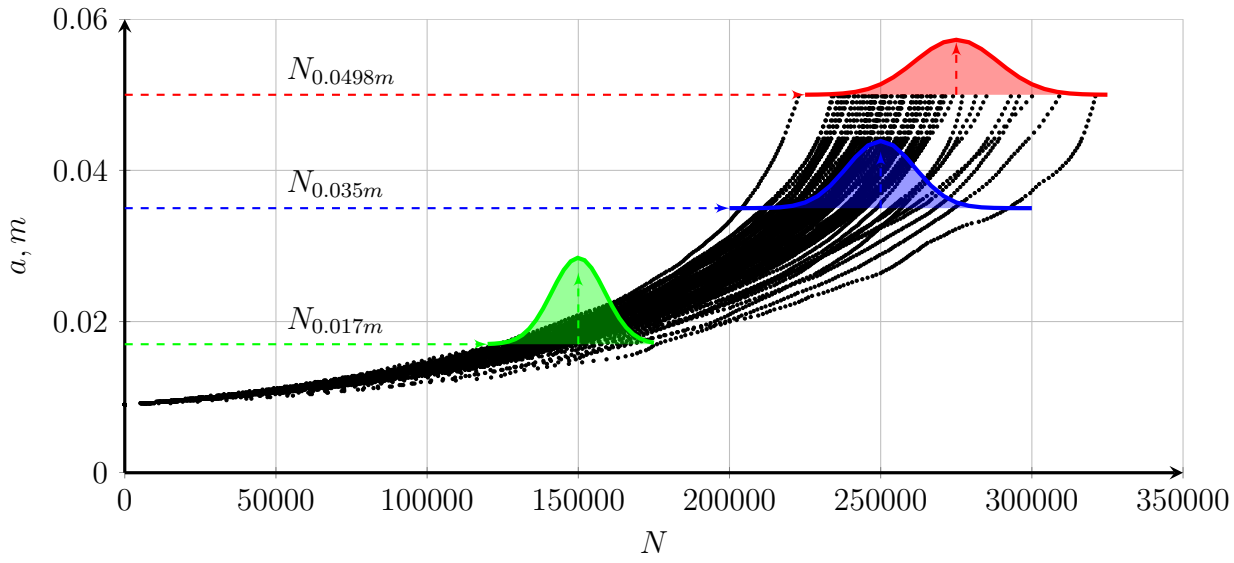

Figure 6.6: Fatigue crack growth results from Virkler experiment [4] with *cuts* made at several crack lengths

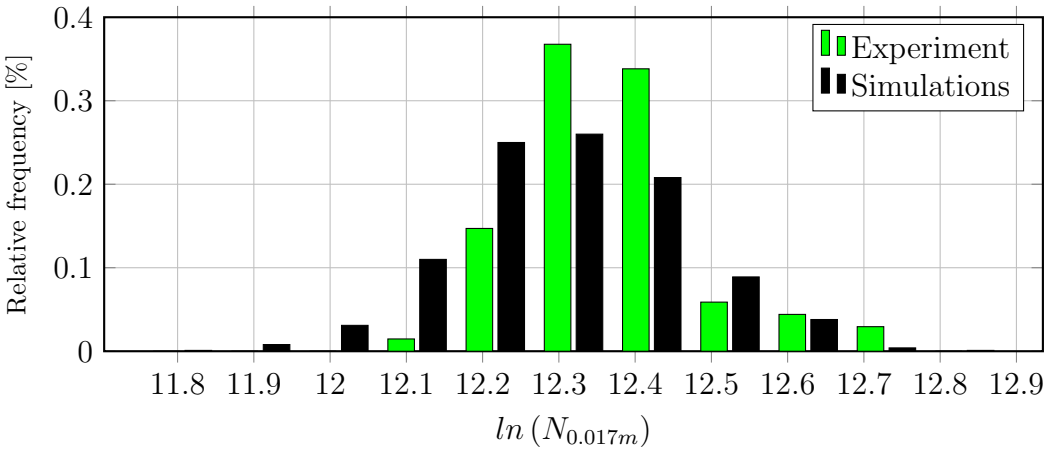

Figure 6.7: Histogram of $ln(N_{0.017m})$ for Al 2024-T3 aluminum alloy experimental [4] and simulated data

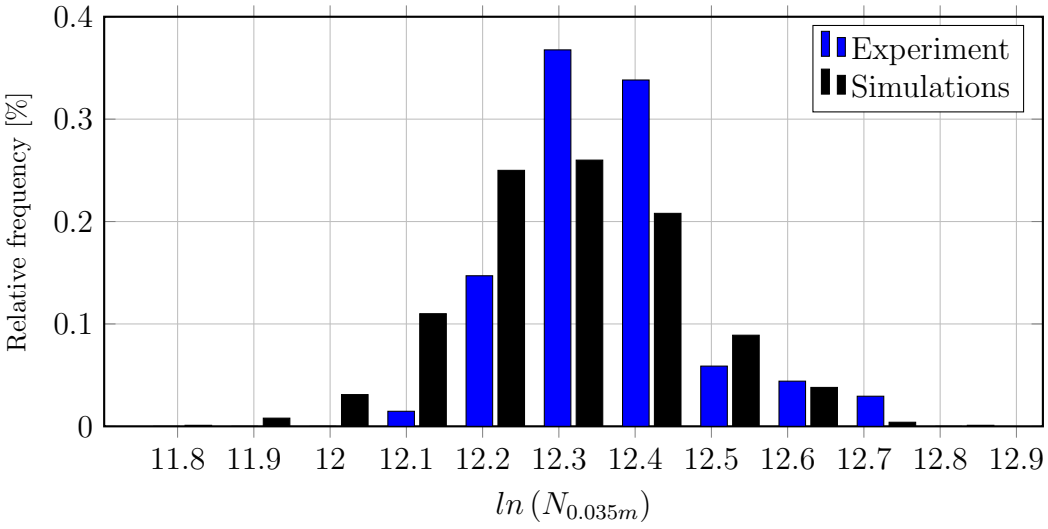

Figure 6.8: Histogram of $ln(N_{0.035m})$ for Al 2024-T3 aluminum alloy experimental [4] and simulated data

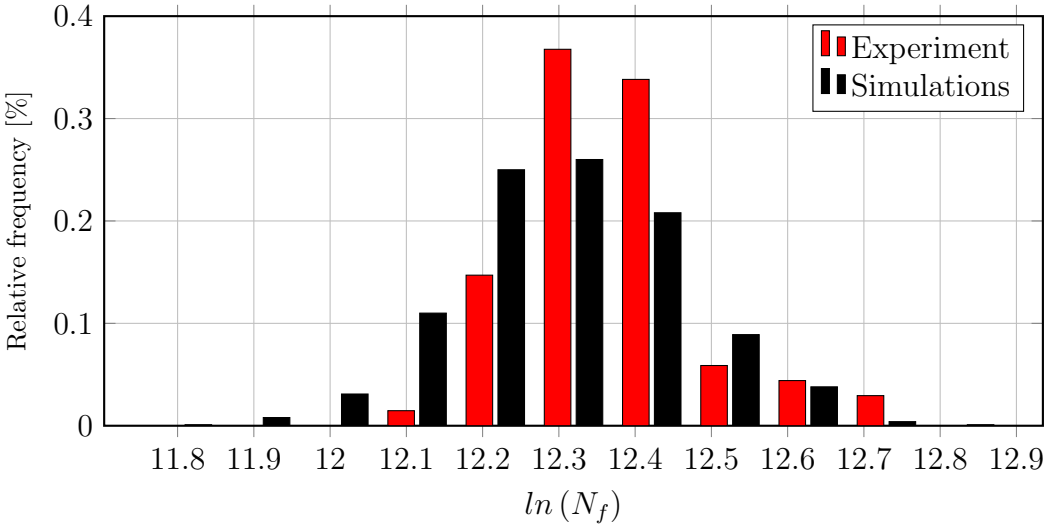

Figure 6.9: Histogram of $ln(N_{0.0498m})$ for Al 2024-T3 aluminum alloy experimental [4] and simulated data

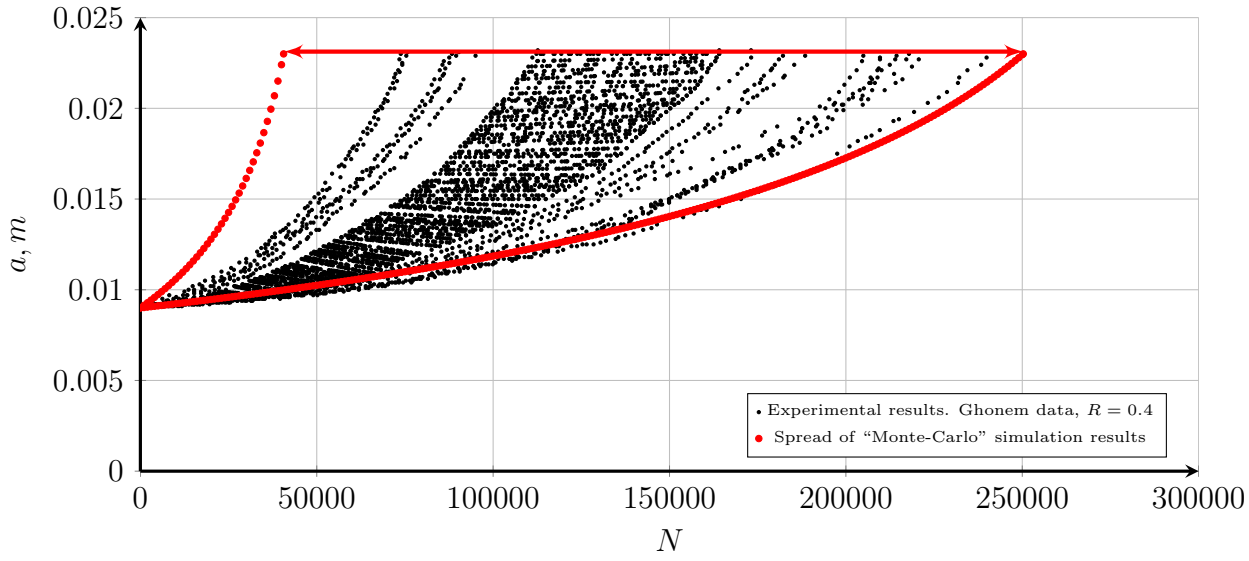

Figure 6.10: Scatter of the "Monte-Carlo" simulation results compared with the experimental data (Al 7075-T6 aluminum alloy, $R = 0.4$)

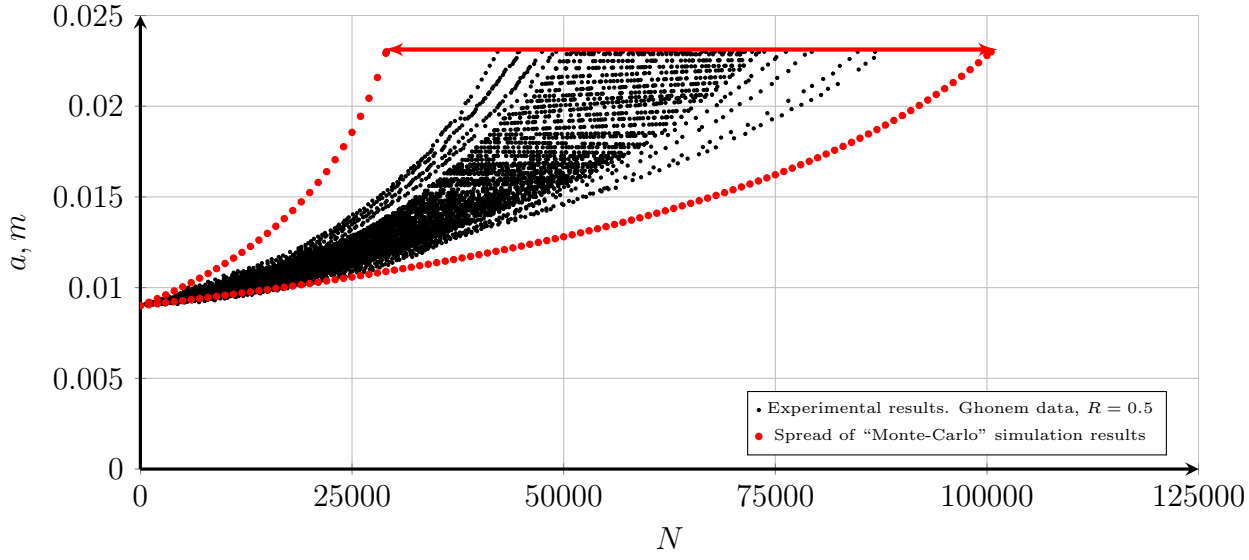

Figure 6.11: Scatter of the "Monte-Carlo" simulation results compared with the experimental data (Al 7075-T6 aluminum alloy, $R = 0.5$)

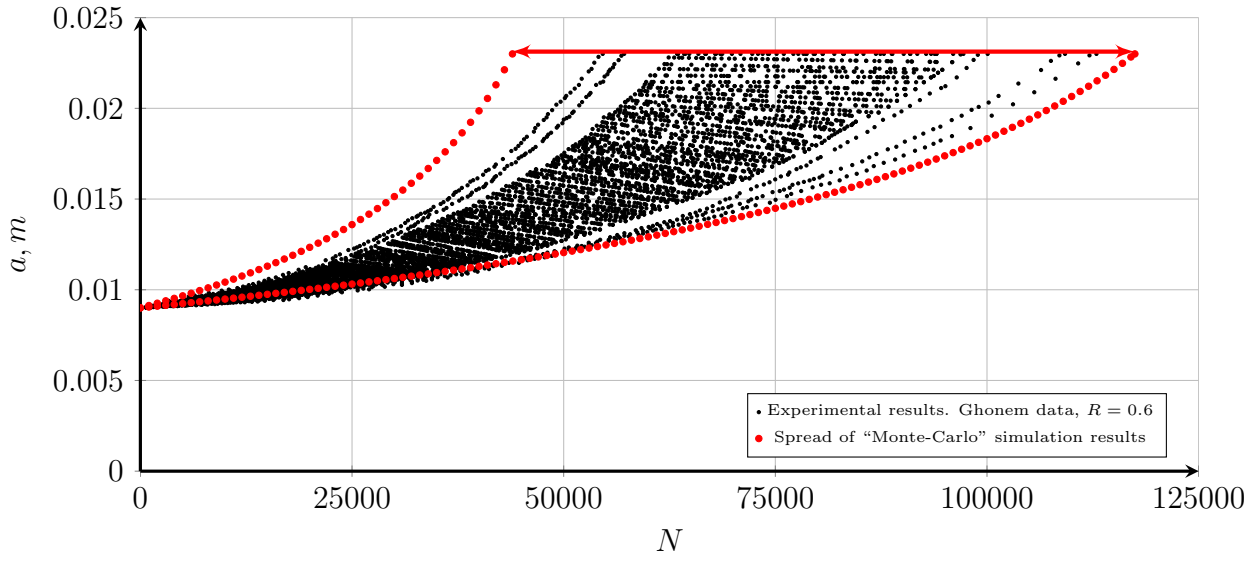

Figure 6.12: Scatter of the "Monte-Carlo" simulation results compared with the experimental data (Al 7075-T6 aluminum alloy, $R = 0.4$)

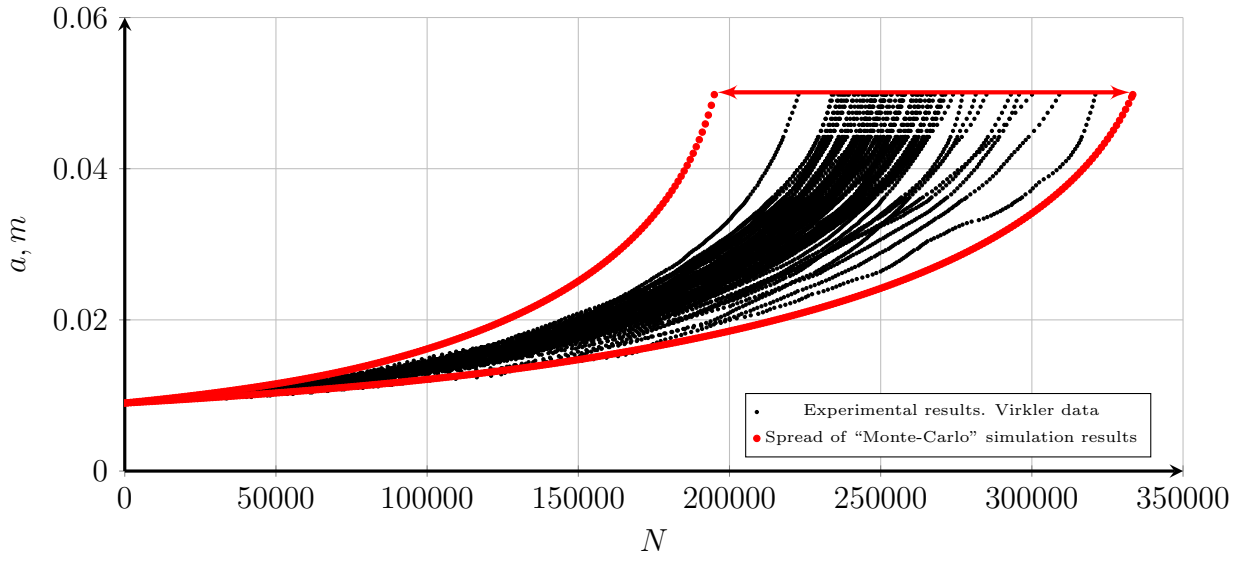

Figure 6.13: Scatter of the "Monte-Carlo" simulations results compared with the experimental data (Al 2024-T3 aluminum alloy, $R = 0.2$)

6.2 Validation of the proposed methodology based on the fatigue crack growth data of semi-elliptical cracks in notches

The concept of how long the aircraft is supposed to be in the service before it should be retired has evolved over years. The designed life of a civil aircraft, for example, was set to approximately 10 years of service in 1950's. These estimations later were proved to be highly conservative and the new design target was set to 20 years period. Still, in the late 1980's airplanes older than 20 years could still be flown based on continuous maintenance and comprehensive inspections. That is why premature retirement is deemed as an unnecessary waste of the valuable assets. For these reasons, variety of life-extension programs are currently ran by US Navy. One of those program has the goal to extend the life of the EA-68 and P-3 planes. In particular, one of the tasks was to perform structural fatigue life analysis of wings, which are partially made of Al 7075-T6 aluminum alloy. Since safety in aviation is the highest priority, any computational analysis had to be backed-up by series of fatigue crack growth experiments. For this reason, Northrop Grumman Corporation has taken 50-mm thick plate (outer wing material), machined it to the thickness of 5.7 mm and performed a series of fatigue life tests [59]. Distinctive feature of those tests is that crack size a_i wasn't measured until it became visible. Therefore, evaluation of the equivalent initial flaw size distribution was required for validation purposes. As the result performed simulations on the basis of the UniGrow fatigue crack growth model and "Monte-Carlo" simulation method were carried out with probabilistic input (initial crack size and material).

6.2.1 Preparation of the data required for fatigue crack growth analysis (geometry, loading and material)

Four types of notched geometries have been tested during the reviewed laboratory investigations: one, two and three-holes specimens as well as the double-sided notch type. While the double-sided notch specimens were tested under the constant amplitude loading spectrum, other three types of specimen were subjected to a variable amplitude loading history. Dimensions of tested specimens are schematically shown in Figures 6.14 and 6.15.

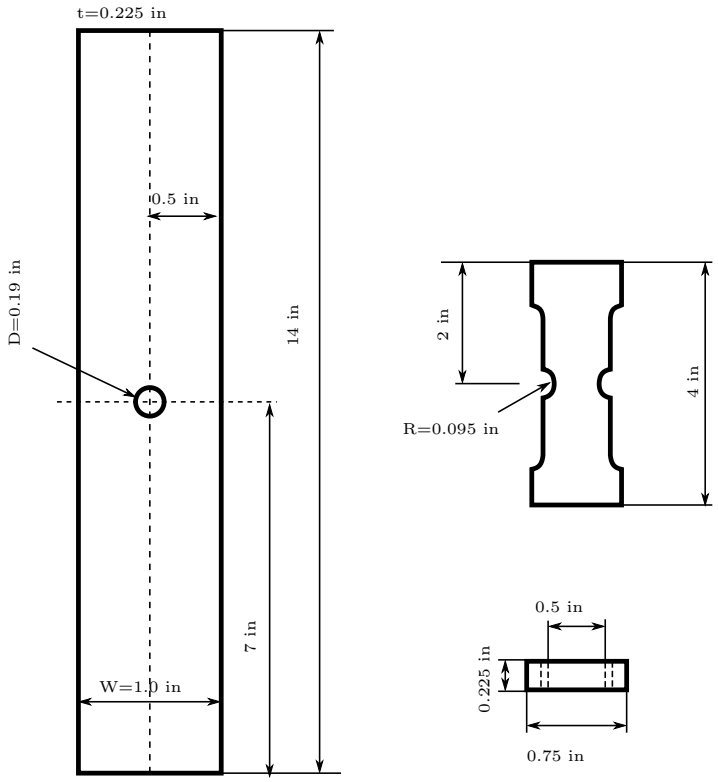

Figure 6.14: The one-hole and double-sided notched specimens made of Al 7075-T6 aluminum alloy

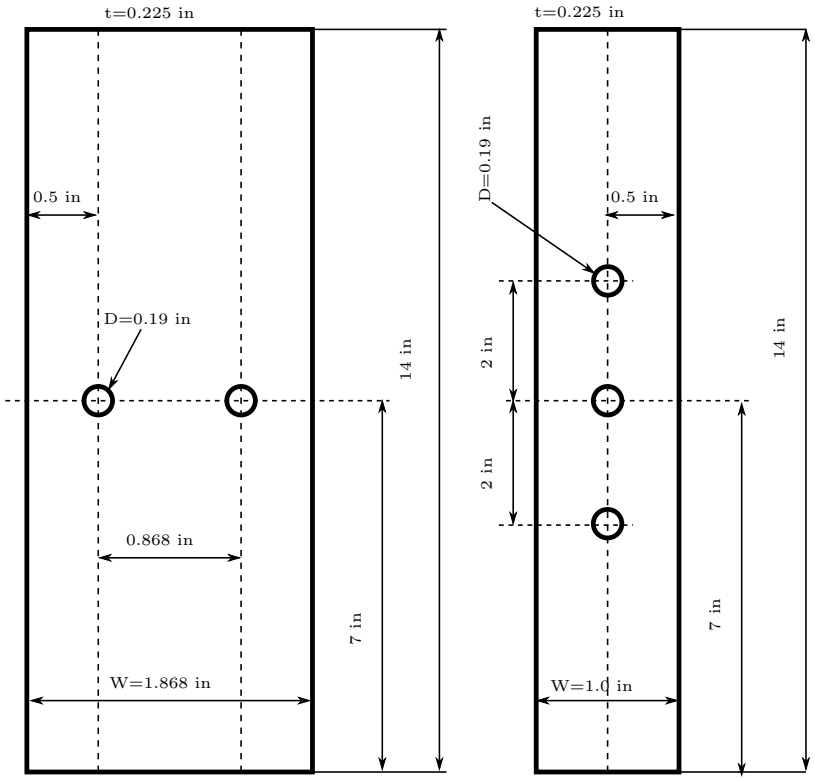

Figure 6.15: Two- and three-hole specimens made of Al 7075-T6 aluminum alloy

The major difference between performed experiments and standard fatigue crack growth test has to be noted now. As per ASTM E647 [15], the specimen used in fatigue crack growth experiment is supposed to have a precrack so the initial crack length a_0 is known. Contrary to this requirement, experimental investigations performed by Northrop Grumman Corporation didn't have any precracking on specimens done. Therefore, the initial crack length a_0 was not measured directly.

Recurring wing spectrum made of 2519 cycles, two hundreds of which are shown in the Figure 6.16 was applied for the one- two- and three-hole specimens. This spectrum is a predominantly tensile, though some compressive stresses were present. The constant amplitude loading history used for double-sided notched specimens have been applied at stress-ratio, $R = 0$ and with three different amplitudes: $\Delta S_1 = 25\ MPa, \Delta S_2 = 30\ MPa, \Delta S_3 = 40\ MPa$.

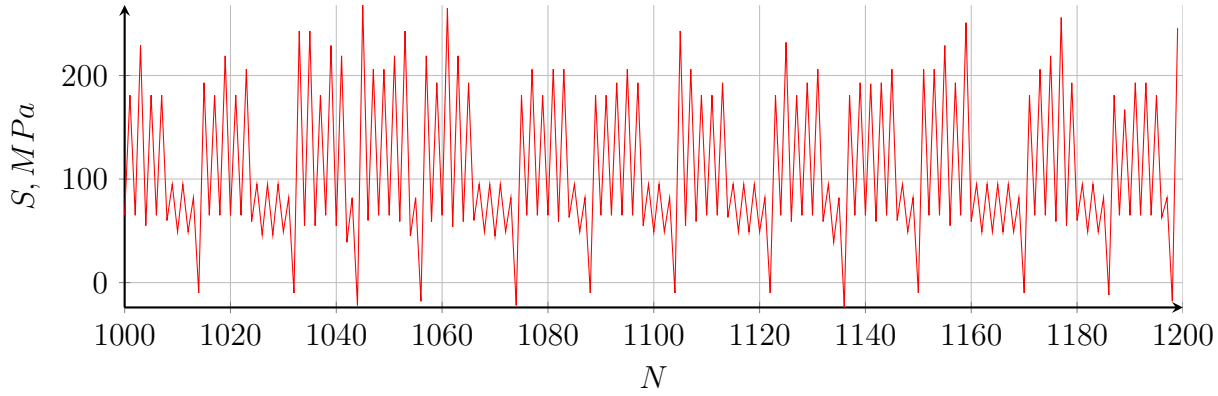

Figure 6.16: Excerpt from the wing loading spectra [37]

Proper evaluation of the equivalent initial flaw size is of great importance for prediction of the fatigue life. Since double-notched specimens were tested under the applied constant amplitude loading history, the data in form of final crack size a_f vs. the number of applied loading cycles N_f can be used to assess the equivalent initial flaw size distribution. This data together with schematic illustration of the procedure for evaluation of the equivalent initial flaw size distribution is schematically shown in Figure 6.17. It is important to note that for the two-hole and three-hole specimen types (see Figure 6.15) post-test quantitative fractography was used by Northroop Grumman [59] in order to to evaluate the $[N_i, a_i]$ fatigue crack growth curve and extrapolate the approximate initial crack size a_0. The resultant initial crack was determined to have a semi-elliptical shape (see Figure 6.19).

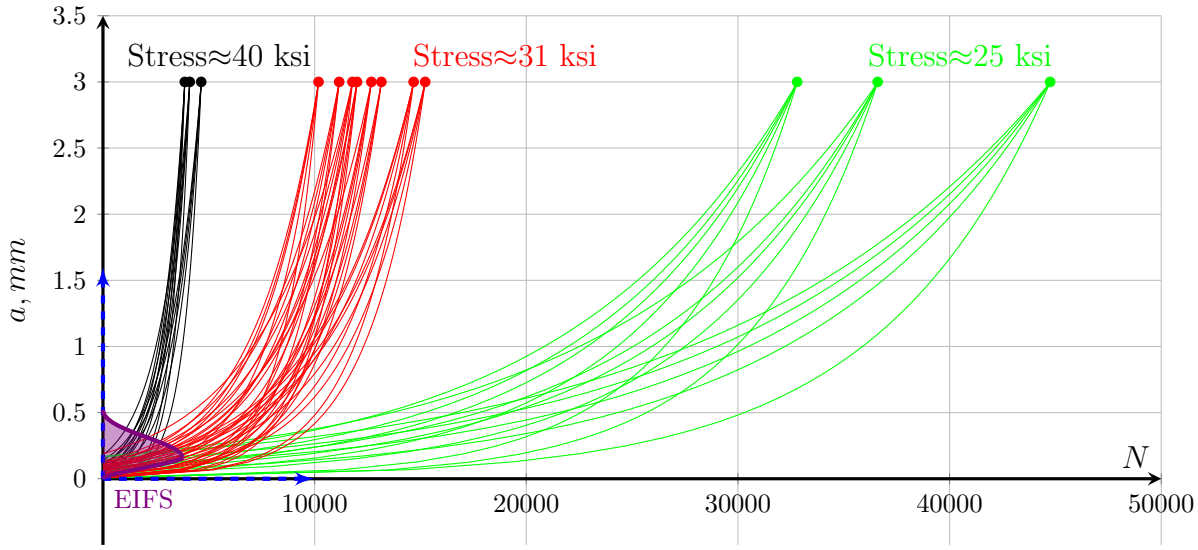

Figure 6.17: Estimation of the equivalent initial flaw size distribution.

Review of available fractography images of crack nucleation sites in the Al 7075-T6 aluminum alloy from reference [54] together with the analysis of equivalent initial flaw size distribution has led to the approximation of a_0 with a two-parameter Weibull distribution:

$$\begin{cases} F(a_0) = 1 - e^{-\left(\frac{a_0}{\lambda}\right)^k} \\ \lambda = 0.000019102, \;\; k = 0.374 \end{cases} \tag{6.1}$$

The mean value and standard deviation of the initial crack size are equal to:

$$\begin{cases} \mu_{a_0} = \lambda \Gamma\left(\frac{1}{k} + 1\right) \approx 77 \mu m \\ \sigma_{a_0} = \lambda^2 \left[\Gamma\left(\frac{2}{k} + 1\right) - \Gamma^2\left(\frac{1}{k} + 1\right)\right] \approx 0.07 \mu m \end{cases} \tag{6.2}$$

The UniGrow fatigue crack growth model requires the knowledge of the da/dN vs $\Delta\kappa$ relationship in form of $[C_i, \gamma_i]$ coefficients to perform fatigue life analysis. Since Al 7075-T6 aluminum alloy is a widespread material, $[\Delta\kappa, (da/dN)]$ plot for this alloy was already available [66] and used for the fatigue crack growth predictions. Nevertheless, during the life-extension program, Northrop Grumman Corporation [59] had performed series of fatigue crack growth tests using the standard compact tension specimens (thickness, $B = 0.225\ in$; width, $W = 3\ in$). Collapsed fatigue crack growth data in form of $[\Delta\kappa, (da/dN)]$ obtained from both sources for comparison purposes is presented in Figure 6.18. As it can be seen from this figure, fatigue crack growth data obtained solely by Northrop Grumman Corporation is less scattered. Which is obvious since the data from different laboratories is supposed to have more variability. Therefore, it was decided to use the same $[C_i, \gamma_i]$ coefficients and distributions of C_i parameters as the ones used for validation of Ghonem [6] statistical fatigue crack growth experiments.

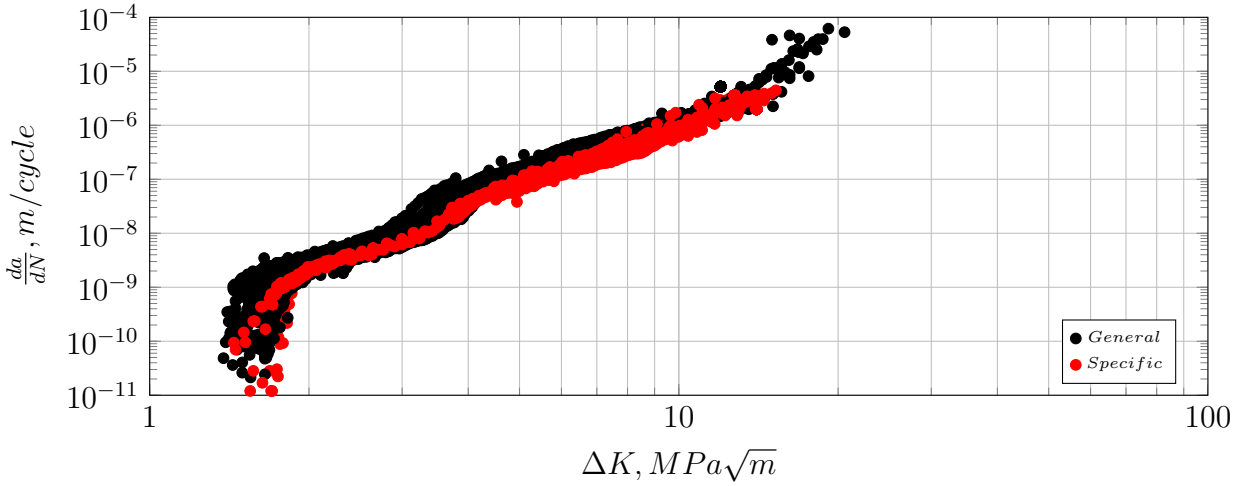

Figure 6.18: Combination of $\Delta\kappa$ plots

6.2.2 Validation results

The fatigue crack growth analysis starts from evaluation of the stress intensity factor applied to the given structure or specimen. Initial crack was assumed to have a semi-elliptical shape (see Figure 6.19). Therefore, fatigue crack growth analysis was performed using the appropriate two-dimensional weight function [21] necessary for calculating the stress intensity factor, K.

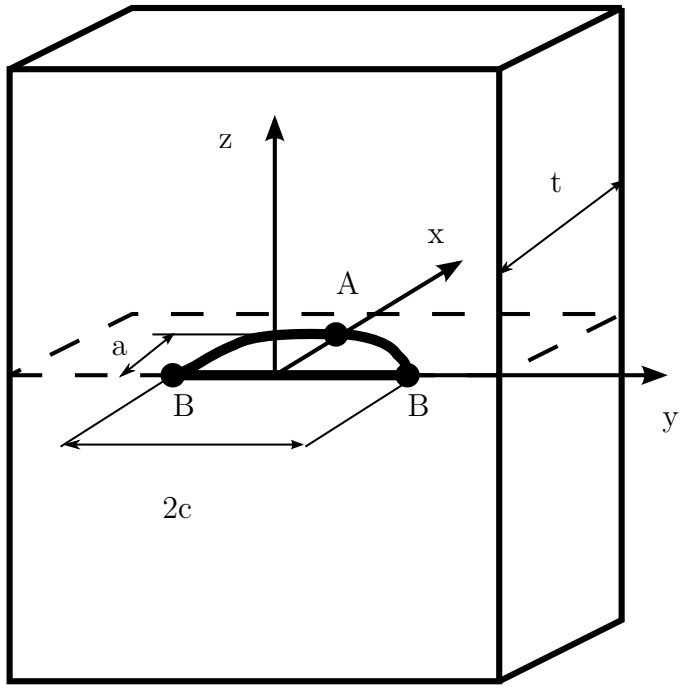

Figure 6.19: The model of a semi-elliptical crack in a finite thickness plate

The stress intensity factor of the point A of semi-elliptical crack (Figure 6.19) can be determined as:

$$K_A = \int_0^a \sigma(x) \frac{2}{\sqrt{2\pi(a-x)}} [1 + M_{1,A}\left(1 - \frac{x}{a}\right)^{1/2} + \\ + M_{2,A}\left(1 - \frac{x}{a}\right) + M_{3,A}\left(1 - \frac{x}{a}\right)^{3/2}] dx \tag{6.3}$$

where the geometry factors $M_{1,A}$,$M_{2,A}$ and $M_{3,A}$ are:

$$\begin{cases} M_{1,A} &= \frac{\pi}{\sqrt{2Q}}(4Y_0 - 6Y_1) - \frac{24}{5} \\ M_{2,A} &= 3 \\ M_{3,A} &= 2\left(\frac{\pi}{\sqrt{2Q}}Y_0 - M_{1,A} - 4\right) \end{cases} \tag{6.4}$$

The stress intensity factor of the point B of semi-elliptical crack can be found from equation (6.5):

$$K_B = \int_0^a \sigma(x) \frac{2}{\sqrt{\pi x}} \left[1 + M_{1,B}\left(\frac{x}{a}\right)^{1/2} + M_{2,B}\left(\frac{x}{a}\right) + M_{3,B}\left(\frac{x}{a}\right)^{3/2}\right] dx \tag{6.5}$$

where weight function geometry factors $M_{1,B}$,$M_{2,B}$ and $M_{3,B}$ are equal to:

$$\begin{cases} M_{1,B} &= \frac{\pi}{\sqrt{4Q}}(30F_1 - 18F_0) - 8 \\ M_{2,B} &= \frac{\pi}{\sqrt{4Q}}(60F_0 - 90F_1) + 15 \\ M_{3,B} &= 2(1 + M_{1,B} + M_{2,B}) \end{cases} \tag{6.6}$$

Coefficients Y_0, Y_1, F_0 and F_1 needed for stress intensity factor calculations can be found in reference [21].

Fatigue live data obtained from the double-notched specimens were used for evaluation of the equivalent initial flaw size distribution using the method described in the previous chapter. Therefore, running of the "Monte-Carlo" simulations for this type of specimen had no practical value. The next specimen in consideration was the plate with a single hole (see Figure 6.14). Since no post-fractography analysis was performed after this test completion, available data was presented in form of the stress-life diagram. In order to simulate those tests using the numerical simulation method, statistical distribution of initial crack sizes (6.1) together with statistical distribution of fatigue crack growth parameters C_i for Al 7075-T6 aluminum alloy (see Figure 6.4) were used. The predicted results (shown in Figure 6.20) are very close to the measured data and can be considered as slightly conservative. Nevertheless, it is important to note that they fall well within the scattered data of predicted values of numbers of cycles to failure, N_f.

The next experiment in consideration was performed using the two-holes specimen. For this type of specimen post-fractography analysis was used to backward extrapolate the crack size. The lowest crack size detected using theses method was about 0.1mm and was estimated to appear around 40000 cycles. Collection of experimental points obtained using the post-fractography analysis together with results of simulation are shown in Figure 6.21. It should be noted that since number of simulation runs is very high (1000), resultant fatigue crack growth curves are visually indistinguishable. Therefore, it was decided to

show the spread of results. Two horizontal "*cuts*" were made for simulation data. As the result, Log-Normal distributions were fitted and plotted in Figure 6.21b. This data can be used to estimate the number of applied loading cycles required to reach crack of specified size with certain degree of probability. Also two vertical "*cut*" was made at $N = 31000$ for the same simulation data. Results of simulation from the UniGrow program for this "*cut*" are shown in Figure 6.22b. This type of data should be useful for the non-destructive evaluation purposes. This is due it shows spread of potential values of the crack size a_i within the given structure. Obtained "Monte-Carlo" simulation results show good correlation with the experimental data.

Final experiment in review was done using the three-holes specimen type. Post-fractography analysis was also used for this part of investigation. As in previous cases, evaluated equivalent initial flaw size distribution together with spread of the fatigue crack growth coefficients for Al 7075-T6 aluminum alloy were used for "Monte-Carlo" simulations. Experimental results together with results of simulation are presented in Figure 6.23. Distribution evaluated from the horizontal (probability density function) "*cut*" is presented in Figure 6.23b. For vertically assembled data, results from the "Monte-Carlo" UniGrow program are shown in Figure 6.24b. Results from performed "Monte-Carlo" simulations for three-hole specimen also show good correlation with the experimental data.

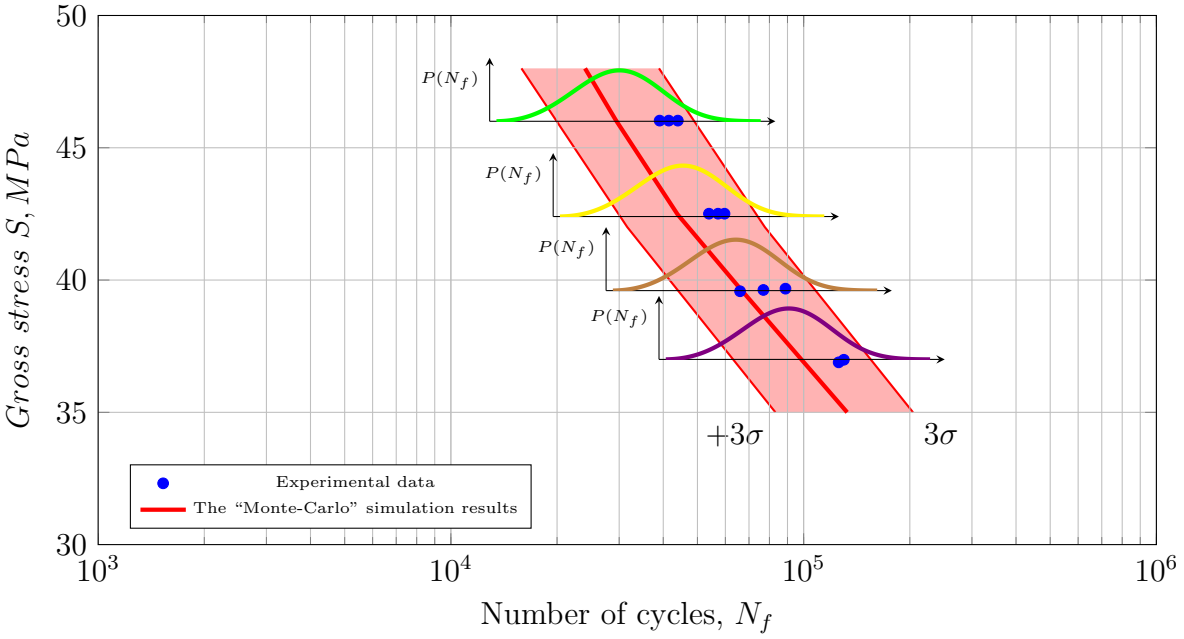

(a)

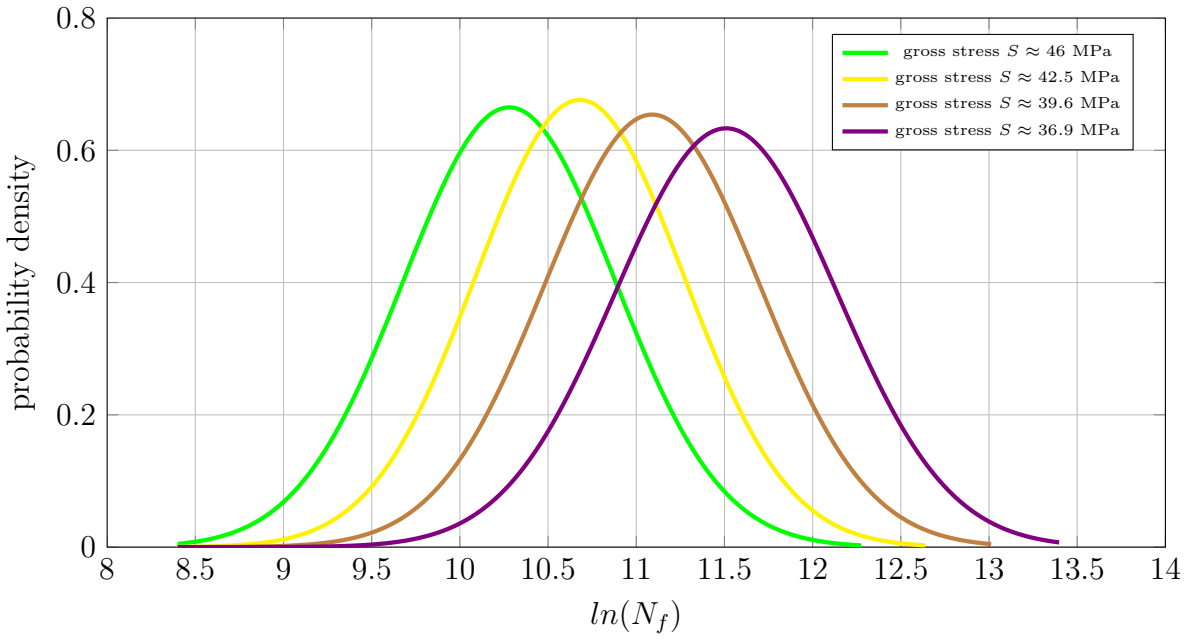

(b)

Figure 6.20: (a) Experimental results [59] and (b) "Monte-Carlo" simulation results for one-hole specimens in form of P(N) probability density function.

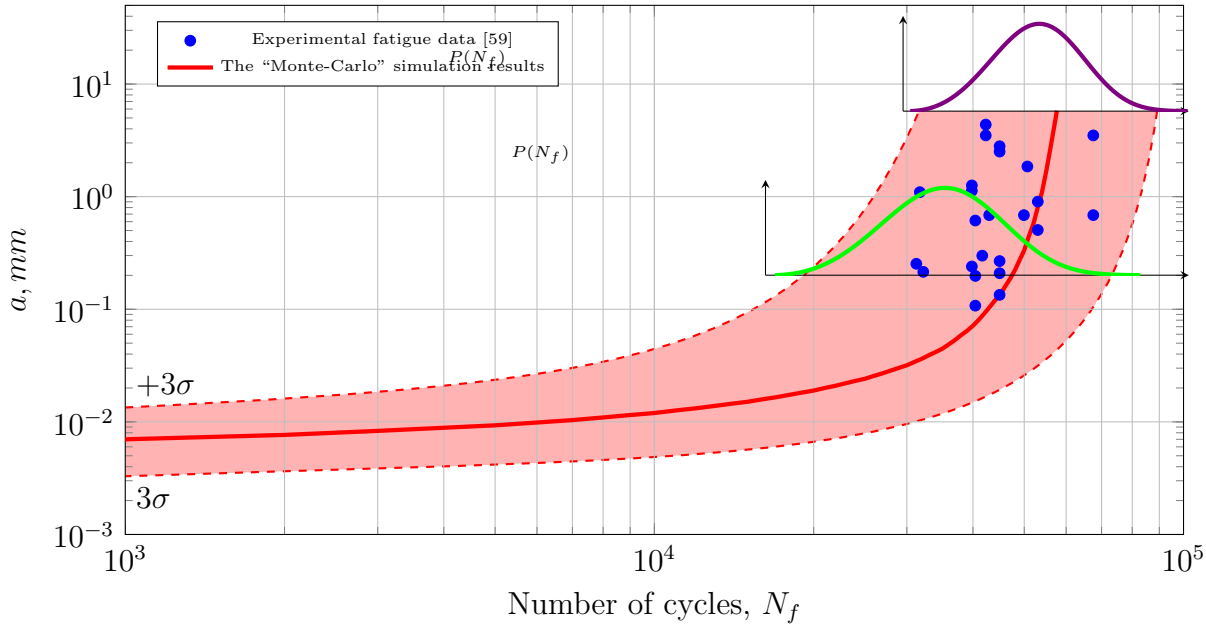

(a)

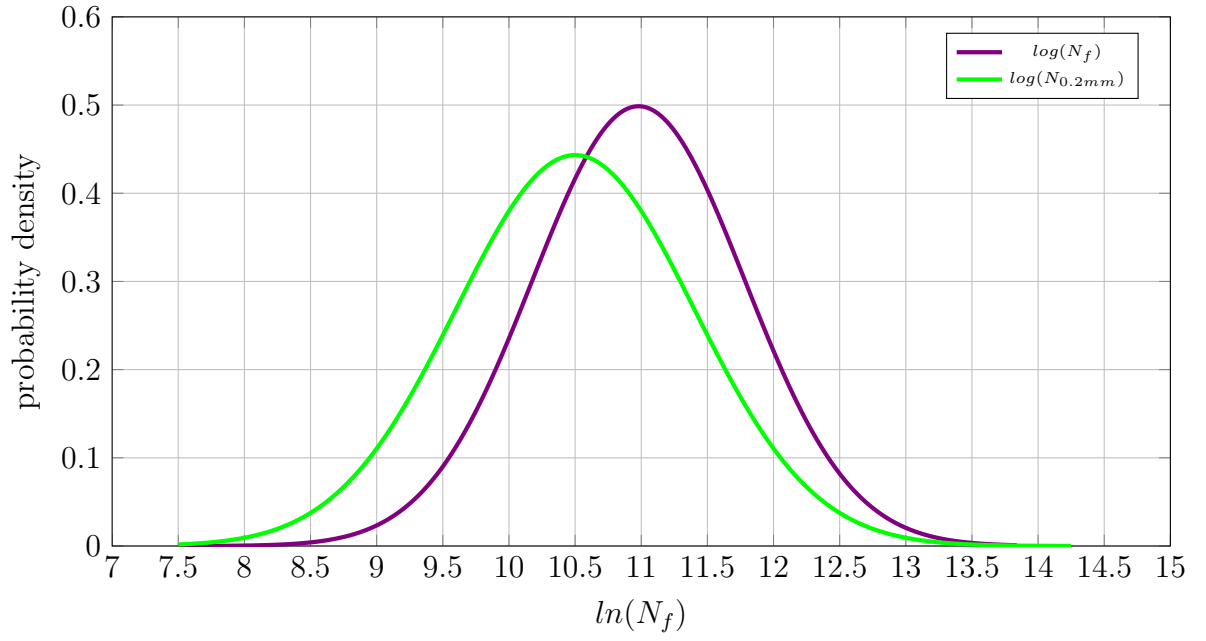

(b)

Figure 6.21: (a) Experimental results [59] and (b) "Monte-Carlo" simulation results for one-hole specimens in form of P(N) probability density function.

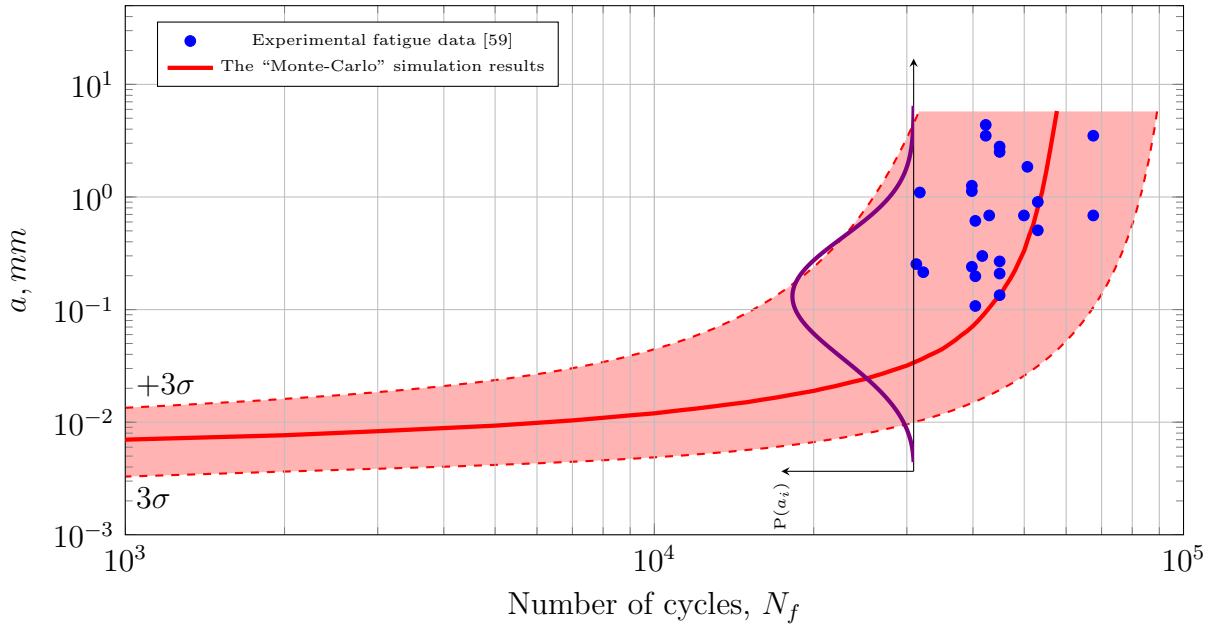

(a)

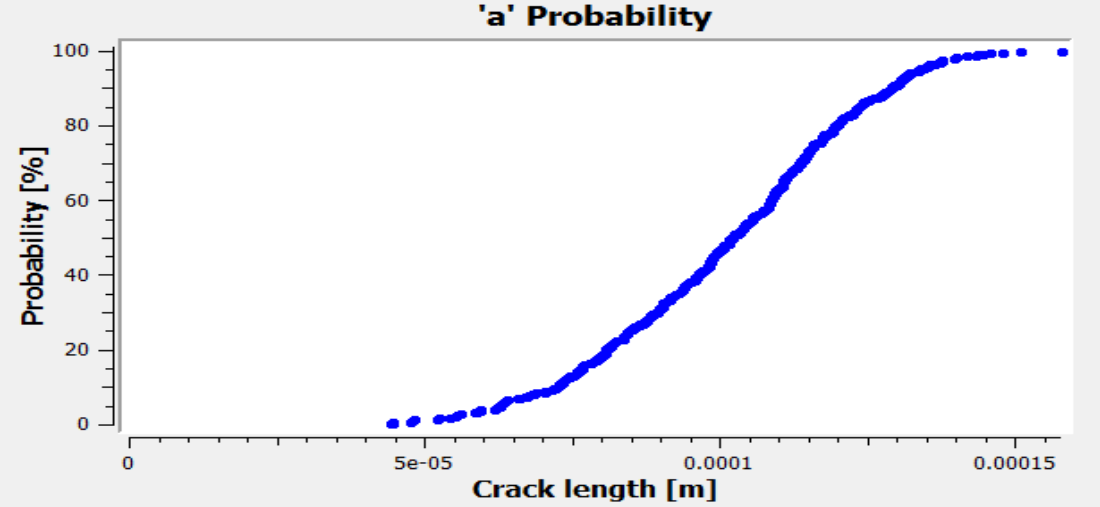

(b)

Figure 6.22: (a) Experimental results [59] and (b) "Monte-Carlo" simulation results for two-hole specimens in form of P(a) cumulative distribution function.

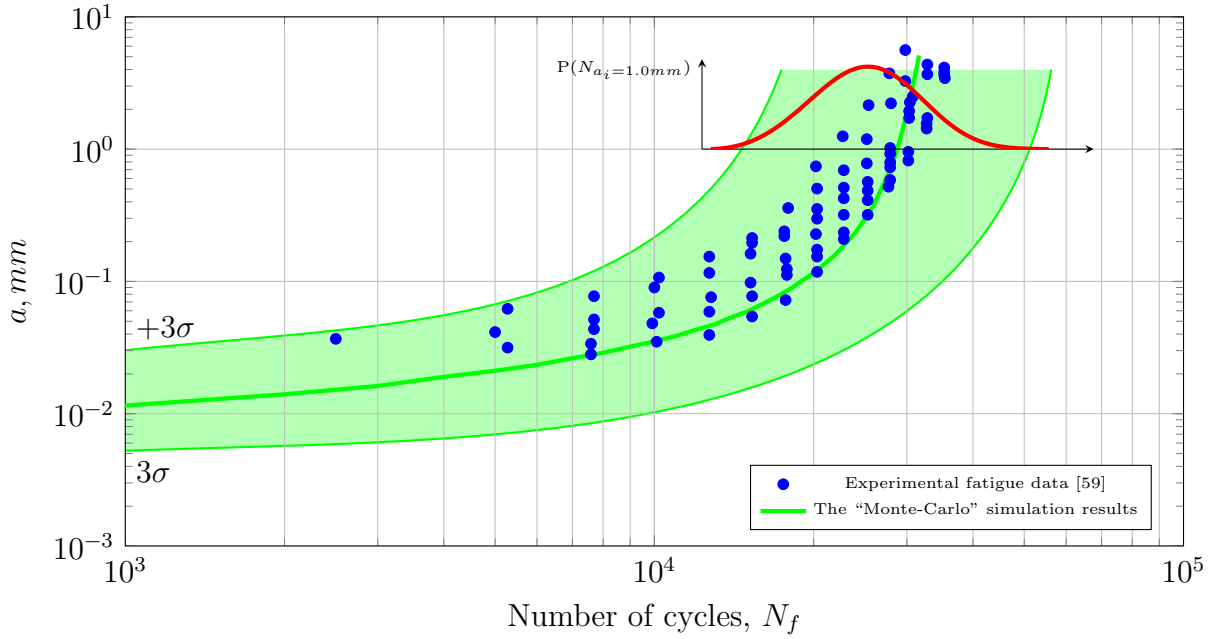

(a)

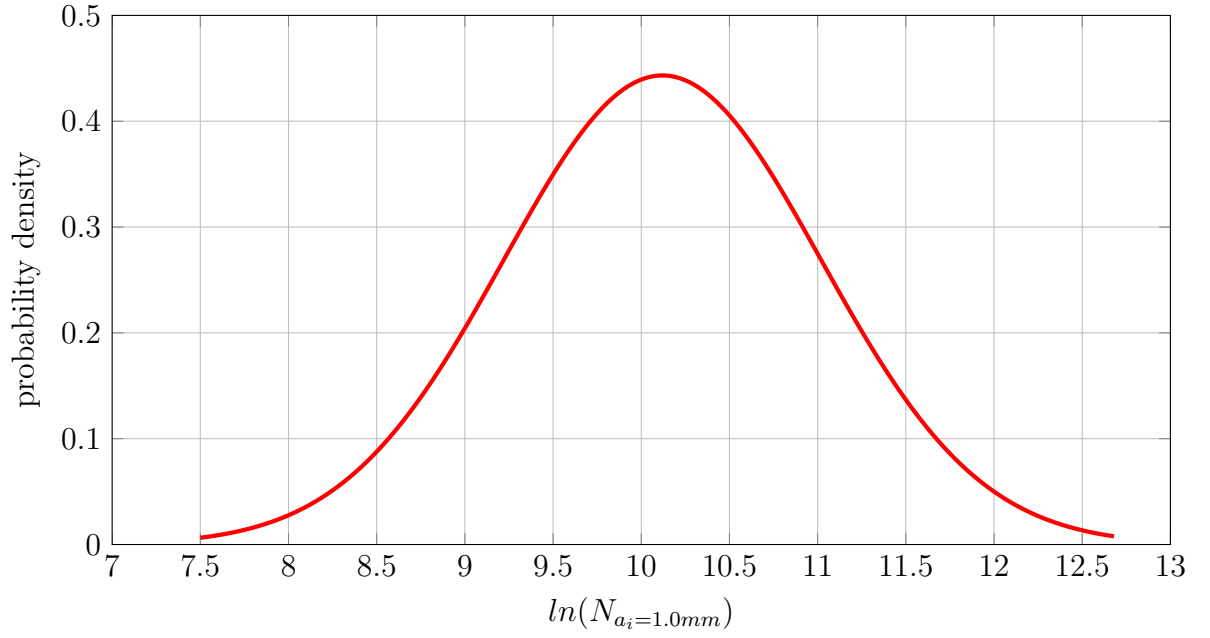

(b)

Figure 6.23: (a) Experimental results [59] and (b) "Monte-Carlo" simulation results for three-hole specimens in form of P(N) probability density function.

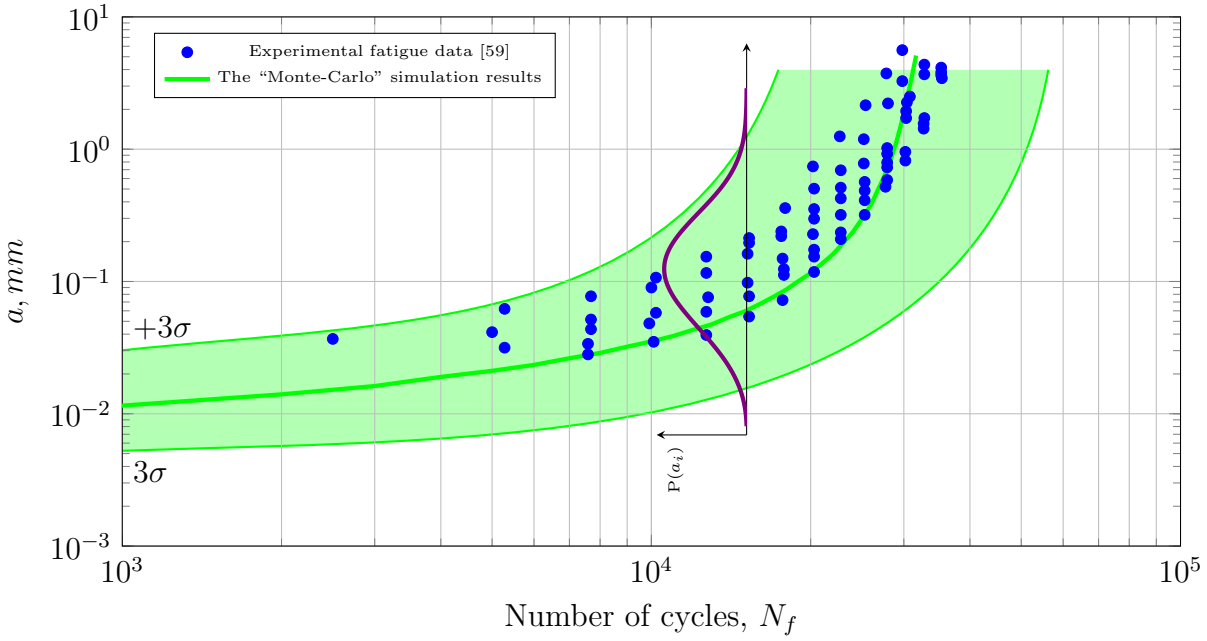

(a)

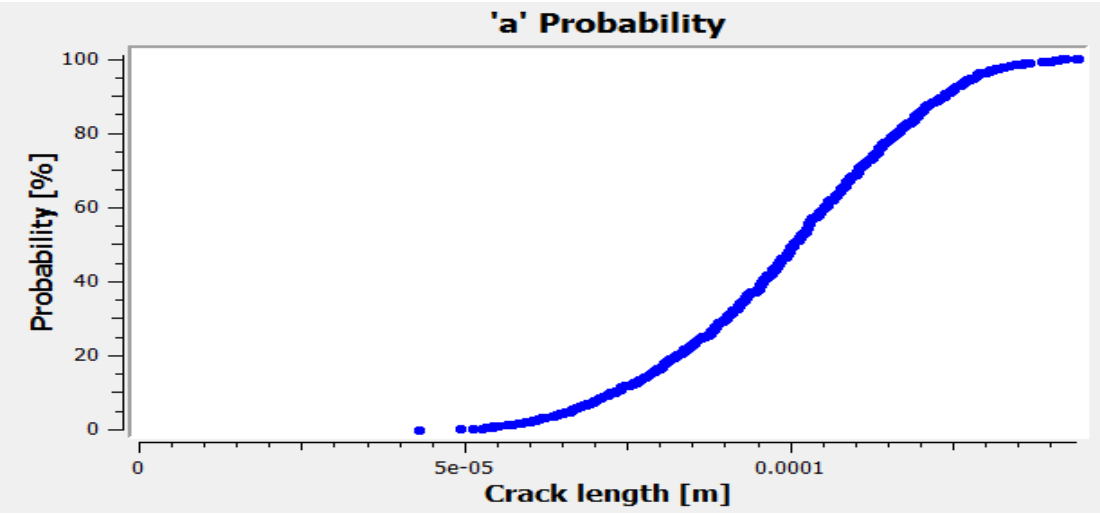

(b)

Figure 6.24: (a) Experimental results [59] and (b) "Monte-Carlo" simulation results for three-hole specimens in form of P(a) cumulative distribution function.

Chapter 7

Conclusions and Future Recommendations

The new fatigue life estimation method based the advanced deterministic fatigue crack growth model UniGrow and the "Monte-Carlo" simulation method has been proposed. This method enables to account for variable nature of the material response to the applied cyclic load and implies the spread of potential initial flaw sizes in the given for analysis structure. The proposed random variables model was validated on the basis of available statistical fatigue crack growth data [4, 6] and by using the data from P3 aircraft life-extension program [59]. Results of fatigue crack growth "Monte-Carlo" simulations are in agreement with experimental data.

Analysis of the UniGrow fatigue crack growth model in its previous form was the starting point of undertaken research. Several deficiencies of the model has been pointed out. Short crack problem and stress analysis of the medium in vicinity of the crack tip were defined as the most critical areas for improvement. As a result of the performed work, short crack correction factor was implemented into fatigue crack growth calculations. The ESED method [65] was implemented for estimation of the residual stress distribution. The

results of comparison with Neuber [48] rule has revealed the following: resultant residual stress profiles obtained using different methods have no significant difference. From other side, imposed plane-strain condition significantly change the residual stress distribution profile. Consequently this impacts the prediction of the fatigue crack growth. Therefore, stress-strain condition at the crack tip has to be carefully analyzed beforehand. As the result, four types of stress analysis were implemented for the UniGrow fatigue crack growth model. They are based on combinations of Neuber or ESED methods with imposed Plane-Stress or Plane-Strain conditions.

Analysis of available methods to estimate value of the ρ^* parameter has been performed. Reviewed methods were shown to have their own drawback and to be conceptually different with one another. Therefore, the new way to evaluate the ρ^* parameter was formulated and coded into a dedicated software package. Proposed method takes into account the dual nature of the ρ^* parameter. The advantage of this method is that it enables further evaluation of the probability distribution of the fatigue crack growth coefficients, C_i. Study of the sensitivity of fatigue crack growth analysis to the chosen value of the ρ^* parameter has been accomplished. It was shown that the ρ^* value chosen from the defined range has no or very little impact on fatigue crack growth predictions given that fatigue crack growth coefficients are corresponding to the chosen value of the ρ^* parameter.

Two methods to combine any deterministic fatigue crack growth model with the "Monte-Carlo" simulation method are known. They are random variables and random process approaches. The choice of the random variables method over the random process one has been justified during the course of the studies. Then, deterministic fatigue crack growth UniGrow model was tested for bias. The performed analysis has shown that the UniGrow fatigue crack growth model can be deemed as unbiased. Combination of the UniGrow fatigue crack growth concept with the "Monte-Carlo" simulation method into the random vari-

ables model was presented. Methods to evaluate probability distributions of fatigue crack growth coefficients, C_i and equivalent initial flaw size a_0 were introduced. Finally, the proposed methodology was programmed into the UniGrow fatigue crack growth software package so the developed model can be used by third-party.

Several recommendations for the future research can be made. To start with, experimental statistical fatigue crack growth investigation similar to the ones by Vikler [4] and Ghonem [6] for the steel and titanium alloys might prove as very useful for the following model validation. Further investigation of the proposed method to evaluate the equivalent initial flaw size distribution are also of interest. Another missing piece for the model in current form is application of the random loading. As of now it can be artificially incorporated into the analysis through some external sampling of the long history and supplying it to the UniGrow fatigue crack growth software. Study of the impact of the randomness in loading sequence on fatigue life modeling is essential next step of future research based on the proposed model. Finally, test of the UniGrow fatigue crack growth model against the almost identical model which will perform the stress analysis using the finite element method is of great interest. The idea of using finite element method was initially abandoned due to high demand concerning the computational time needed for the analysis. However new computers may make such a task feasible and therefore cost analysis of computational time versus prediction accuracy should be done.

References

[1] A. Noroozi, G. Glinka, and S. Lambert, "A two parameter driving force for fatigue crack growth analysis," *International Journal of Fatigue*, vol. 27, no. 10-12, pp. 1277 – 1296, 2005. Fatigue Damage of Structural Materials V 5th International Conference on Fatigue Damage of Structural Materials.

[2] S. Hudak Jr, A. Saxena, R. Bucci, and R. Malcolm, "Development of standard methods of testing and analyzing fatigue crack growth rate data," tech. rep., DTIC Document, 1978.

[3] T. R. Porter, "Method of analysis and prediction for variable amplitude fatigue crack growth," *Engineering Fracture Mechanics*, vol. 4, no. 4, pp. 717 – 736, 1972.

[4] D. A. Virkler, B. M. Hillberry, and P. K. Goel, "The statistical nature of fatigue crack propagation," *Journal of Engineering Materials and Technology*, vol. 101, no. 2, p. 148, 1979.

[5] A. Rosenberger, "Variability in component life due to fatigue crack growth variability (preprint)," tech. rep., DTIC Document, 2008.

[6] H. Ghonem and S. Dore, "Experimental study of the constant-probability crack growth curves under constant amplitude loading," *Engineering Fracture Mechanics*, vol. 27, no. 1, pp. 1 – 25, 1987.

[7] F. Kozin and J. Bogdanoff, "On the probabilistic modeling of fatigue crack growth," *Engineering Fracture Mechanics*, vol. 18, pp. 623–632, Jan 1983.

[8] S. Mikheevskiy and G. Glinka, "Elastic plastic fatigue crack growth analysis under variable amplitude loading spectra," *International Journal of Fatigue*, vol. 31, no. 11-12, pp. 1828 – 1836, 2009. Fatigue Damage of Structural Materials {VII}.

[9] P. Paris and F. Erdogan, "A critical analysis of crack propagation laws," *Journal of Fluids Engineering*, vol. 85, no. 4, pp. 528 – 553, 1963.

[10] G. R. Irwin, "Analysis of Stresses and Strains Near the End of a Crack Traversing a Plate," *J. Appl. Mech.*, 1957.

[11] M. Creager and P. Paris, "Elastic field equations for blunt cracks with reference to stress corrosion cracking," *International Journal of Fracture Mechanics*, vol. 3, no. 4, pp. 247–252, 1967.

[12] Y. Murakami and N. Z. Gakkai, *Stress Intensity Factors Handbook*. Society of Materials Science, Japan, 2001.

[13] H. Tada, G. Irwin, P. Paris, P. Productions, and D. R. Corporation, *The Stress Analysis of Cracks Handbook*. Paris Productions and Del Research Corporation, 1985.

[14] G. Sih, L. U. I. of Fracture, and S. Mechanics, *Handbook of Stress-intensity Factors*. Handbook of Stress-intensity Factors, Lehigh University, Institute of Fracture and Solid Mechanics, 1973.

[15] *ASTM E647-05 Standard Test Method for Measurement of Fatigue Crack Growth Rates*. ASTM International, 2013.

[16] A. Moftakhar and G. Glinka, "Calculation of stress intensity factors by efficient integration of weight functions," *Engineering Fracture Mechanics*, vol. 43, no. 5, pp. 749 – 756, 1992.

[17] H. F. Bueckner, "A novel principle for the computation of stress intensity factors," *Zeitschrift fuer Angewandte Mathematik & Mechanik*, vol. 50, no. 9, pp. 529 – 546, 1970.

[18] J. R. Rice, "Some remarks on elastic crack-tip stress fields," *International Journal of Solids and Structures*, vol. 8, no. 6, pp. 751 – 758, 1972.

[19] E. Atroshchenko, S. Potapenko, and G. Glinka, "Weight function for an elliptical planar crack embedded in a homogeneous elastic medium," *International Journal of Fracture*, vol. 165, pp. 39–45, Sep 2010.

[20] E. Atroshchenko, S. Potapenko, and G. Glinka, "Stress intensity factor for a semi-elliptical crack subjected to an arbitrary mode i loading," *Mathematics and Mechanics of Solids*, vol. 19, pp. 289–298, May 2014.

[21] G. Shen and G. Glinka, "Weight functions for a surface semi-elliptical crack in a finite thickness plate," *Theoretical and Applied Fracture Mechanics*, vol. 15, pp. 247–255, Aug 1991.

[22] M. Miller and J. Gallagher, "An analysis of several fatigue crack growth rate (fcgr) descriptions," in *Fatigue Crack Growth Measurement and Data Analysis*, pp. 205–205–47, ASTM International, Jan 1981.

[23] R. G. Forman, V. E. Kearney, and R. M. Engle, "Numerical analysis of crack propagation in cyclic-loaded structures," *Journal of Fluids Engineering*, vol. 89, no. 3, pp. 463 – 464, 1967.

[24] K. Walker, "The effect of stress ratio during crack propagation and fatigue for 2024-t3 and 7075-t6 aluminum," *Effects of Environment and Complex Load History on Fatigue Life*, p. 1114, Jan 1970.

[25] P. Chong-Myong and S. Ji-Ho, "Crack growth and closure behavior of short fatigue cracks," *Engineering fracture mechanics*, vol. 47, no. 3, pp. 327–343, 1994.

[26] W. Elber, "The significance of fatigue crack closure," *Damage Tolerance in Aircraft Structures*, p. 23023013, Jan 1971.

[27] H. Hardrath, *Recent developments in analysis of crack propagation and fracture of practical materials*. 1978.

[28] J. Newman, J.C., "A crack opening stress equation for fatigue crack growth," *International Journal of Fracture*, vol. 24, no. 4, pp. R131–R135, 1984.

[29] S. R. Institute and N. J. S. Center, *NASGRO reference manual version 5.2*. SWRI, 2008.

[30] K. Donald and P. C. Paris, "An evaluation of ΔK_{eff} estimation procedures on 6061-T6 and 2024-T3 aluminum alloys," *International Journal of Fatigue*, vol. 21, Supplement 1, no. 0, pp. S47 – S57, 1999.

[31] D. Kujawski, "A new (k+kmax)0.5 driving force parameter for crack growth in aluminum alloys," *International Journal of Fatigue*, vol. 23, pp. 733–740, Sep 2001.

[32] S. Dinda and D. Kujawski, "Correlation and prediction of fatigue crack growth for different R-ratios using K_{max} and ΔK^+ parameters," *Engineering Fracture Mechanics*, vol. 71, no. 12, pp. 1779 – 1790, 2004.

[33] L. F. Coffin Jr, "A study of the effects of cyclic thermal stresses on a ductile metal," *trans. ASME*, vol. 76, pp. 931–950, 1954.

[34] K. Smith, T. Topper, and P. Watson, "A stress-strain function for the fatigue of metals(stress-strain function for metal fatigue including mean stress effect)," *Journal of materials*, vol. 5, pp. 767–778, 1970.

[35] J. Schijve, "Observations on the prediction of fatigue crack growth propagation under variable-amplitude loading," *Fatigue Crack Growth Under Spectrum Loads*, p. 3321, Jan 1976.

[36] A. Bacila, X. Decoopman, G. Mesmacque, M. Voda, and V. Serban, "Study of underload effects on the delay induced by an overload in fatigue crack propagation," *International Journal of Fatigue*, vol. 29, no. 911, pp. 1781 – 1787, 2007. Fatigue Damage of Structural Materials {VI} The Sixth International Conference on Fatigue Damage of Structural Materials.

[37] W. Schutz, "Standardized stress-time historiesan overview," *Development of Fatigue Loading Spectra*, p. 3314, Jan 1989.

[38] J. McMillan and R. Pelloux *Fatigue Crack Propagation*, p. 50550531, Jan 1967.

[39] O. E. Wheeler, "Spectrum loading and crack growth," *J. Basic Engineering*, vol. 94, no. 1, p. 181, 1972.

[40] J. Willenborg, R. Engle, and H. Wood, "A crack growth retardation model using an effective stress concept," Tech. Rep. AFFDL-TM-71-1-FBR, 1971.

[41] A. F. R. L. W.-P. A. O. A. V. Directorate and J. Harter, *AFGROW Users Guide and Technical Manual*. Storming Media, 1999.

[42] G. Garrett and J. Knott, "On the effect of crack closure on the rate of fatigue crack propagation," *International Journal of Fracture*, vol. 13, no. 1, pp. 101–104, 1977.

[43] D. Kujawski, "A fatigue crack driving force parameter with load ratio effects," *International Journal of Fatigue*, vol. 23, Supplement 1, no. 0, pp. 239 – 246, 2001.

[44] J. Newman, *FASTRAN-2: A Fatigue Crack Growth Structural Analysis Program*. 1992.

[45] J. A. Harter, "Comparison of contemporary {FCG} life prediction tools," *International Journal of Fatigue*, vol. 21, Supplement 1, no. 0, pp. S181 – S185, 1999.

[46] D. Dugdale, "Yielding of steel sheets containing slits," *Journal of the Mechanics and Physics of Solids*, vol. 8, pp. 100–104, May 1960.

[47] S. Mikheevskiy, *Elastic-Plastic Fatigue Crack Growth Analysis under Variable Amplitude Loading Spectra*. PhD thesis, University of Waterloo, 2009.

[48] H. Neuber, "Theory of stress concentration for shear-strained prismatical bodies with arbitrary nonlinear stress-strain law," *Journal of Applied Mechanics*, vol. 28, no. 4, p. 544, 1961.

[49] K. Molski and G. Glinka, "A method of elastic-plastic stress and strain calculation at a notch root," *Materials Science and Engineering*, vol. 50, pp. 93–100, Sep 1981.

[50] S. Hudak, *A comparison of single-cycle versus multiple-cycle proof testing strategies*, vol. 4318. National Aeronautics and Space Administration, Office of Management, Scientific and Technical Information Division, 1990.

[51] R. J. Cross, A. Makeev, and E. Armanios, "A comparison of predictions from probabilistic crack growth models inferred from virklers data," *Journal of the ASTM International*, vol. 3, no. 10, pp. 1–11, 2006.

[52] J. Yang and S. Manning, "A simple second order approximation for stochastic crack growth analysis," *Engineering Fracture Mechanics*, vol. 53, p. 677686, Mar 1996.

[53] K. Ortiz and A. S. Kiremidjian, "Stochastic modeling of fatigue crack growth," *Engineering Fracture Mechanics*, vol. 29, pp. 317–334, Jan 1988.

[54] A. Merati and G. Eastaugh, "Determination of fatigue related discontinuity state of 7000 series of aerospace aluminum alloys," *Engineering Failure Analysis*, vol. 14, pp. 673–685, jun 2007.

[55] T. Anderson, *Fracture Mechanics: Fundamentals and Applications, Third Edition*. Taylor & Francis, 2005.

[56] M. Bao-Tong and C. Laird, "On fatigue crack size distributions in copper single crystals," *Fat Frac Eng Mat Struct*, vol. 9, pp. 109–116, Feb 1986.

[57] J. Gallagher and F. Giessler, "Usaf damage tolerant design handbook: guidelines for the analysis and design of damage tolerant aircraft structures," Tech. Rep. AFFDL-TR-79-3021, 1979.

[58] K. J. Miller, "The short crack problem," *Fat Frac Eng Mat Struct*, vol. 5, pp. 223–232, Jul 1982.

[59] J. Newman, E. Anagnostou, and D. Rusk, "Fatigue and crack-growth analyses on 7075-t651 aluminum alloy coupons under constant- and variable-amplitude loading," *International Journal of Fatigue*, vol. 62, p. 133143, May 2014.

[60] J. Kendall and J. King, "Short fatigue crack growth behaviour: data analysis effects," *International Journal of Fatigue*, vol. 10, no. 3, pp. 163 – 170, 1988.

[61] N. Fleck, "Influence of stress state on crack growth retardation," in *Basic Questions in Fatigue: Volume I*, pp. 157–157–27, ASTM International, Jan 1988.

[62] D. Ye, S. Matsuoka, N. Suzuki, and Y. Maeda, "Further investigation of neubers rule and the equivalent strain energy density (esed) method," *International Journal of Fatigue*, vol. 26, no. 5, pp. 447 – 455, 2004.

[63] G. Glinka, "Calculation of inelastic notch-tip strain-stress histories under cyclic loading," *Engineering Fracture Mechanics*, vol. 22, pp. 839–854, Jan 1985.

[64] A. H. NorooziSani, *Development of a Two-Parameter Model (K_{max}, ΔK) for Fatigue Crack Growth Analysis*. PhD thesis, University of Waterloo, 2007.

[65] G. Glinka, "A notch stress-strain analysis approach to fatigue crack growth," *Engineering Fracture Mechanics*, vol. 21, no. 2, pp. 245 – 261, 1985.

[66] Newman, Wu, Swain, Zhao, Phillips, and Ding, "Small-crack growth and fatigue life predictions for high-strength aluminium alloys. part ii: crack closure and fatigue analyses," *Fat Frac Eng Mat Struct*, vol. 23, pp. 59–72, Jan 2000.

[67] T. Zhu and J. Li, "Ultra-strength materials," *Progress in Materials Science*, vol. 55, no. 7, pp. 710 – 757, 2010.

[68] S. Bogdanov, S. Mikheevskiy, and G. Glinka, "Probabilistic analysis of the fatigue crack growth based on the application of the monte-carlo method to unigrow model," *Matls. Perf. Charact.*, p. 20130066, Jun 2014.

[69] H. Kitagawa and S. Takahashi, "Applicability of fracture mechanics to very small cracks or the cracks in the early stage," in *Second International Conference on Mechanical Behavior of Materials. ASM, Metals Park, Ohio. 1976, 627-631*, 1976.

[70] F. Bergner and G. Zouhar, "A new approach to the correlation between the coefficient and the exponent in the power law equation of fatigue crack growth," *International Journal of Fatigue*, vol. 22, no. 3, pp. 229 – 239, 2000.

[71] E. Charkaluk, A. Constantinescu, F. Szmytka, and S. Tabibian, "Probability density functions: From porosities to fatigue lifetime," *International Journal of Fatigue*, vol. 63, no. 0, pp. 127 – 136, 2014.

[72] J. M. Karandikar, N. H. Kim, and T. L. Schmitz, "Prediction of remaining useful life for fatigue-damaged structures using bayesian inference," *Engineering Fracture Mechanics*, vol. 96, no. 0, pp. 588 – 605, 2012.

[73] C. Annis, "Probabilistic Life Prediction Isn't as Easy as It Looks," *Journal of ASTM International*, vol. 1, 2004.

[74] P. C. Paris, M. Gomez, and W. Anderson, "A rational analytic theory of fatigue," *The Trend in Engineering*, 1961.

[75] L. N. McCartney and B. Gale, "A generalized theory of fatigue crack propagation," *Proceedings of the Royal Society A: Mathematical, Physical and Engineering Sciences*, vol. 322, pp. 223–241, Apr 1971.

[76] P. Shull, *Nondestructive Evaluation*. CRC Press, may 2002.

[77] D. Straub, *Generic approaches to risk based inspection planning for steel structures*, vol. 284. vdf Hochschulverlag AG, 2004.

[78] M. K. Rabinovich and M. V. Markuskev, "Effect of grain size on the crack resistance of aluminum alloys," *Metal Science and Heat Treatment*, vol. 36, pp. 429–436, aug 1994.

[79] P. Noronha, S. Henslee, D. Gordon, Z. Wolanski, and B. Lee, *Fastener hole quality*. Defense Technical Information Center, 1978.

[80] J. D. Hochhalter, *Finite element simulations of fatigue crack stages in AA 7075-T651 microstructure*. PhD thesis, Cornell University, 2010.

[81] Ryschkewitsch, "Nondestructive evaluation requirements for fracture-critical metallic components," Tech. Rep. NASA-STD-5009, NASA, 2008.

[82] D. Turan, A. Karci, and S. Turan, "Microstructural observation of overload effect on the fatigue crack growth of 2024-t3 al-alloy," in *CONFERENCE SERIES-INSTITUTE OF PHYSICS*, vol. 179, pp. 281–284, Philadelphia; Institute of Physics; 1999, 2004.

[83] J. L. Rudd, "Applications of the equivalent initial quality method," tech. rep., DTIC Document, 1977.

[84] R. Wellein, "Applications of pfm in the nuclear industry to reactor pressure vessel, main coolant piping and steel containment," in *Probabilistic fracture mechanics and reliability* (J. Provan, ed.), vol. 6 of *Engineering Application of Fracture Mechanics*, pp. 325–350, Springer Netherlands, 1987.

[85] S. Fawaz, "Equivalent initial flaw size testing and analysis of transport aircraft skin splices," *Fatigue & Fracture of Engineering Materials & Structures*, vol. 26, no. 3, pp. 279–290, 2003.

[86] M. Matsumoto and T. Nishimura, "Mersenne twister: a 623-dimensionally equidistributed uniform pseudo-random number generator," *TOMACS*, vol. 8, p. 330, Jan 1998.

[87] "Boost C++ libraries." `http://www.boost.org/`. Accessed: 2011-10-05.

[88] G. S. Fishman, *Monte Carlo*. Springer New York, 1996.

[89] R. P. Patankar, *Modeling fatigue crack growth for life-extending control*. PhD thesis, 1999.

[90] C. Boller and T. Seeger, *Materials data for cyclic loading*. No. pt. 4 in Materials science monographs, Elsevier, 1987.

[91] M. H. Gruber, *Regression estimators: A comparative study*. JHU Press, 2010.